Defects in low dimensional strongly correlated quantum systems

A Thesis
Submitted to the
Tata Institute of Fundamental Research, Mumbai
For the degree of
Doctor of Philosophy
in Physics

by
Sambuddha Sanyal

Department of Theoretical Physics
Tata Institute of Fundamental Research, Mumbai
December, 2013

DECLARATION

This thesis is a presentation of my original research work. Wherever contributions of others are involved, every effort is made to indicate this clearly, with due reference to the literature, and acknowledgement of collaborative research and discussions.

The work was done under the guidance of **Professor Kedar Damle**, at the Tata Institute of Fundamental Research, Mumbai.

Sambuddha Sanyal
Department of Theoretical Physics
Tata Institute of Fundamental Research, Mumbai
December, 2013

In my capacity as supervisor of the candidates thesis, I certify that the above statements are true to the best of my knowledge.

Prof. Kedar Damle
Department of Theoretical Physics
Tata Institute of Fundamental Research, Mumbai
December, 2013

Acknowledgement

First of all I want to acknowledge my advisor Kedar Damle for giving me interesting problems to work on and also for his able and sincere guidance. I also want to thank him for giving very interesting courses from which I learned lot of things.
I want to thank Deepak Dhar, Vikram Tripathi and Rajdeep Sensharma for various courses, journal clubs and discussions, I benefited a lot from all those interactions. I am specially grateful to Deepak for helping me to improve my writing at the last phase of my PhD. I would like to thank Mandar Deshmukh with whom I worked in an experimental project and enjoyed many discussion, the time I spent in his lab helped me to get a much broader view of condensed matter physics. I must also thank Amol Dighe, Goutam Mondal, Sourendu Gupta, Nilmani Mathur and Sushil Majumdar for various courses and projects which helped me a lot.
I want to thank my collaborator and friend Argha Banerjee for very fruitful discussions and for helping me in various things at the beginning of my graduate school; I enjoyed and learned a lot of things from him outside Physics as well. I also want to acknowledge my another collaborator Anders Sandvik, apart from the topic we worked on I learned a lot of details about perfecting a draft from him. I will like to thank our collaborators John Chalker and Roderich Moessner for giving valuable inputs on the first two problems of this thesis.
I would like to thank Arun Paramekanti for hosting me in a few months visit at UofT, I have benifited a lot from discussions with him and other members of the department. I would specially like to thank Subhro Bhttacherjee for the very enjoyable Physics discussions and the great time we had at Toronto.
I want to acknowledge the computer services section of our department, specially Kapil Ghadiali and Ajay Salve who helped me with lots of problems and maintained the clusters, without which most of the works in this thesis wouldn't have been possible. I would thank the DTP, TIFR office staffs Raju Bhatija, Ramesh Power, Girish Ogale and Mohan Sindhe who made our life hassle free from all official formalities. I would thank the TIFR main office also for the same reason.

I will like to thank my TIFR friends Nikhil, Geet, Rahul, Nilay, Himani, Sayantan, Loganayagam, Jyotirmoy, Umesh, Padmanath, Dipan, Sanmay, Kabir, Kusum, Prithvi, Soham, Takimi, and Sachin for all the interesting activities, adventures and discussions. I must thank specially Geet, Nikhil, Rahul and Himani for helping me to improve my writing. I must also thank all other students in the DTP students room of my time for keeping up an wonderful environment. Beyond the DTP students room I want thank my TIFR friends Saswata, Santanu, Nirupam, Deepnarayan, Aditi for all the crazy activities and great time we had.

I will like to take this opportunity to thank my teacher Tapan Saha, who first motivated me to do take Physics as career and Mahan Maharaj who also motivated me a lot in the college. I want to thank by brother Souriddha for the support and my other relatives for their support and encouragement. I want

to thank my father Late Bijit Sanyal, who induced rational thinking to me at a very young age.
Finally I will thank my mother Bani Sanyal, without her constant support and encouragement my education beyond school wouldn't have been possible.

Abstract

In this thesis we have studied four different problems on the effects of disorders in low dimensional quantum systems. In the first problem we studied the how the low energy properties of a non-interacting system of electron on a bipartite lattice gets effected due to random site dilution. We conclude that the behavior of the density of states the gapless phase is of so called "Gade type" and in the gapped phase is of so called "Griffiths" type. We also tried to understand the possible origin of generation of such states at low energy. In the second problem we have tried to understand the effect of random site dilution in a $SU(2)$ symmetric spin model by mapping the model into a non interacting fermion gas, this map helped us to understand the behavior of the spin system from the results of the non-interacting electronic systems of previous problem. We conclude that from the magnetic response of the system that at low energy the system stabilizes to a "random-singlet" phase. In the third problem we have focused on the ground state properties of finite size antiferromagnetic which can arise in a thermodynamic system as a result of random site dilution. In the fourth problem we focused on the effects of a single impurity on the spin texture in an antiferromagnetically ordered spin chain.

Contents

Chapter 1

Synopsis

A majority of solid state systems in the real world deviates from an ordered arrangement of atoms or ions. Such deviations from a perfect crystalline structure are called defects or disorders in the systems. Defects in crystalline solids not only demand different set of theoretical techniques from the one used for idealized pure systems, but also shows interesting behavior which are different from the pure system. In this synopsis we will overview our work on three different studies to understand effects of defects in strongly correlated systems.

Local changes in the strongly correlated system properties due to defects is interesting as the response of the system in the vicinity of an impurity is a measurable quantity with local probes like NMR and STM, also such responses can give us important hints about the properties of the ground state. In the first problem of the synopsis, we have tried to understand origins of multiplicative logarithmic corrections to the scaling predictions of spin textures in presence of a missing site in the Néel ordered phase of the one-dimensional Heisenberg antiferromagnet. We used standard Bosonization techniques and RG improved perturbation theory to calculate [1] the spin texture in the Néel ordered phase and compared those results with the numerical results [1] obtained by QMC for a different model with same Néel ordered phase in one-dimension. The details of the analysis is presented in first section of this synopsis.

In the second problem of the synopsis we tried to understand certain ground state properties of finite size antiferromagnetic systems, which is important because in computational studies working with finite size systems is inescapable. Also experiments have shown that when a square lattice Heisenberg antiferromagnets (SLHAF) is randomly diluted with non magnetic impurities it shows a percolation transition; with dilution above the percolation threshold the magnetic order of the system breaks in many puddles of finite size [2]. In finite size clusters of SLHAF the ground state can be a either singlet or a doublet which can have fundamentally different behavior. Properties of singlet ground state in a SLHAF have been analyzed before, both numerically [3] and analytically [4]; whereas for doublet such detailed analytical understanding is lacking. In this problem we focus on the doublet ground state properties of SLHAF [5]. Using three different approximate analytic approaches we characterize

a universal relation (with respect to the microscopic details of the Hamiltonian) between the singlet and doublet antiferromagnetic ground state magnetic order in those clusters, observed from numerical experiments [5]. The details of the universal relation and details of the analysis is presented in the second section of this synopsis.

In the third problem of the synopsis we tried to understand certain behavior of disordered quantum spin liquids(QSL). QSLs are very interesting low energy states of strongly correlated matter, where at temperatures lower than the scale of exchange coupling, there is no conventional magnetic order due to interplay between quantum fluctuation and geometric frustration. Several experimental [6, 7, 8, 9] proposals exist where such a state can be realized. This work is related to a realization of the $SU(2)$ invariant spin liquid with spinful Majorana fermion excitation previously discussed at mean field level by Biswas et al [10] to model the phenomenology of $EtMe_3Sb[Pd(dmit)_2]_2$ [11, 12]. In the third problem of this synopsis, we considered an exactly solvable spin model [13] with such SU(2) invariant Majorana QSL ground state and studied the low temperature susceptibility in presence of random site dilution, which is a kind of defect common to experimental systems.

1.1 Vacancy-induced spin texture in one dimensional $S = 1/2$ Heisenberg antiferromagnet

In this part we consider a one-dimensional spin chain with a $S = 1/2$ moment at every site, with nearest neighbors interacting via Heisenberg antiferromagnetic interaction (1DHAFC). We study the vacancy induced spin texture in this system, in the Néel ordered phase.

Even though for $S = 1/2$ 1DHAFC, the thermodynamic properties can be exactly calculated in the ground state using Bethe Ansatz [14], such calculations are often too complicated to be useful in calculating correlation functions [15]. Here we took an alternative route to study this problem i.e. the bosonization approach, which is asymptotically exact in the limit of low energies and long wavelengths. Using bosonization techniques one can map $S = 1/2$ 1DHAFC to a $1 + 1$ dimensional bosonic field theory with a 'sine-Gordon' action, which has a scale invariant free-field part perturbed by a non-linear cosine interaction [16]. The renormalization group (RG) analysis of such cosine interaction perturbing the scale invariant free-field action is an well known example of 'marginally irrelevant' interactions in the neighborhood of a well-characterized scale free RG fixed point. Such marginally irrelevant interaction can give violation of scaling predictions at critical points due to the presence of logarithmic corrections that multiply the scaling predictions. However, the physics of the multiplicative correction for a marginal operator is quite general and applicable in other models like the textbook example of ϕ^4 theory. The importance of studying the same physics in the context of $S = 1/2$ chain is that we can access the system by a number of numerical and exact methods. So it represents an ideal testing ground for this important result.

More generally this problem is relevant in the context of similar multiplicative logarithmic violations of scaling, which have been argued to exist [3, 17] at the critical point of a continuous quantum phase transition [18, 3] between the usual Néel ordered antiferromagnetic ground state and a spontaneously dimerized non-magnetic state with valence-bond order in a two dimensional $S = 1/2$ SLHAF. The questions about nature of that phase transition, existence of such corrections and the origin of the same are not clear and under debate [3, 19, 17, 20, 21, 22].

In this problem, we tried to understand the origin of similar multiplicative logarithmic corrections by studying the Néel ordered phase of this analytically and numerically tractable $S = 1/2$ 1DHAFC. We calculate the spin texture around a missing site from the corresponding bosonic field theory by keeping careful track of the effects of the marginal cosine interaction term using one loop RG improved perturbation theory. Those field theory results for spin texture, are compared to available numerical results [1], which was calculated previously using Quantum Monte-Carlo (QMC) [1] for a one-dimensional chain with nearest neighbor Heisenberg exchange J and six-spin coupling $Q = 4qJ$ (JQ model). Our main conclusion is that this marginal cosine interaction leads to multiplicative logarithmic corrections of scaling in the power-law Néel phase. We compare these analytical predictions with our numerical results for $q < q_c$ (in the Néel phase, above q_c the JQ model goes to a VBS phase) and find good agreement with the data. By good agreement we mean that the strength of the log corrections is larger for q further away from the critical point, and vanishes for $q = q_c$, which is consistent with the bosonized field theory results.

1.1.1 Details of calculation

Using bosonization, $S = 1/2$ 1DHAFC with a non-magnetic impurity (or open boundaries) can be modeled in low energy as the following effective Hamiltonian [16], where ϕ is the bosonic field with $[\phi(x), \widetilde{\phi}(y)] = -i\Theta(x-y)$ ($\Theta(x)$ is the step function).

$$H = H_0 + H_1 \tag{1.1}$$

where the free field part H_0 is written as

$$H_0 = \frac{u}{2}\int_0^L dx \left[\left(\frac{d\phi}{dx}\right)^2 + \left(\frac{d\widetilde{\phi}}{dx}\right)^2\right] , \tag{1.2}$$

and the interaction term H_1 reads

$$H_1 = -\frac{u\epsilon_0}{r_0^2}\int_0^L dx \cos\left(\frac{2\phi(x)}{R}\right) ; \tag{1.3}$$

here r_0 is an ultraviolet regulator defined later and

$$\frac{1}{2\pi R^2} = 1 - \pi\epsilon_0 . \tag{1.4}$$

The last constraint that relates R to the bare coupling constant ϵ_0 at scale r_0 arises from the $SU(2)$ spin invariance of the underlying microscopic theory [23]. Within this bosonized formulation, the operator $S^z(r)$ at site $r = ja$ is represented as

$$S^z(r) = \frac{a}{2\pi R}\frac{d\phi}{dr} + \frac{\mathcal{A}}{\sqrt{r_0}}(-1)^{\frac{r}{a}} \sin\left(\frac{\phi(r)}{R}\right) . \tag{1.5}$$

The alternating part of this is denoted by $N_z(r)$ and compared with available numerical results. We first calculate the alternating part($N_z(r)$) of $\langle S^z(r)\rangle_\uparrow$(the numerical calculation [1] was done in the doublet ground state $S^z_{tot} = +1/2$, created by one missing site in a periodic lattice with even number of sites) by using bare perturbation theory [24, 23, 25] of first order in ϵ_0 for a finite system of length L. However, the bare perturbation theory result turns out to depend logarithmically on the value of the ultraviolet cutoff r_0 via a logarithmic ultraviolet divergence proportional to $\epsilon_0 \log \frac{L}{r_0}$.

This logarithmic divergence makes bare perturbation theory suspect, since a notionally small $\mathcal{O}(\epsilon_0)$ correction turns out to have a logarithmically diverging coefficient. To extract useful information from the bare perturbation theory, it is therefore necessary to appeal to the Callan-Symanzik equation[1] for the one point function $S = \langle \frac{1}{\sqrt{r_0}} \sin\left(\frac{\phi(r)}{R}\right)\rangle_\uparrow$. Using the general form of solution of the Callan-Symanzik equation for one-point correlation and comparing that with the bare perturbation theory results we obtain the alternating part of $\langle S^z(r)\rangle_\uparrow$ as,

$$N_z(r) = c\sqrt{a}\frac{F_0}{\sqrt{L}}\left(\frac{\epsilon_0}{\epsilon(L)}\right)^{\frac{1}{4}}(1+\epsilon(L)R) , \tag{1.6}$$

with

$$F_0(\frac{r}{L}) = -\sqrt{\frac{\pi \sin\theta_r}{2}} , \tag{1.7}$$

and

$$R(\frac{r}{L}) = \frac{\pi}{2}\log\frac{2\pi}{\sin\theta_r} + 2\left(\int_0^{\theta_r} + \int_0^{\pi-\theta_r}\right)\phi\cot\phi d\phi , \tag{1.8}$$

with $\theta_r \equiv \frac{\pi r}{L}$.

Expressing $\epsilon(L)$ as (obtained by solving the one loop expression for the beta function)

$$\epsilon(L) = -\frac{|\epsilon_0|}{1+2\pi|\epsilon_0|\left\{\log\left(\frac{L}{r_0}\right) + \frac{1}{2}\log\left(\log\left(\frac{L}{r_0}\right)\right)\right\}} , \tag{1.9}$$

we choose the short-distance cutoff as $r_0 = a$, and set the length L to $L = (N+1)a$. Eqns(6.43),(6.44), (6.45) with these inputs constitutes a theoretical prediction with two free parameters (the overall amplitude c, and the bare coupling ϵ_0 at the lattice scale), and we find below that this provides an extremely good two-parameter fit of the available numerical data in the power-law ordered antiferromagnetic phase of the one dimensional JQ_3 model(Figure 6.1).

In addition, the spin texture at $q = q_c$,($q_c = 0.04$ is known from numerics) the critical end-point of this power-law ordered Néel phase, fits extremely well to the general prediction with $\epsilon_0 = 0$(Figure 6.3).

[1]The Callan-Symanzik equation is a differential equation describing the evolution of the correlation functions under variation of the energy scale at which the theory is defined.

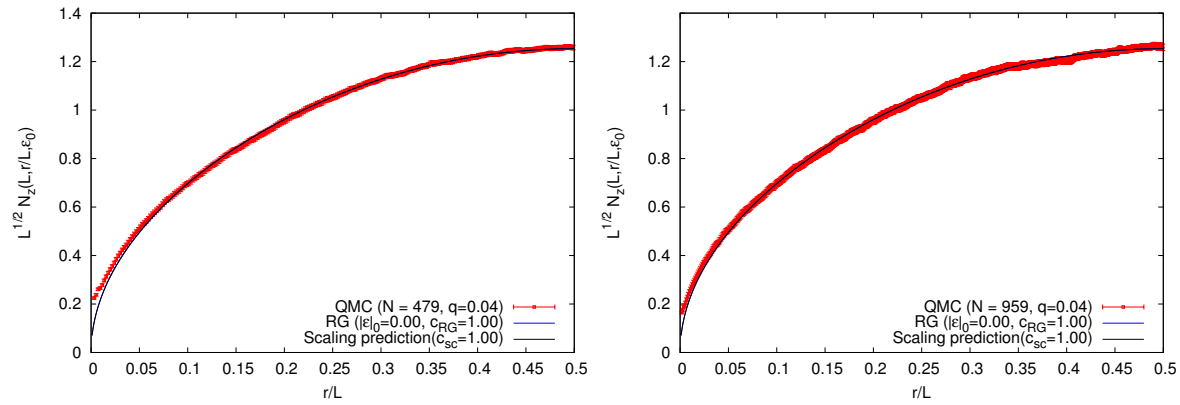

Figure 1.1: $L^{1/2}N_z(r)$ plotted versus r/L (where $L = N + 1$ for chains with $N = 959$ and $N = 479$ spins and open boundary conditions) and compared with the scaling prediction F_0 for $q = q_c = 0.04$, the approximate location of the quantum critical point separating the power-law Néel phase from the VBS ordered phase in the one dimensional JQ_3 model. Note the data at both sizes fits essentially perfectly to the scaling prediction with the same prefactor c_{sc}. Also note that the best two-parameter fit corresponding to our RG improved perturbation theory result also gives $|\epsilon_0| = 0$, and thus coincides with the scaling answer.

1.1.2 Comparing numerical and analytical results

In Figure (6.3), we have shown the numerical data [1] for the alternating part of the spin texture to compare it with the scaling prediction at the critical point $q = q_c$ and RG prediction for the same, for two system sizes. As can be seen from these two figures, the scaling prediction fits extremely well to all the data at both sizes. Also, a two-parameter fit using the RG-improved perturbation theory result yields a best-fit value of ϵ_0 indistinguishable from $\epsilon_0 = 0$. This confirms the location of the critical point, as the bare coefficient of the marginally irrelevant cosine interaction is expected to be zero at the transition point. This almost perfect fit to the scaling prediction is contrasted with the results shown in Figure (6.1), which show numerical results at two representative points($q = 0$ and $q = 0.02$) in the power-law Néel phase compared with the one-parameter fit obtained from the scaling prediction. As shown in these two figures, the scaling prediction cannot predict well the numerical results for $q < q_c$. Additionally we note that the misfit of scaling predictions with numerical results increases as we go further from the critical point(i.e. smaller q). In the same figures, we also show the best two-parameter fit obtained by using our RG improved perturbation theory results. We show here that the best-fit values of $|\epsilon_0|$ increase as one goes further away from $q = q_c$, which is consistent with the expectation that the bare coefficient of the cosine interaction vanishes as q approaches q_c. Also we show that the RG improved perturbation theory provides a much better fit at $q = 0.02$ than at the Heisenberg point $q = 0$, consistent with the fact that our calculation is perturbative in the renormalized coupling $\epsilon(L)$, and is

supposed to be a better approximation when the bare value of $|\epsilon_0|$ is smaller to begin with.

To summarize the first work, we did a field theoretical analysis to understand the origin of multiplicative logarithmic corrections in the critical scaling form, observed numerically on the verge of the Néel to VBS transition of an one dimensional antiferromagnetic model.

1.2 Antiferromagnetic systems with doublet ground states

In the second problem we have investigated ground state properties of the square lattice Heisenberg antiferromagnets(SLHAF) with $S = 1/2$ moments at every site of a finite size cluster. Such kind of finite size systems can be relevant when the antiferromagnetic order breaks into puddles in an SLHAF due to randomly dilution with non magnetic impurities above the percolation threshold.

On the other hand in computational studies, to obtain information about the system in the thermodynamic limit one needs to know how the physical quantities of interest are dependent on the size of the system and the thermodynamic limit extrapolation of the same [26, 27] . For example, consider $S = 1/2$ SLHAF defined on a rectangular region of a two-dimensional lattice, where the sides of the rectangle are L_x (L_y) in the x (y) direction in lattice units and periodic boundary conditions are imposed in both directions. The antiferromagnetic order parameter is defined as the singlet ground state average of square of staggered magnetization. It is is given by:

$$m_0^2 = \frac{1}{N_{\rm tot}} \sum_{\vec{r}\vec{r}'} \eta_{\vec{r}} \eta_{\vec{r}'} \langle \mathbf{S_r} \cdot \mathbf{S_{r'}} \rangle_0, \tag{1.10}$$

with $N_{tot} \equiv L_x L_y$. Here $\eta_{\vec{r}}$ is $+1$ when $\vec{r} \in A$-sublattice, -1 when $\vec{r} \in B$-sublattice on a bipartite graph, $\langle ... \rangle_0$ and subscript 0 denotes expectation values over the singlet ground state. Usually numerical studies [28, 29] of the finite size properties of the system are done by taking a sequence of $L_x \times L_y$ systems, keeping both L_x and L_y even and imposing periodic boundary conditions(PBC) in both directions. From the analytical side, the form of finite size dependence of m^2 and the leading effects on low energy spectrum, are derived with even L_x, L_y and PBC [26]. However, some numerical studies [27] use "cylindrical" samples with PBC in one direction and pinning fields on one pair of edges to keep the spins fixed on the boundaries, focusing on the dependence of ground state properties on the aspect ratio L_y/L_x in various lattices.

The common thing about all those approaches is that they focus on systems with an *even* number of spin-half moments(N_{tot}). According to the Lieb-Mattis theorem the ground state of such a system is a singlet [30] with $S_{\rm tot} = 0$. Certainly there can be another kind of finite size cluster with a very different ground state i.e. SLHAF on an $L \times L$ square lattice with odd L and open boundary condition imposed in both of the directions. According to Lieb-Mattis [30] theorem such a system should have a doublet ground state with total spin $S_{\rm tot} = 1/2$. A measure of antiferromagnetic ordering in such a

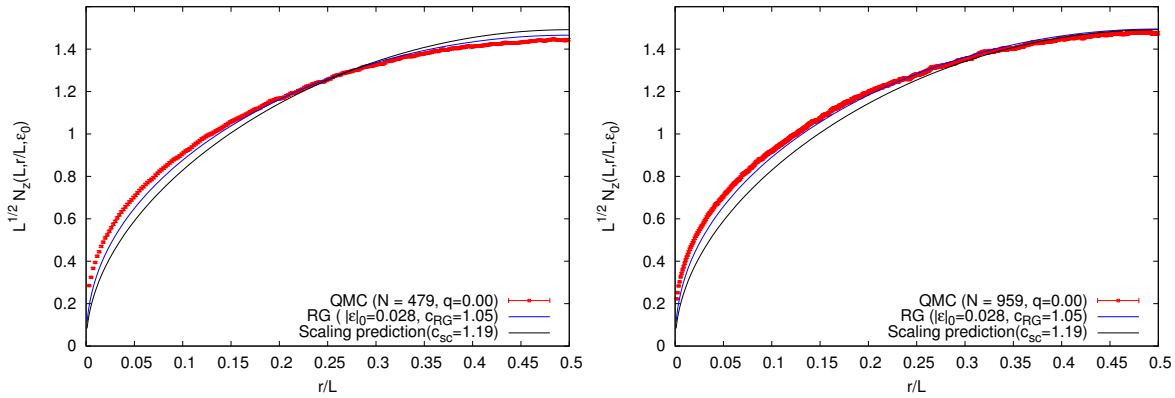

Figure 1.2:

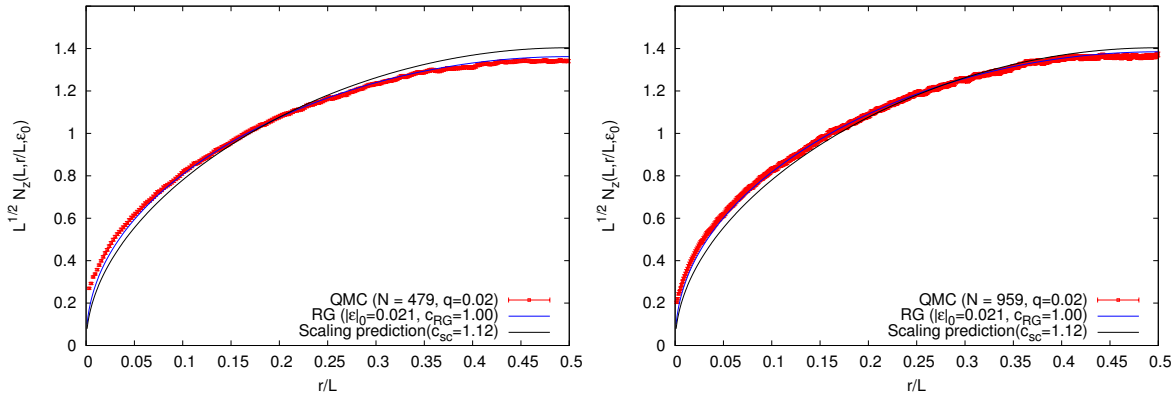

Figure 1.3: $L^{1/2}N_z(r)$ plotted versus r/L in the power-law ordered Néel phase at $q = 0.0$ in the top figures and $q = 0.02$ at the bottom figures, where $L = N + 1$ for chains with $N = 959$(right) and $N = 479$(left) spins and open boundary conditions. Those are compared with the scaling prediction with a common best-fit prefactor c_{sc}. Note that for all the figures the deviation of the data from the scaling prediction cannot be simply ascribed to an overall multiplicative factor that grows with N, since the *shape* of the curves is slightly different. For top two figures data at both sizes is also fit to the best two-parameter fit corresponding to our RG improved perturbation theory result, and the agreement is seen to be quite reasonable, but not perfect, for the best fit values of c_{RG} and $|\epsilon_0|$ listed in the legend. Whereas for the bottom two figures, data at both sizes is also fitted to the best two-parameter fit corresponding to our RG improved perturbation theory result, and the agreement is seen to be excellent for the best fit values of c_{RG} and $|\epsilon_0|$ listed in the legend.

system could be staggered component of this ground state spin texture (defined as $\Phi^z(\vec{r}) \equiv \langle S^z_{\vec{r}} \rangle_\uparrow$),

$$n^z_\uparrow = \frac{1}{N_{\rm tot}} \sum_{\mathbf{r}} \eta_{\mathbf{r}} \langle S^z_{\mathbf{r}} \rangle_\uparrow. \tag{1.11}$$

Where $\langle \dots \rangle_\uparrow$ and subscript $\uparrow$ denotes expectation values calculated in the $S^z_{\rm tot} = +1/2$ sector of the doublet ground state($\eta_{\vec{r}} = +1$ on the A sublattice and -1 on the B sublattice). The quantities $n^z_\uparrow$, calculated in a particular sector of the doublet ground state and m_0, calculated in singlet ground state are different ways of measuring antiferromagnetic order in ground states of different nature.

In this work we focus on the the functional dependence of $n^z_\uparrow$ on m_0, which is a property of the spontaneously broken $SU(2)$ symmetry of the Néel state in the thermodynamic limit. It might be possible to describe the low energy physics of SLHAF in doublet ground state by some effective theory with a local term to capture the open boundary, where the effective field theory parameters[2] can be extracted from the knowledge of the microscopic Hamiltonian. Such an effective field theory description is not available since it is not clear what kind of local terms will capture the effect of open boundaries and how to project out the $S_{tot} = +1/2$ sector of the ground state in the field theory description.

From QMC studies [5] by deforming nearest neighbor interacting Heisenberg antiferromagnet with additional multispin interactions, it turns out that irrespective of the model Hamiltonian $n^z_\uparrow$ can be fitted as an universal polynomial function of m_0 in the antiferromagnetic phase. The function is given by:

$$n^z_\uparrow \approx (\frac{1}{3} - \frac{a}{2} - \frac{b}{4}) m_0 + a m_0^2 + b m_0^3, \tag{1.12}$$

where $a \approx 0.288$ and $b \approx -0.306$. Here we tried to understand this functional dependence $n^z_\uparrow(m_0)$ in the antiferromagnetic phase from three approximate analytical methods: spin wave theory, sublattice mean field theory and rotor model. In next subsection we will describe the details of the analysis and the conclusions.

1.2.1 Details of the approximate analytical calculation

Spin wave analysis: Spin wave theory is a perturbative approach to understand the long wavelength behavior of spin systems. Still it is surprisingly accurate in the description of SLHAF, even in the predictions for finite size systems with periodic [31] and semi-open boundaries [4]. Motivated by this success of spin wave theory in predicting finite size results of SLHAF, we developed a formalism to do linear spin-wave expansion for a SLHAF with open boundary. The method is based on the

[2]The effective, long-distance/time and zero temperature description of 2D Heisenberg model is given by non linear sigma model(NLSM). Such effective low-energy/momentum description of the system is completely determined by two ground state parameters i.e. spinwave velocity c, spin stiffness constant ρ_s. The values of those two parameters have to be determined from the microscopic Hamiltonian. The partition function looks like, $\mathcal{Z} = \int \mathcal{D}\hat{n}(x,\tau)\delta(\hat{n}^2 - 1) exp[-S_B - S_{\hat{n}}]$, where S_B is the Berry phase term and it is not important in the present context. For d-dimensional antiferromagnets $S_{\hat{n}} = \int d\tau d^d x [\frac{\chi_\perp}{2} (\overrightarrow{\bigtriangledown} \hat{n})^2 + \frac{\rho_s}{2} (\partial_\tau \hat{n})^2]$ and $c^2 = \frac{\rho_s}{\chi_\perp}$. One can choose $c = 1$ to set the scale and that leaves only one free parameter ρ_s. Hence all the physical quantities should be a function of ρ_s. Like the antiferromagnetic order parameter m_0^2(equation 2.16) can be calculated from this NLSM description as a function of ρ_s and can be fitted with the experimental/numerical results of m_0^2 to obtain the value of ρ_s for a particular microscopic system.

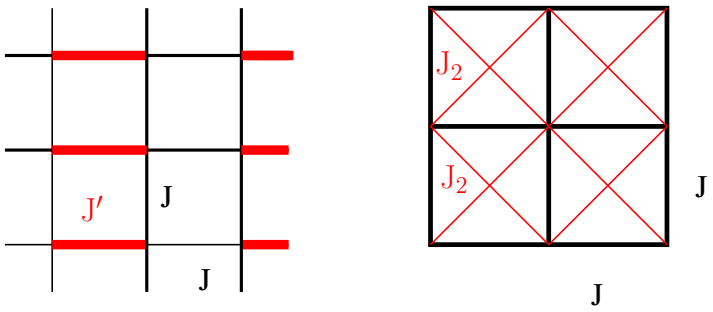

Figure 1.4: An illustration of the interactions present in the JJ' (left panel) and JJ_2 (right panel) model Hamiltonians. In this illustration, black bonds denote exchange interaction strength of J, while a red bond represents exchange strength of J' (J_2) in the left (right) panel

Holstein-Primakoff [32] representation of spin operators by bosons. The Heisenberg spin Hamiltonian is represented by a bosonic Hamiltonian as a result, which is truncated to quadratic order in boson operators by large S expansion to obtain the first quantum corrections to the classical energy of the system(the Néel state being the classical ground state). For periodic systems since there is a translational symmetry in the problem, so one can work in the Fourier space to find the spin-wave modes and calculate the leading order spin wave corrections in $n_{\uparrow}^{z}$ and m_0 for various models in the large- S limit. This calculation is pretty standard and routinely done in literature, but the corresponding analysis of systems with free boundary conditions, with odd numbers of sites is not standard and has been developed in this part of the thesis. From our spin-wave analysis it turns out that the universality discussed in the previous section is well captured by spin-wave theory. As discussed in the previous section, we study two deformations of Heisenberg antiferromagnet which are known as $JJ^{'}$ [33] and JJ_2 [34] models[Figure 5.1] in literature. The spin-wave expansion results in the following relationship between $n_{\uparrow}^{z}$ and m_0 , which is qualitatively same as the available numerical results

$$n_{\uparrow}^{z} = (1 - \alpha - \beta/S)m_0 + (\alpha/S)m_0^2 + \mathcal{O}(S^{-2}), \tag{1.13}$$

with $\alpha \approx 0.013$ and $\beta \approx 1.003$ for spin-S antiferromagnets[Figure 5.8]. Moreover, by studying the Fourier transform[3] of the ground state spin-texture in the momentum space for various deformations of the pure antiferromagnet, we found that spin wave expansion predicts that the spin-texture near the antiferromagnetic wave-vector is an universal(with respect to various deformations of the microscopic Hamiltonian) function of the wavevector[Figure 5.9].

Sublattice mean-field theory: We explore two other ways to explain this universal function for antiferromagnets(Equation 1.13) with a spin-S moment at every site. One of them is a simple mean-field picture in which the system can be described in terms of the dynamics of two giant spins vectors

[3]This Fourier transform is done numerically on the data to see the weight of the various modes in hte momentum space. To be specific we are concerned about the weight of the modes near the antiferromagnetic wavevector. For an odd size antiferromagnet it is convenient to use antiperiodic boundary condition as periodic boundaries induce frustration in this case.

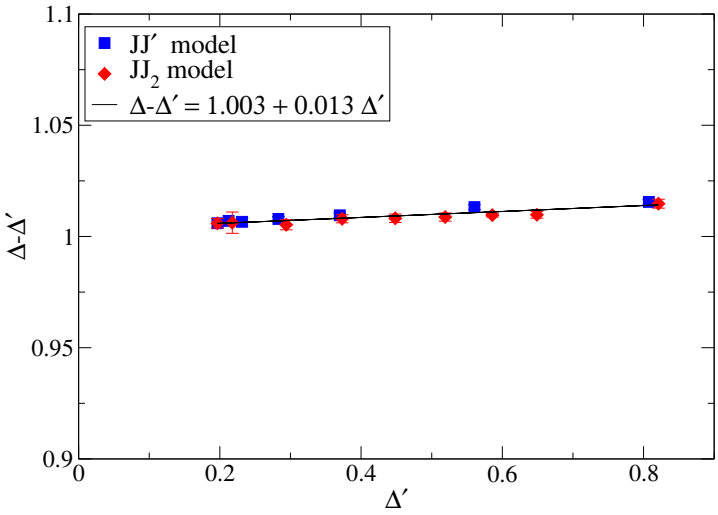

Figure 1.5: Using finite-size extrapolations to the $L \to \infty$ limit, to obtain $\Delta(n^z_\uparrow = S - \Delta)$ for various values of J_2/J and $J^{'}/J$, we compare the result with $\Delta'(m_0 = S - \Delta')$. Specifically, we now ask if the universality seen in the QMC results [5] is reflected in these semiclassical spin-wave corrections to $n^z_\uparrow$ and m_0. The obtained spin-wave corrections apparently satisfy a universal linear relationship $\Delta - \Delta' \approx 1.003 + 0.013\Delta'$ as one deforms away from the pure square lattice antiferromagnet for JJ' and JJ_2 models(Figure 5.1). This implies that $n^z_\uparrow(m_0)$ to leading order in $1/S$ will be $\frac{n^z_\uparrow}{m_0} = 1 - \frac{\Delta - \Delta'}{S} + \mathcal{O}(S^{-2})$. We highlight this point by plotting the figure in way such that it is clear that $\Delta - \Delta'$ is almost 1 with a very small slope of $1/S$ order. Using our numerically established universal result to relate $\Delta - \Delta'$ to Δ', we obtain the universal relationship $n^z_\uparrow = \alpha m_0 + \beta m_0^2$ with $\alpha \approx 0.987 - 1.003/S$ and $\beta \approx 0.013/S$.

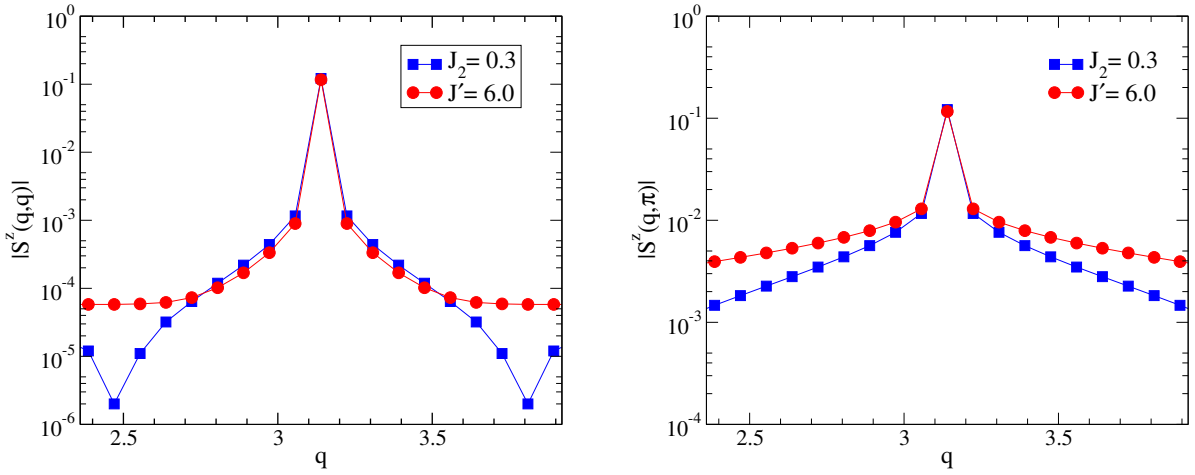

Figure 1.6: Fourier transform (with antiperiodic boundary conditions assumed for convenience) of the spin-wave data for $\Phi^z(\vec{r})$ (assuming $S = 3/2$ and calculated using $L = 75$ for JJ_2 and JJ' model) along cuts passing through the antiferromagnetic wavevector (π, π). Note the nearly universal nature of the results in the neighborhood of the antiferromagnetic wavevector, which in any case accounts for most of the weight of the transformed signal. Note that this are only two cuts of the two dimensional (q_{k_x}, q_{k_y}) plane, if one considers the entire two dimensional plot, near the point (π, π) there will be significant overlap to see the universality.

$\vec{S}_A$ and $\vec{S}_B$, composed of the total spin of the A and B sublattices respectively. When the number of spins in B sublattice(N_B) is one more than that in A sublattice(N_A) (or vice versa), one can take the total spin quantum number of $\vec{S}_A$ as $S_B + S$ and the total spin quantum number of $\vec{S}_B$ as S_B.

The effective Hamiltonian to describe this mean field picture is given by,

$$H_{MF} = J_{MF}\vec{S}_A \cdot \vec{S}_B \tag{1.14}$$

with $\mathbf{S}_A$ and $\mathbf{S}_B$ being coupled antiferromagnetically ($J_{MF} > 0$). We focus on the $|0\rangle_{MF} = S_{\rm tot} = S$, $S^z_{\rm tot} = S$ ground state of this effective Hamiltonian as this corresponds to the $S_{\rm tot} = S$,$S^z = S$ ground state considered in the analysis, which can be obtained by the angular momentum addition of S_B and $S_B + S$. In this effective Hamiltonian picture, $n^z_\uparrow$ is $\langle 0|(S^z_A - S^z_B)/N_{\rm tot}|0\rangle_{MF}$. Similarly, when $N_A = N_B$, one can also calculate $m_0^2 = \langle(\mathbf{S}_A - \mathbf{S}_B)^2\rangle_{J=0}/N^2_{\rm tot}$ within the same sublattice-spin approach, with the ground state being in the singlet sector. This allows to extract the ratio $n^z_\uparrow/m_0$ the thermodynamic limit as

$$n^z_\uparrow = \frac{S}{S+1}m_0. \tag{1.15}$$

This effective mean-field picture is exact for a Hamiltonian of an infinite-range model in which *every* A sublattice-spin interacts with *every* B sublattice-spin via a *constant* (independent of distance) antiferromagnetic exchange coupling J_{MF}. So this simple mean field model will become asymptotically exact in the limit of infinitely long-range unfrustrated couplings in the Heisenberg model. In that limit, we also expect $m_0 \to S$, and thus, our mean field theory predicts that $n^z_\uparrow \to (S/S+1)m_0$ when $m_0 \to S$. This is the constraint that we impose into our fit of $n^z_\uparrow(m_0)$.

Rotor model: Another way to understand the functional form $n^z_\uparrow(m_0)$ is in terms of a quantum rotor picture, where the rotor vector is the Néel vector $\vec{n}$ of an antiferromagnetic system with an odd number of sites. As we know that ground state of the SLHAF with nearest neighbor interactions has Néel order and with that system, one can associate a Néel vector($\vec{n}$) pointing at some definite direction in space. Even though for a finite size system with singlet ground state there is no real preferred orientation for this Néel vector, it was shown by Anderson [35] that the Néel state will be a superposition of practically degenerate states and the Néel vector will slowly precess through those states. That motion of Néel vector can be modeled as a rigid rotor. In the case of an antiferromagnet with an even number of $S = 1/2$ moments, the low-energy effective rotor Hamiltonian of the order parameter(Néel vector) is

$$H_{rotor} = \frac{\vec{L} \cdot \vec{L}}{2\chi N_{\rm tot}}. \tag{1.16}$$

Here $\vec{L}$ is the angular momentum conjugate to the "quantum rotor" coordinate $\hat{n} \equiv \vec{n}/|\vec{n}|$, χ is the uniform susceptibility per spin, and $N_{\rm tot}$ is the total number of spins.

In the case of antiferromagnets with an odd number of sites, the number of spin-S moments on A-sublattice is one more than that on B-sublattice(or vice versa), i.e. $N_A = N_B + 1$. For this system, we postulate a rotor Hamiltonian, following the work of Chandrashekharan on quantum rotor descriptions of insulating antiferromagnets doped with a single mobile charge-carrier [36]. In that description $\vec{L}$ of 1.16 is replaced by the angular momentum operator $\vec{L}'$ conjugate to a quantum rotor coordinate $\hat{n}$, which parametrizes a unit-sphere with a fundamental magnetic monopole at its origin. [37] The low-energy effective Hamiltonian for this case becomes,

$$H^S_{rotor} = \frac{\vec{L}' \cdot \vec{L}'}{2\chi N_{\rm tot}} \tag{1.17}$$

where the superscript reminds us that the lowest allowed angular momentum quantum number l of the modified angular momentum operator $\vec{L}'$ is $l = S$. The angular wavefunction [37] of the $|l = S, m_l = S\rangle$ ground state of this modified rotor Hamiltonian is the *monopole harmonic* $Y_{-S,S,S}(\theta, \phi)$. To calculate $n^z_\uparrow/m_0$ we calculate $\langle n^z_\uparrow\rangle_\uparrow$ i.e. the expectation value of $\hat{n}^z \equiv \cos(\theta)$ in this monopole harmonic wave function on the unit sphere. It leads to

$$\langle n^z_\uparrow\rangle_\uparrow = \frac{S}{S+1} m_0, \tag{1.18}$$

which is exactly the same expression we got from sublattice mean-field theory.

Conclusion: The rotor model is a more general phenomenological approach than the sublattice mean-field theory which doesn't take into account any nonzero wave vector modes or the amplitude fluctuations of the Néel order parameter, also the model makes no assumptions about any long range interactions. It still reproduces the sublattice mean-field theory results which is asymptotically exact in the limit of infinite-range unfrustrated interactions. Thus, a more general phenomenological approach that goes beyond sublattice-spin mean-field theory but ignores all non-zero wavevector modes also

gives

$$n^z_\uparrow = \frac{m_0}{3}, \tag{1.19}$$

for $S = 1/2$. Since both numerical results and spin-wave results show clear deviations from this result, we conclude that such non-zero wavevector modes are essential for a correct calculation of the universal function $n^z_\uparrow(m_0)$.

To summarize this section, we did approximate analytical studies to understand an interesting universal relationship between certain aspects of the ground state spin texture, observed from numerical experiments. In the process we uncovered some interesting features of ground state properties of an antiferromagnetic system in doublet ground state or in general, any multiplet ground state.

1.3 Vacancies in SU(2) invariant Majorana spin liquid

Due to the effect of weak disorder, in the mean field proposal of $SU(2)$ invariant Majorana QSL state [10] the magnetic susceptibility goes to a constant value at $T \to 0$. Understanding the effect of missing sites or strong disorders in such a state can be useful as in experimental conditions often samples have such kind of disorder. In the third problem we focus on the effects of random site dilution in an exactly solvable $SU(2)$ symmetric spin model (Yao-Lee model, equation4.2 [13]), which has a spin liquid(QSL) ground state with gapped or gapless spinfull fermionic excitation in presence of time-reversal symmetry.

In this context the gapless phase of Kitaev's spin model is very interesting because it has a spin liquid ground state with very short range spin correlations but broken rotational symmetry. Kitaev's spin model on a honeycomb lattice was exactly solved by mapping it to a free Majorana fermion hopping problem, Willans et al [38] have shown that such a method also works in presence of randomly located vacancies (dubbed as "random site dilution"). By that token the problem of random site dilution in the spin model maps to a problem of random site dilution in a free Majorana fermion hopping problem on a bipartite (e.g. honeycomb) lattice. And the susceptibility of the spin model maps to the compressibility or density of states of the corresponding free fermion system as

$$\chi(T \to 0) \sim \frac{\rho(T)}{T}. \tag{1.20}$$

Thus computing the density of states of the randomly diluted free fermion problem at very low energy gives the behavior of magnetic susceptibility at $T \to 0$ limit.

The free Majorana fermion hopping problem corresponding to the gapped phase of Kitaev's model with many vacancies was analyzed using perturbative techniques [38] and it was shown that low temperature magnetic susceptibility behaves as $\chi(T) \sim \frac{1}{T(log(\frac{1}{T}))^{1.7}}$. Analyzing the problem in the more interesting gapless phase by same method is difficult as finite size effects becomes more important

and the integrals appearing in Green's function calculation doesn't converge. On the other hand it can be shown [13] that by similar mapping the $SU(2)$ symmetric Yao-Lee model (equation4.2 [13]), can be mapped to very similar free fermion hopping problem as that of Kitaev's (detailed explanation is provided in next subsection) with similar gapped and gapless phases, for the same parametric values of exchange coupling. So in this work, by performing exact calculations of density of states for that randomly diluted free fermion hopping problem at very low energy on large size systems, we tried to understand the low temperature magnetic response of Kitaev's model and Yao-Lee model in presence of many vacancies in the both gapped and gapless phases.

The spin model to free Majorana fermion hopping map connects the disordered spin problem with the earlier studies on particle-hole symmetric localization on bipartite random hopping problem [39] where the spectrum is symmetric about zero energy($E = 0$). From numerical works [39] it is known that in the particle-hole symmetric pure problem introducing random bond disorder generate lots of new states near $E = 0$. In an effort to understand the physical mechanism behind generation of such states, the functional form of density of states in the $E \to 0$ limit is an important quantity to study. It was shown that random bond disorder in particle-hole symmetric hopping problem has universal behavior in the functional form of density of states at low energy depending on whether it is defined on a bipartite or nonbipartite graph and whether the spectrum in absence of disorder is gapped or gapless [39, 40]. From the work of Motrunich et al [39] on bipartite random hopping problem in two dimension at the strong disorder limit, the predictions are following:

In the gapless phase the density of states $\rho(E)$ (E being the energy) will have the Gade [40] functional form

$$\rho(E) \sim \frac{1}{E} e^{-c|lnE|^{\frac{1}{x}}}. \tag{1.21}$$

with x=3/2 and c is a constant whose values depends on the disorder concentration and type of disorder. In the gapped phase the density of states shows the Griffiths [41] form given by

$$\rho(E) \sim E^{-1+d/z}, \tag{1.22}$$

with a variable dynamical exponent z at dimension d ($d = 2$ here).

In contrast from the perturbative calculation of Willans et al [38] on randomly diluted Kitaev's model, the gapped phase density of states follows the Dyson form given by

$$\rho(E) \sim \frac{1}{E[log[1/E]]^{1+x}}, \tag{1.23}$$

with $x \sim 0.7$. In this work on randomly diluted bipartite hopping problem we tried to resolve this conflict and we conclude that Motrunich et al's [39] prediction for the functional form of density of states is correct in asymptotically low energy limit at both gapped and gapless phases.

There is another interesting aspect of this work. Using real space renormalization group analysis Ma-Dasgupta-Hu [42] and Fisher [43] have previously shown that one dimensional Heisenberg spin chain

with randomly distributed exchange coupling have a stable phase at low energy, in which each spin is paired with one other spin that may be very far away (dubbed as "random-singlet" phase). Such random singlet phase has a diverging low temperature susceptibility due to lack of any long range order of the form $\chi(T) \sim \frac{1}{T}h(log(1/T))$ (h is some decreasing function of its argument that makes this density states integrable) . As a first example of such kind of Physics in higher dimension, Bhatt-Lee [44] have shown numerically that three dimensional Heisenberg antiferromagnet doped with non-magnetic impurities doesn't show any magnetic order at very low temperature (lower than exchange coupling energy) due to such random singlet formation. The higher dimensional studies of the system are numerical and it is not clear whether such random-singlet phase observed there is the stable low energy phase of such system. From our exact calculation of density of states (or susceptibility , equation 1.20) we seem to have found that the true low temperature phase of the system is of "random-singlet" like on a randomly diluted two dimensional bipartite lattice.

1.3.1 Analysis of SU(2) symmetric extension model with spin liquid ground state

Construction of a SU(2) symmetric Kitaev model requires a lattice with coordination number three and a tricolourability property for the links of the lattice. The SU(2) invariant spin model [13] we study is defined on a brickwall lattice (topologically equivalent to honeycomb lattice). In that lattice each link can be assigned a type-label x, y or z such that every vertex has exactly one link of each type. So the link Hamiltonian $H_{<jk>_\lambda}$ on a λ-type link $< jk >_\lambda$ ($\lambda = x, y, z$) connecting sites j and k can be defined as,

$$H_{\langle jk\rangle_\lambda} = -J_{\langle jk\rangle_\lambda}(\tau_j^{\lambda_{\langle jk\rangle}}\tau_k^{\lambda_{\langle jk\rangle}})(\sigma_j.\sigma_k). \tag{1.24}$$

The model has two different spin degrees of freedom σ^α ($\alpha = x, y, z$) and τ^α at every site. Which are represented by $SU(2)$ invariant Majorana fermion representation as $\sigma^x = -ic^yc^z$ (and all counterclockwise permutations) and $\tau^x = -ib^yb^z$ (and all counterclockwise permutations). Note that any model with this kind of structure will look like a bilinear in both Majorana operators b and c. Now that we have two independent Pauli matrices as every site and we are writing each one of them by SU(2) symmetric representation of three Majorana fermions, we have double counted the single site Hilbert space. To get back to the original Hilbert space the typical choice [45] is $c^xc^yc^zb^xb^yb^z = i$ (or alternatively $c^xc^yc^zb^xb^yb^z = -i$). So the Hamiltonian in terms of the Majorana fermions becomes

$$H = i\sum_{<jk>_\lambda} J_{<jk>_\lambda}u_{<jk>_\lambda}(\sum_{\alpha=x,y,z} c_j^\alpha c_k^\alpha). \tag{1.25}$$

Where the outer sum is over all three types of links $< jk >_\lambda$ ($\lambda = x, y, z$). Here the products $ib_j^{\lambda_{<jk>}}b_k^{\lambda_{<jk>}}$ on the λ links $< jk >_\lambda$ (with $\lambda = x, y, z$) become static Z_2 gauge fields $u_{<jk>_\lambda}$ and the Hamiltonian becomes a bilinear in c Majorana fermion operators which are coupled to those static Z_2 gauge fields. Note that the SU(2) symmetry of the original spin model is reflected in equation (4.9) as a global $SO(3)$ symmetry between the three copies of Majorana fermions. At this stage the only difference between this model and the original Kitaev's model is that, this model has three different flavors of c-fermions which means we have three copies of Kitaev's original solution with each of

those fermion flavors being coupled with the same gauge field. Due this resemblance with the original Kitaev's model, the properties of this free Majorana fermion hopping problem of our $SU(2)$ symmetric model, is same as that of Kitaev's original model.

Free Majorana fermions on a bipartite lattice: Some additional simplification is possible for the random hopping problem on a bipartite graph, over equation 4.9. Since $t_{\langle jk\rangle_\lambda}(= u_{\langle jk\rangle_\lambda} J_{\langle jk\rangle_\lambda})$ only connects A-sublattice sites to B-sublattice sites, instead of working with the pure imaginary but hermitian matrix defined by the original hopping problem, we can work with a real symmetric matrix. This can be seen by re-writing the Schrodinger equation in the following way,

$$\begin{aligned} \sum_k t_{\langle jk\rangle_\lambda}(i\phi_k^\mu) &= \epsilon_\mu \phi_j^\mu \\ \sum_j t_{\langle jk\rangle_\lambda}\phi_j^\mu &= \epsilon_\mu (i\phi_k^\mu). \end{aligned} \tag{1.26}$$

Here, j is a A-sublattice site and k is a B-sublattice site. We note that it is advantageous to study the matrix H^2 $(= -t^2_{\langle jk\rangle_\lambda})$ instead of H $(= it_{\langle jk\rangle_\lambda})$ the hopping Hamiltonian. For bipartite lattices in H^2 the two sublatitces are decoupled with same absolute values of eigenvalues (differing in sign), that reduces the size of the matrix to be considered to half of the original. Moreover, for very small numbers the H^2 is more numerically stable.

Computation of Density of states: At this stage(equation 1.27) we approach the problem of site dilution in SU(2) symmetric Majorana spin liquid as an eigenvalue problem where finding the density of states is basically counting number of eigenvalues in a certain interval. To count the number of eigenvalues below a certain energy value we use the Sturm method. The method suggest an way to compute the number of eigenvalues above a particular number λ for a real symmetric matrix A, by calculating the number of sign agreements between the successive leading principal minors of the matrix $(A - \lambda I)$. That translates to finding the number of eigenvalues below some particular $-\epsilon$ for the matrix $A = H^2$, which has eigenvalues $-\epsilon_\mu^2$.

Here one of our goals is to get as large size as possible in order to reduce finite size corrections in low energy, so we use some schemes to reduce computational memory cost. We considered semiopen boundary condition such that the free fermion hopping matrix becomes a banded matrix with a narrow band, which has a lower memory cost in various operations compared to the full matrix. In order to ease the process of evaluating the principle minors the matrix $(A - \lambda I)$ is triangularized using standard Gaussian elimination. We make use of a numerically stable algorithm by Martin and Wilkinson [46] for such kind of calculations on banded matrices which is also very memory efficient. By that algorithm, there is no need to store the whole matrix at any stage of the calculation, only a bandwidth square number of elements is needed to be stored.

Since here we are trying to probe very low energy states of the system due to large number of impurities, we tried to make our computation as accurate as possible for extremely small numbers. For that purpose we make use of the GNU Multiple Precision Arithmetic Library [47], which uses efficient

algorithms [48] to stretch the precision for basic arithmetic operations well beyond the machine precision. The only limit in the maximum achievable precision is imposed by the virtual memory of the machine.

Using a combination of the previously mentioned memory efficient algorithms and the high precision libraries, we managed to reliably calculate integrated density of states of the disordered system upto size 51200 sites and $\sim 10^{-150}$ precision. The cost of such high precision memory efficient algorithm is the computation time. Still we managed to obtain significant statistics[4] for our conclusions and we are working on improving that statistics.

1.3.2 Results

Gapped phase: We calculate the density of states in presence of a finite number of vacancies upto very low energy($E_{min} = 10^{-150}$) and large size systems($N = 51200$). We obtain reliable data by carefully implementing Lieb's theorem [49] in all plaquettes of our disordered fermion hopping problem such that the system under study is always in the energy minimizing ground state flux sector[5].

The key point in our observation is that the behavior of integrated density of states(IDOS) goes through a crossover at a very low energy. Before going in to the detail of the crossover we will introduce a few notations and express all the DOS forms in that for convenience. Instead of energy we will use the quantity $\Gamma = log(1/E)$ and instead of DOS we will plot IDOS, $N(\Gamma)$. Now with the new notations, in Figure 1.7 in the left plot plot we have reproduced the result of Willans et al [38] in the energy range considered by them. Our exact calculation shows same result as their perturbative calculation, which is the "Dyson" form $N(\Gamma) \sim \Gamma^{-x}$(look at equation 2.9 for the corresponding $\rho(E)$ expression) with $x \sim 0.8$ (Willan's et al predicted $x \sim 0.7$ [38]).

In figure 1.7 IDOS shows the "Dyson" form upto an energy $E \sim 10^{-20}$. At an energy lower than $E \sim 10^{-40}$, the behavior of IDOS is better described by either Griffiths form $N(\Gamma) \sim e^{-\frac{d}{z}\Gamma}$(look equation 2.7 for the corresponding $\rho(E)$ expression) with a very high value of dynamical exponent ($z \sim 110$) or modified Gade form $N(\Gamma) \sim \Gamma^{1-\frac{1}{x}} e^{-c\Gamma^{\frac{1}{x}}}$ (look equation 2.6 for the corresponding $\rho(E)$ expression) with $x = 3/2$. From the IDOS data set we have it is really hard to distinguish between those two forms, as Griffiths is an exponential and Gade is a stretched exponential.

The results obtained here, can be contrasted with the corresponding results from the studies of strong disorder in bipartite random hopping (BPRH) by Motrunich et al [39], which predicts the Griffiths form, in the gapped phase.

[4] We calculate the integrated density of states by averaging over a large number of disorder realizations with fixed concentration.

[5] Lieb's theorem: For a half-filled band of electrons hopping on a planar, bipartite graph the magnetic flux enclosed by a loop of size $4m$ is π, whereas the magnetic flux enclosing by a loop of size $4m + 2$ is 0(where m is an integer). The theorem can was proved only in presence of certain symmetries. In the disordered fermion hopping problem those symmetries are not present, but Willans et al [38] have shown with the aid of perturbative and numerical calculation that the theorem holds even in the absence of those symmetries.

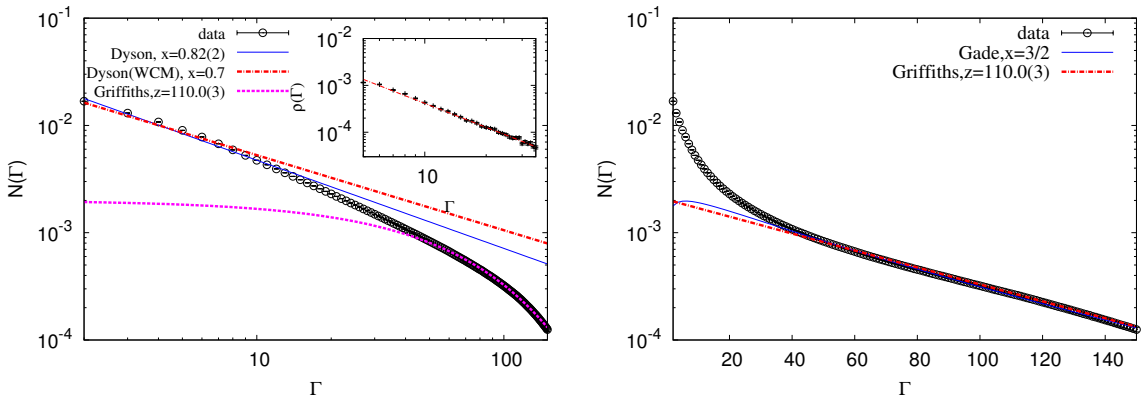

Figure 1.7: Integrated density of states $N(\Gamma)$ plotted against Γ(=$log(1/E)$) for the gapped phase of Kitaev's model on a honeycomb lattice with semiopen boundary condition. The parameter values used here $J_x = J_y = 1, J_z = 4(\alpha = J_z/J_x)$. The results are obtained with 5% impurity concentration, for sample of 51200 sites, averaged over 1000s of disorder realizations. Left panel: the main plot in left panel emphasizes the crossover from Dyson form($N(\Gamma) \sim \Gamma^{-x}$) to some other form behavior of low energy IDOS. Inset of left panel shows a zoomed portion in the higher energy range of the plot, to compare Willans et al [38] result. For comparison the inset plot is made for a sample with 3200 sites and 5% impurity concentration , same as Willans et al [38]. Right panel: this plot shows a fit for the crossover from Dyson form to Griffiths($N(\Gamma) \sim e^{-\frac{d}{z}\Gamma}$) or modified Gade form($N(\Gamma) \sim \Gamma^{1-\frac{1}{x}} e^{-c\Gamma^{\frac{1}{x}}}$, $x = 3/2$) in the behavior of low energy IDOS. From this plot it is hard to decide that for high values of Γ, which of the two forms fits better with the data. The only thins we can say that certainly the IDOS looks straighter than the Dyson form, so indeed there is a crossover in functional form of IDOS. The fits made here are within the range of $\Gamma = 40$ to 140. The z value fluctuates when we change the range. For example for the range of $\Gamma = 25$ to 80, z is 76.

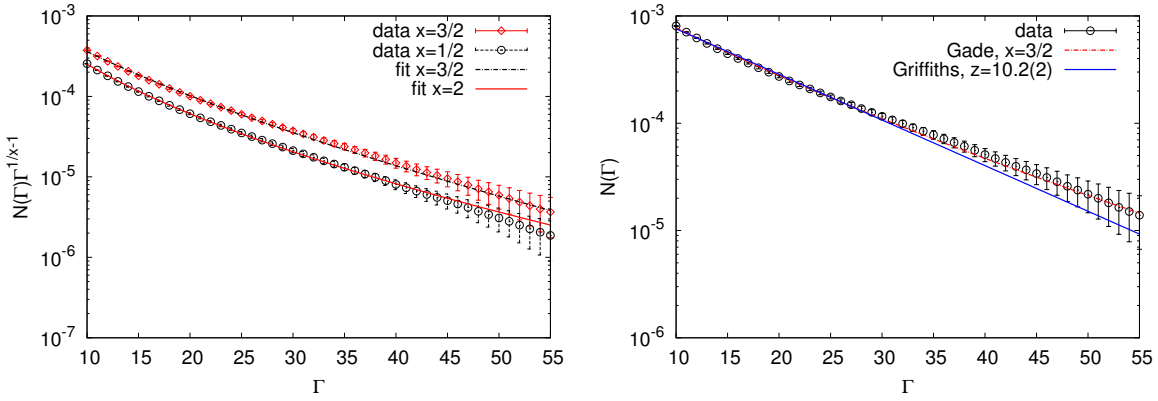

Figure 1.8: Integrated density of states $N(\Gamma)$ plotted against Γ for the gapless phase of Kitaev's model on a honeycomb lattice with semiopen, armchair boundary condition. The parameter values used here $J_x = J_y = J_z = 1(\alpha = J_z/J_x)$. The results are obtained with 5% impurity concentration, averaged over 1000s of disorder realizations. Left panel: for convenience to fit the data in the form $N(\Gamma) \sim \Gamma^{1-\frac{1}{x}} e^{-c\Gamma^{\frac{1}{x}}}$ we plot $N(\Gamma)\Gamma^{-1+\frac{1}{x}}$ to Γ. Here we compare between Gade form($x = 2$) and modified Gade form($x = 3/2$). We conclude that modified Gade form is a better fit to the data. Right panel: here we compare between Gade form and Griffiths form($N(\Gamma) \sim e^{-\frac{d}{z}\Gamma}$). Again we conclude that modified Gade form is a better fit to the data.

Gapless phase: We calculate the density of states in presence of finite number of vacancies upto very low energy($E_{min} = 10^{-55}$) and large size systems($N = 39200$) and contrast our result with the corresponding results of critical delocalized phase in the BPRH universality class [39]. In the delocalized phase the IDOS at low energy follows the "Gade" form $N(\Gamma) \sim \Gamma^{1-\frac{1}{x}} e^{-c\Gamma^{\frac{1}{x}}}$ (look equation 2.6 for the corresponding $\rho(E)$ expression) with $x = 3/2$(Figure 3.9, dubbed as "modified Gade" form to contrast with the original "Gade" [40] form with exponent 2.

Conclusion: From this work our conclusion is following: in the gapless phase even upto very low energy the density of states is of Gade form (equation 2.6), on the other hand in the gapped phase the Dyson form persists upto a certain energy scale (Figure 1.7) then there is a crossover in the form and finally the form changes either to Gade form or Griffiths form. It is hard to distinguish between a power law (equation 2.7) and stretched exponential (equation 2.6) from our current set of data.

So the predictions from Motrunich et al [39], which they provided for random bond disorder also holds in presence of random dilution. In the gapped phase the prediction of Willans et al [38] on the form of density of states turns out to be true (equation 2.9, $x = 1.7$, Figure 1.7)in the higher energy range($E > 10^{-20}$ in $J = 1$ scale) but at the $E \to 0$ limit the density of states takes either modified Gade(equation 2.6) or Griffiths form(equation 2.7, Figure 3.9). It is is hard to resolve between these two forms from our data.

In addition we conclude from the Equations 1.20 and 2.6, 2.7 that susceptibility will behave as

$\chi(T \to 0) \sim \frac{1}{T}h(log(1/T))$($h$ is some decreasing function of its argument that makes this density states integrable), this is the signature of random singlet phase and from these results it seems to be the true low temperature phase of the randomly diluted $SU(2)$ spin model with a Majorana spin liquid ground state, defined on a two dimensional bipartite lattice.

Chapter 2

Introduction

Understanding emergent phenomena in many body systems at different levels of complexity is one of the main goals of physics. Disorder effects in such systems are of special interest not only because they are ubiquitous in nature but also because the effects of disorder can lead to genuinely different behavior compared to that of the pure system. Sometimes studying the changed behavior of a complex system in presence of disorder also improves understanding of the pure system. In this thesis our goal is to understand effects of disorder in some specific examples of low dimensional many electron systems at zero temperature.

A class of phases observed in solid state systems (e.g. metals, band insulators, semiconductors, semi metals, integer quantum hall systems) can be understood from a model of weakly interacting or non interacting many electron system. It turns out in such a non-interacting system of electrons, a metallic phase in the clean system can be driven to an insulating phase in the presence of disorder. This phenomena was discovered by Anderson [50] and is known as Anderson localization. The nature or existence of such an transition depends strongly on the dimensionality of the problem. Later it was discovered that the properties (such as susceptibility, specific heat) of this kind of systems in the metallic and insulating phase varies depending on the nature of the pure system and the kind of disorder introduced. Different behavior corresponds to different "universality classes" which are determined by the overall symmetries of the disordered system; such as time reversal symmetry, particle-hole symmetry and spin rotation symmetry.

Characterizing the metal-insulator insulator transition in these different universality classes of non interacting disordered many electron systems and understanding the physics of such systems is a subject of interest as it corresponds to the behavior of various physical systems like dirty graphene, topological insulators, superconductors etc.

On the other hand there is another class of phases observed in solid state systems (e.g. Mott insulators, magnetic systems, high T_c superconductors, quantum spin liquids, fractional quantum hall systems) where the role of interaction is not negligible, nor small enough to treat perturbatively. It

turns out in an interacting electronic system, a metallic phase can be driven to an insulating phase depending on the strength of interaction compared to the bandwidth. This phenomena was discovered by Mott[51] and is known as Mott localization. The most well studied experimental example where Mott transition is realized is in the family of cuprates.

A very different kind of metal-insulator transition is observed in doped semiconductors, where the response of the system in both metal and insulator side is anomalous compared to the previous cases. This anomaly is believed to be due to the fact that the metal to insulator transition is driven by an interplay between Mott and Anderson localization. The phenomenology of such a system can be captured by a model of disordered Heisenberg quantum antiferromagnet. This model is well understood and analyzed in one dimension where at low temperature the system stabilizes in a very special interesting random singlet phase as shown by Dasgupta and Ma [42]. In higher dimension an exact solution of this model is not known so far; but by approximate RG calculation for certain kind of disorder in three dimension, Bhatt and Lee [44, 52] have predicted occurrence of a similar phase with no long range order. However the higher dimensional theoretical calculations doesn't capture all the experimental features of the transition, and there are unresolved issues like whether random-singlet like phase is the true low energy phase in higher dimension.

In a pure Mott insulator where the interaction is much stronger than the kinetic energy of electronic hopping between atomic orbitals, the system can be modeled in low energy as a spin Hamiltonian with Heisenberg antiferromagnetic interaction. Such antiferromagnetic phases shows an wide range of differently ordered phases due to the interplay of competing nature of interaction caused by the geometry of the system and quantum fluctuation. Often in the experimental realization of such kind of phases, impurities are unavoidable even in the purest possible samples. Response of such impurities can actually serve as a local probe to the system. By NMR and STM experiments one can scan the local response of system near those point defects; for example such measurements performed on the cuprates shows that near a non-magnetic impurity the staggered magnetization enhances locally. Similarly a single spinless impurity in an one dimensional $S = 1$ antiferromagnet induces staggered magnetization locally. The decay of the staggered magnetization from the impurity gives valuable information about the spin correlations in the ground state of the pure system and manifests the presence of a finite spin-gap (Haldane gap).

With this brief overview of the few areas relevant to the following discussion of this thesis, we motivate the need to study disorder in low dimensional many body quantum system.

2.1 Modeling disorder in correlated many body quantum system

The most general yet simple model of many electron system to capture the physics of both Anderson transition and Mott transition is the single band Hubbard model:

$$H = \sum_{\langle ij\rangle,\sigma} t_{ij}(c^{\dagger}_{i,\sigma}c_{j,\sigma} + h.c.) + \frac{U}{2}\sum_{i,\sigma}(n^2_{i,\sigma} - 1) + \sum_i V_i n_i. \tag{2.1}$$

This model is defined on a lattice where every site is occupied by an atom and the atomic orbital of neighboring sites can overlap (the simplest case) to allow conduction of electrons in the outermost shell of each atom. Electrons are allowed to hop from one atomic orbital to another atomic orbital by obeying Pauli exclusion principle such that at the atomic orbital of each atom there can be either no electron or one electron or two electrons of opposite spins at a time.

The single-band assumption is related to the fact that only one band per atomic orbital is considered; it is a good enough approximation to capture most of the phenomenology. The first term of the model is a kinetic term describing hopping of electrons between the atomic orbitals located between sites i and j. In the Hamiltonian written in second quantization language the creation operator $c^{\dagger}_{i,\sigma}$ represent creation of an electron at site i, with σ spin-1/2 eigenstate. The hopping probability amplitude t_{ij} in first quantized notation between sites i and j is given by,

$$t_{ij} = \int d\mathbf{r}\psi_i(\mathbf{r})\left(\frac{\Delta^2}{2m} + U_{ion}\right)\psi_j(\mathbf{r}). \tag{2.2}$$

In this equation $\psi_i(\mathbf{r})$ represents the orbital wavefunction at site i and U_{ion} is the periodic potential created by the lattice; the bandwidth(denoted by D) in the model is dependent on the U_{ion} part of this term. The operator $n_i(=\sum_\sigma n_{i,\sigma})$ represents the fermion number operator at each site. Thus the second term is the term representing two electrons with different spins (by Pauli exclusion principle) occupying same site with effective Coulomb interaction energy U. In first quantization notation it is given by

$$U = \int d\mathbf{r}_1 d\mathbf{r}_2 |\phi_i(\mathbf{r}_1)|^2 \frac{e^2}{|\mathbf{r}_1 - \mathbf{r}_2|}|\phi_i(\mathbf{r}_1)|^2, \tag{2.3}$$

where we are ignoring the long range Coulomb interaction. The third term in the model denotes a random on site potential V_i at site i, which can be physically attributed to the presence of random site impurities.

This simple model turned out to be a very successful model to capture the phenomenology of Mott insulators. It shows different phases depending on the relative values of t_{ij}, U_{ion}, D and U. In one dimension for arbitrary filling this problem is exactly solvable by Bethe ansatz [14]. But in two dimensions, no exact solutions is known so far. We will describe two limiting cases for which we will discuss the theoretical approaches to the problem.

In a many body system the possibilities exist that $U > 0$ (coulomb repulsion between like charged electrons), $U < 0$ (effective attraction can be mediated by electron-phonon interaction as in superconducting phase), $U = 0$ (uncorrelated free electron system, can be metal,band insulator, semiconductor, semi-metal etc. depending on the filling factor). Depending on various values of the ratio U/D one can

expect other various kind of possibilities. Here, we focus on disorder effect in those specific situations, all of which are deep in the Mott insulating regime $t << U$. However, we will see that the low energy properties of one of them (chapter 4) is essentially determined by the physics of free fermions with a certain kind of disorder (chapter 3).

2.2 Disorder in $U << t_{ij}$ limit

First consider the limit $U \to 0$ in which the disordered Hubbard model reduces to

$$H = \sum_{\langle ij \rangle, \sigma} t_{i\sigma, j\sigma'} (c^{\dagger}_{i,\sigma} c_{j,\sigma'} + h.c.) + \sum_{i} V_i n_i. \tag{2.4}$$

In absence of any disorder i.e. $V_i = V$ and $t_{i\sigma,j\sigma'} = t$, this model is the well known single particle tight binding model. For convenience of the rest of the discussion we can write this Hamiltonian in a matrix form as

$$H = \mathbb{C}^{\dagger}_{A} \mathbb{H}_{A,B} \mathbb{C}_{B}. \tag{2.5}$$

The subscripts $A \equiv (i, \sigma), B \equiv (j, \sigma)$. The vectors $\mathbb{C}_A = c_{i,\sigma}$ and $\mathbb{C}_B = c_{j,\sigma}$. And the matrix $\mathbb{H}_{A,B} = t_{i\sigma,j\sigma'} + V_i \delta i\sigma, j\sigma'$. Depending on the constraints imposed on symmetry properties on this first quantized Hamiltonian matrix $\mathbb{H}$, the model captures the behavior of a wide class of physical system. As mentioned in 2.1 in this $U \to 0$ limit one can explain metal, semiconductor and band-insulators etc. The model in Eq. (2.4) is a very general one where the only condition imposed on the Hamiltonian matrix $\mathbb{H}$ is that it has to be hermitian. Apart from that when special symmetry properties are imposed on this general model, it faithfully captures the physics of disordered graphene, topological insulators, quasiparticles in dirty superconductors etc. As a specific example consider Graphene, which is described by an Hamiltonian $\mathbb{H}_{A,B}$ with bipartite structure, particle-hole symmetry, time-reversal symmetry and sublattice symmetry.

2.2.1 Symmetry classification in single particle random Hamiltonians

An important quantity characterizing the randomness in a quantum mechanical Hamiltonian is the density of states. To see why knowing the density of states is important consider the general spectrum from an ensemble of random valued matrices $\mathbb{H}_{A,B}$. In most general case, one can think that the spectrum of this ensemble will consist of closed disjoint intervals (called bands); also there can be open intervals between two such bands (called gaps). Now consider at the energies near the band edges i.e. eigenstates near the boundary of band energies; for the spectrum to have such eigenstates there has to be large regions in the system where all the hopping and on site potential is of same energy (near lower or upper band edge). For a random valued distribution to have all same values near the minima or maxima is of extremely low probability (dubbed as a rare fluctuation event) and can be shown to be exponentially suppressed, this is known as Lifshitz tails [53] of the spectrum. The characterization the spectrum with this kind of rare fluctuations at band edges or band center or divergence at band center can be done conveniently by looking at the density of states, often it is more convenient to get spectral

information uniquely from the integrated density of states given the fact it is a monotonic function with energy of the system.

Considering the physical reasons it is also interesting to understand the behavior of density of states in random Hamiltonians. As in non-interacting electronic system it determines the measurable thermodynamic quantities like specific heat, susceptibility. So while characterizing the properties of disordered systems described by single particle Hamiltonian, the low energy density of states for such systems are often studied. As an example of such systems with different symmetries, consider the BdG equations for spinless and spin-singlet paired superconducting systems; the quasiparticle excitations in the former is described a single particle Hamiltonian which is charge conjugation symmetric whereas for the later case the same is described by a charge conjugation antisymmetric Hamiltonian. Observations for density of states in dirty systems with such different symmetries were put together by Atland and Zirnbauer [54] to show that there only 10 different universal classes of random single particle Hamiltonians (breaks all those symmetries which commute with the Hamiltonian e.g. translational, rotational symmetry) are possible. Those 10-classes are characterized by more-internal discrete symmetries which anticommutes with the Hamiltonian e.g. time-reversal, particle-hole and chirality. Without going into the entire details of that classification we will discuss the universal character of density of states in some of the universality classes of the random single particle Hamiltonians relevant to our work in this thesis.

General single particle system with random-bond disorder The most general class of this 10-fold classification is the famous Anderson localization class, occurring in a general Hamiltonian which doesn't posses any of the time-reversal, particle-hole or chiral symmetry. Thus $\mathbb{H}_{A,B}$ for that Hamiltonian is represented by a hermitian matrix. Conventionally disorder is introduced in this Hamiltonian by drawing the entries of the matrix $\mathbb{H}_{A,B}$ from a random valued distribution, and the disorder strength is increased when the distribution is broader. For such kind of disorder in this Hamiltonian the density of states shows an exponentially suppressed Lifshitz tail at the band edge. Such tails are present in the spectrum irrespective of the fact whether the Hamiltonian is gapped or gapless. This class of Hamiltonians shows very different behavior with randomness in different dimensions.

Particle-hole symmetric single particle system with random bond disorder Now consider the class of random Hamiltonians which is particle-hole symmetric, for such class of Hamiltonians the spectrum is symmetric with respect to zero energy and even in the presence of randomization this special zero energy point is protected which leads to different universal behavior from the previous case. When this Hamiltonian is realized on a bipartite graph in addition to particle-hole symmetry it also possesses chiral symmetry. That kind of Hamiltonians with random bond disorder was analyzed by Motrunich et al. [39] and from their work it in known that the density of states is singular near the special zero energy ($E = 0$) point, thus randomization generates lots of states near $E = 0$. It was observed that random bond disorder in particle-hole symmetric hopping problem has universal

behavior in the functional form of density of states at low energy depending on the Hamiltonian being gapped or gapless [39, 40]. For bipartite random hopping problem (BPRH) in two dimension at the strong disorder limit, the predictions are following:

In the gapless or delocalized phase the density of states $\rho(E)$ (E being the energy) will have the functional form

$$\rho(E) \sim \frac{1}{E} e^{-c|lnE|^{\frac{1}{x}}}. \tag{2.6}$$

Where $x = 3/2$ and c is a constant whose values depends on the disorder concentration and type of disorder. This delocalized phase is knowns as a critical Gade [40] phase as such a behavior of density of states was predicted by Gade by analyzing 2-dimensional Dirac equation with random mass and random vector potential. The mechanism of generating a large number of low energy states near $E = 0$ with such stretched exponential kind of divergences in density of states can be modeled as the states occurring near the extrema of a 2D random Gaussian surface. But as is evident here, these states are not like the rare fluctuations described before; instead they are the usual fluctuations in a 2D random Gaussian surface with the property that disorder strength (width of the random distribution) renormalizes with the length scale of the problem.

In the gapped or localized phase the density of states shows the form,

$$\rho(E) \sim E^{-1+d/z}, \tag{2.7}$$

with a variable dynamical exponent z at dimension d ($d = 2$ here). This form is known as Griffiths [41] form as it is same as that obtained from the Griffith's effect in disordered quantum system. The gapless or delocalized phase discussed above can be derived to the gapped or localized phase by making some special bonds that produce a complete dimer cover of the lattice, stronger than the rest. To visualize this consider hopping problem on a bipartite honeycomb lattice and to get the gapped phase in this lattice one can make the bonds along the y direction of the honeycomb lattice stronger than others, so those are the special bonds in this case. The power-law contributions to the low-energy DOS in such bipartite gapped phases comes from the low-energy states associated with the end-points of the quasi one dimensional strings along which the background dimer pattern is broken. When such a situation occurs often, the density of states shows the Griffiths form.

However the characterization of this this delocalization-localization (or can be said metal-insulator) transition in two dimension is not completely well understood in the literature. It is believed that the "Gade" phase is a signature of criticality in this phase transition. In contrast in one dimension and quasi-one dimension there is a simple picture where the system goes from one localized phase to another via a critical point with divergent z. In the critical point the low energy density of states takes the so called "Dyson" form given by

$$\rho(E) \sim \frac{1}{E[log[1/E]]^{1+x}}, \tag{2.8}$$

with $x \sim 2$. This form is known as Dyson form as such a form for a disordered linear chain was predicted by Dyson [55] many years ago.

Particle-hole symmetric single particle system with random dilution In the studies of system certainly another different kind of random disorder can be considered i.e. instead of taking the elements of the matrix $\mathbb{H}_{A,B} = t_{i\sigma,j\sigma'} + V_i\delta i\sigma, j\sigma'$ from a random valued distribution one can simply delete bond hopping parameters at random locations; which is physically equivalent to knocking of atoms from random locations in the lattice. In other words here this is equivalent to putting zero's in randomly selected entries of the matrix $\mathbb{H}$, while maintaining the particle-hole symmetry and bipartite structure (or chiral symmetry) of the Hamiltonian. The discussions in the previous case of random disorder doesn't obviously apply here to intuitively guess the behavior of density of states near zero energy of random dilution problem, as random dilution is a much more abrupt way of introducing disorder which changes the spatial structure and symmetries of the lattice. What happens to the density of states near $E = 0$ for this class of Hamiltonian(One can name this class as bipartite random dilution class or BPRD class) in 2D is the main question we tried to answer in the chapter 3 of this thesis. Other relevant open issues related to this questions can be, characterizing the nature of localization to delocalization phase transition in presence of random site dilution and providing a physical picture to the density of states behavior near the band center in both of the phases. In this thesis we provide a complete characterization of the functional form of density of states near the band center at both localized and delocalized phases. We also tried to give a partial understanding to the origin of such states. In addition we tried to understand the nature of the transition mentioned before.

The behavior of density of states near zero energy for this kind of disorder in the gapped phase of free-fermion hopping problem on a honeycomb lattice was analyzed previously by Willans et al. They have shown that density of states in that case follows the Dyson form,

$$\rho(E) \sim \frac{1}{E[log[1/E]]^{1+x}}, \tag{2.9}$$

with $x \sim 0.7$. Over a limited dynamical range in energy, this result is different from that of the gapped case behavior in the previously discussed random-disorder problem. This poses a puzzle since on general universality grounds one might expect Griffith's behavior. This puzzle is resolved in chapter 3 where we show that Eq. 2.9 represents a crossover and the true low energy DOS is indeed of Griffith's form in the gapped phase. In addition we also study the delocalization phase and compare our results as the Gade form of DOS. However from our work we conclude that for random site dilution in free fermion hopping problem on honeycomb lattice, Motrunich et al's [39] prediction for the functional form of density of states holds true in asymptotically low energy limit at both gapped (Eq. 2.7) and gapless phases (Eq. 2.6). We leave further discussion on the details of this work and our understanding of the issues discussed above for chapter 3 of the thesis.

2.3 Disorder in $U >> t_{ij}$ limit

In the $U \to \infty$ limit the energy cost for a electron hopping from one atomic orbital to another atomic orbital is very high, thus there is no charge transport across the system; this describes a Mott insulating

state. However virtual hopping of electrons are still possible due to quantum fluctuations, for which the spin sector of this system is very much alive and thus in low energy limit the Mott insulating phase is described by a Heisenberg spin Hamiltonian. The standard way to derive the effective low energy Hamiltonian is by starting in the atomic limit with a finite U and $t = 0$, and then perturb that atomic ground state by turning on a small hopping t. For simplicity consider two sites, for which in the atomic limit the ground state has four possibilities as one singlet ($\frac{1}{\sqrt{2}}(|\uparrow,\downarrow\rangle - |\downarrow,\uparrow\rangle)$ and three triplets ($|\uparrow,\uparrow\rangle, |\downarrow,\downarrow\rangle, \frac{1}{\sqrt{2}}(|\uparrow,\downarrow\rangle + |\downarrow,\uparrow\rangle)$. Now turning on a small hopping t causes virtual hopping between a singlet and another exited singlet state as follows,

$$\frac{1}{\sqrt{2}}(|\uparrow,\downarrow\rangle - |\downarrow,\uparrow\rangle) \rightleftarrows \frac{1}{\sqrt{2}}(|\uparrow\downarrow,0\rangle - |0,\downarrow\uparrow\rangle)\,. \tag{2.10}$$

This is the only allowed virtual process with an energy cost $J = \frac{4t^2}{U}$, any other process involving the triplet ground states are not allowed by Pauli exclusion principle. This low energy process can be captured by a Heisenberg interaction term as $(\mathbf{S}_1.\mathbf{S}_2)$ between the two spin states with exchange interaction J. For N sites similarly the ground state has 2^N degenerate spin states and when the full degenerate perturbation theory is performed with the perturbation parameter $\frac{t}{U}$, the low energy effective Hamiltonian of the system with half filling turns out to be

$$H = J\sum_{\langle ij\rangle}\left(\mathbf{S}_i\mathbf{S}_j - \frac{1}{4}\right). \tag{2.11}$$

Away from half filling this Hamiltonian contains a hopping term of the excess electrons or holes, with the creation/annihilation operators of the relevant Hilbert space. In this thesis we will focus on understanding effect of impurity doping on the spin Hamiltonian, which will be referred as the spin sector of Mott insulator.

2.3.1 Impurity doping in Quantum Spin liquid

Quantum Spin liquids (QSL) are known as very interesting low energy states of strongly correlated matter, where at temperatures lower than the scale of exchange coupling, there is no conventional magnetic order due to interplay between quantum fluctuation and geometric frustration. Several experimental [6, 7, 8, 9] proposals exist where such a state can be realized. In the chapter 4 of this thesis we will analyze an exactly solvable $SU(2)$ invariant spin model(known as Yao-Lee model) which has a ground state realizing an $SU(2)$ invariant spin liquid with spinful Majorana fermion excitation. Such kind of spin liquid states were previously discussed at mean field level by Biswas et al [10] to model the phenomenology of $EtMe_3Sb[Pd(dmit)_2]_2$ [11, 12]. Due to the effect of weak disorder, in that mean field proposal of $SU(2)$ invariant Majorana QSL state [10] the magnetic susceptibility goes to a constant value at $T \to 0$. Understanding the effect of missing sites or strong disorders in such a state can be useful as in experimental conditions often samples have such kind of disorder. In the chapter 4 of this thesis we will focus on studying such kind of disorders in the exact spin liquid ground state of the Yao-Lee model, and this gives one motivation behind that study; the other motivation is described in 2.3.2.

2.3.2 Impurity doping driven metal-insulator transition in a Mott insulator

A very interesting phenomena to understand in the correlated system is the interplay between Mott and Anderson localization. Real systems where this kind of physics is realized is the doped semiconductors like Phosphorus or Boron doped silicon (Si:P and Si:B, [56]). Experiments on such doped semiconductors shows very unique behavior due to the competition between disorder and interaction. For example in the zero temperature limit the magnetic susceptibility behaves like a power law as

$$\chi(T \to 0) \sim \frac{1}{T^{\alpha}}, \tag{2.12}$$

with $0 < \alpha < 1$ in both metal and insulator phases. Also the behavior of magnetic susceptibility is smooth across the metal insulator transition which was believed to be a second order transition. This phenomenon suggested that the anomalous behavior in the magnetic properties might be due to the spin sector of Mott insulators. The specific heat measurements also manifests similar anomalous behavior and similar singularities as that of the magnetic susceptibility, indicating a divergence in the number of states at low energy.

The power law divergence observed in both magnetic susceptibility and specific heat measurements can be understood from a model of disordered quantum antiferromagnet with the Hamiltonian

$$H = \sum_{\langle ij \rangle} J_{ij} \mathbf{S}_i . \mathbf{S}_j, \tag{2.13}$$

with all $J_{ij} > 0$. Using real space renormalization group analysis Ma-Dasgupta-Hu [42] and Fisher [43] have previously shown that in one dimension this model has a stable phase at low energy, in which each spin is paired with one other spin that may be very far away (dubbed as "random-singlet" phase). Such a phase was observed for J_{ij} being drawn from a Gaussian distribution and in the strong disorder limit. This random singlet phase has a diverging low temperature susceptibility due to the presence of a large density of the form

$$\chi(T) \sim \frac{1}{T} h(log(1/T)). \tag{2.14}$$

Where h is some decreasing function of its argument that makes this density of states integrable. This prediction was confirmed by experiments on one dimensional random bond spin chains [57].

However such exact RG calculation turned out to be difficult in higher dimension; for such systems Bhatt-Lee [44] have developed an approximate numerical RG technique and studied this model by assuming J_{ij} as an exponential function of the distance between the two positions of donor atoms. In two-dimension it was shown that susceptibility is of the form $\chi(T) \sim 1/T^{\alpha}$ (with $\alpha < 1$ depending on the doping concentration). In three-dimension it was shown that the insulating phase has no long range magnetic ordering and the susceptibility diverges with a weaker form than in two-dimension. On the other hand the metallic phase of Si:P cannot be explained by Bhatt-Lee scenario with such itinerant electrons and local spin moments. In that side the specific heat coefficient is much stronger suggesting a stronger divergence in the number of degrees of freedoms at low temperature.

In this thesis we study random site dilution in the SU(2) invariant Yao-Lee spin model [13](Eq. 4.2), defined on a brickwall lattice (topologically equivalent to honeycomb lattice). This model has a quantum spin liquid(QSL) ground state with gapped or gapless spinfull fermionic excitation in presence of time-reversal symmetry, as mentioned in the 2.3.1.

The model is exactly solvable by mapping it into a free lattice gas of Majorana fermions on a brickwall lattice in the background of a static Z_2 gauge field. The random dilution in the spin model can be shown to be random site dilution of the fermion hopping problem, and the magnetic susceptibility of the spin model gets mapped to the compressibility of the free-fermion hopping problem. In chapter 4 of this thesis we will discuss the details of this mapping and show that because of this connection the results obtained in the BPRH problem discussed before can be directly used to calculate the behavior of the magnetic susceptibility in both gapped and gapless phase of the spin model. This connection allows one to know the true low behavior of the spin model by exact solution. Our main result by this exact solution analysis is following: we found that the magnetic susceptibility behavior in both gapped and gapless phases of Yao-Lee spin model is same as the random-singlet form (Eq. (2.14)). Thus it seems that the true low temperature phase of the randomly diluted $SU(2)$ spin model with a Majorana spin liquid ground state, defined on a two dimensional bipartite lattice has a phase with random singlet like susceptibility in both the metallic and insulator side. However since we do not know the exact transition point of this metal insulator transition we cannot make a clear statement whether this random singlet behavior persists deep in the metallic phase. In chapter 4 of this thesis we will provide our detailed analysis and conclusions about this problem.

2.3.3 Non-magnetic impurity doped 2D Heisenberg antiferromagnet

One of the most well studied Mott insulating compound is La_2CuO_4 which realizes a two-dimensional (2D) quantum (spin-1/2) antiferromagnet. Apart from disorder effects mentioned in the previous sections, non-magnetic impurity doping in such compounds shows another class of phenomena. By controlled doping [2] with randomly distributed non magnetic impurities(Zn or Mg) on the copper-oxygen planes of La_2CuO_4, this system goes through a percolation transition which was studied via neutron scattering and NMR tools. Those studied shows the system $La_2Cu_{1-z}(Zn,Mg)_zO_4$, is well described by the Hamiltonian

$$H = J\sum_{ij} p_i p_j \mathbf{S}_i \mathbf{S}_j. \tag{2.15}$$

Where the sum is over nearest-neighbor (NN) sites, J is the antiferromagnetic Cu-O-Cu superexchange, S is the $S = 1/2$ operator at site i, $p_i = 1$ on magnetic sites, and $p_i = 0$ on nonmagnetic sites. The long range antiferromagnetic order survives even at the percolation threshold of doping atoms at which point the largest connected cluster of copper atoms could be considered as weakly connected. With a little doping at the percolation threshold (known to be $p^* \sim 0.40725$), the long range order disappears as that macroscopically large connected cluster can break into small isolated finite size clusters as in Figure 2.1. In those finite size clusters the system can be in both singlet or doublet ground state, and so it is important to understand the ground state properties of such system.

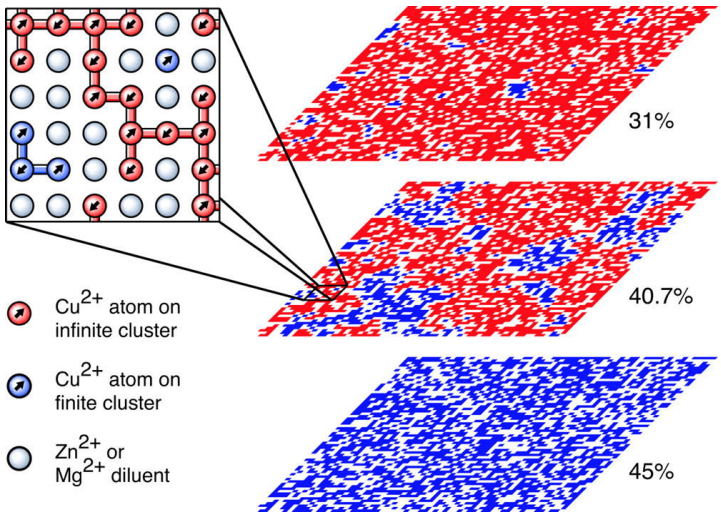

Figure 2.1: Schematic of finite-sized sections of the infinite square lattice with random site dilution levels well below ($p^* \sim 0.31$), just below ($p^* \sim 0.407$), and above ($p^* \sim 0.45$) the percolation threshold $p^* \sim 0.40725$. The inset is a close-up view for $p^* \sim 0.407$, showing the role that magnetic Cu and nonmagnetic Zn/Mg ions play in the experimental system. Figure taken from [2].

Studying finite size systems is also interesting from the computational point of view, as computational studies are inescapably limited to finite size systems. To obtain information about the system in the thermodynamic limit one needs to know how the physical quantities of interest are dependent on the size of the system and the thermodynamic limit extrapolation of the same[26, 27] . For example, consider $S = 1/2$ SLHAF defined on a rectangular region of a two-dimensional lattice, where the sides of the rectangle are L_x (L_y) in the x (y) direction in lattice units and periodic boundary conditions are imposed in both directions. The antiferromagnetic order parameter is defined as the singlet ground state average of square of staggered magnetization. It is is given by:

$$m_0^2 = \frac{1}{N_{\rm tot}} \sum_{\vec{r}\vec{r}'} \eta_{\vec{r}} \eta_{\vec{r}'} \langle \mathbf{S}_{\mathbf{r}} \cdot \mathbf{S}_{\mathbf{r}'} \rangle_0, \tag{2.16}$$

here $N_{tot} \equiv L_x L_y$. Here $\eta_{\vec{r}}$ is $+1$ when $\vec{r} \in A$-sublattice, -1 when $\vec{r} \in B$-sublattice on a bipartite graph and $\langle\rangle_0$ and subscript 0 denotes expectation values over the singlet ground state. Usually numerical studies[28, 29] of the finite size properties of the system are done by taking a sequence of $L_x \times L_y$ systems, keeping both L_x and L_y even and imposing periodic boundary conditions(PBC) in both directions. From the analytical side, the form of finite size dependence of m^2 and the leading effects on low energy spectrum, are derived with even L_x, L_y and PBC[26]. Some numerical studies [27] use "cylindrical" samples with PBC in one direction and pinning fields on one pair of edges to keep the spins fixed on the boundaries, focusing on the dependence of ground state properties on the aspect ratio L_y/L_x in various lattices.

The common thing about all those approaches is that they focus on systems with an *even* number of spin-half moments(N_{tot}). According to the Lieb-Mattis theorem the ground state of such a system

is a singlet [30] with $S_{\rm tot} = 0$. Certainly there can be another kind of finite size cluster with a very different ground state i.e. SLHAF on an $L \times L$ square lattice with odd L and open boundary condition imposed in both of the directions. According to Lieb-Mattis[30] theorem such a system should have a doublet ground state with total spin $S_{\rm tot} = 1/2$. A measure of antiferromagnetic ordering in such a system could be staggered component of this ground state spin texture (defined as $\Phi^z(\vec{r}) \equiv \langle S^z_{\vec{r}} \rangle_\uparrow$),

$$n^z_\uparrow = \frac{1}{N_{\rm tot}} \sum_{\mathbf{r}} \eta_{\mathbf{r}} \langle S^z_{\mathbf{r}} \rangle_\uparrow. \tag{2.17}$$

Where $\langle \dots \rangle_\uparrow$ and subscript $\uparrow$ denotes expectation values calculated in the $S^z_{\rm tot} = +1/2$ sector of the doublet ground state($\eta_{\vec{r}} = +1$ on the A sublattice and -1 on the B sublattice). The quantities $n^z_\uparrow$, calculated in a particular sector of the doublet ground state and m_0,calculated in singlet ground state are different ways of measuring antiferromagnetic order in ground states of different nature. The functional dependence of $n^z_\uparrow$ on m_0 is a property of the spontaneously broken $SU(2)$ symmetry of the Néel state in the thermodynamic limit. It might be possible to describe the low energy physics of SLHAF in doublet ground state by some effective theory with a local term to capture the open boundary, where the effective field theory parameters[1] can be extracted from the knowledge of the microscopic Hamiltonian. Such an effective field theory description is not available since it is not clear what kind of local terms will capture the effect of open boundaries and how to project out the $S_{tot} = +1/2$ sector of the ground state in the field theory description.

The facts known about the functional dependence of $n^z_\uparrow$ and m_0 from numerical experiments is that, there exists universal relationship between $n^z_\uparrow$ and m_0 in the thermodynamic limit [17]. By universality we mean that the relation is a low energy property of the antiferromagnetic phase and doesn't depend on the microscopic details of the Hamiltonian. We confirm this by studying several deformations of Heisenberg antiferromagnet on a square lattice and by noting that for all the deformations, the functional dependence of $n^z_\uparrow$ on m_0 remains the same in the antiferromagnetic phase. An approximate analytical understanding of the relationship between $n^z_\uparrow$ and m_0 will be the topic of detailed discussion in chapter 5.

2.3.4 Single non-magnetic impurity in one dimensional antiferromagnet

As mentioned before the in one dimension the spin sector of Mott insulating Hubbard model is the playground of many analytical and numerical methods. Additionally one dimensional Heisenberg

[1] The effective, long-distance/time and zero temperature description of 2D Heisenberg model is given by non linear sigma model(NLSM). Such effective low-energy/momentum description of the system is completely determined by two ground state parameters i.e. spinwave velocity c, spin stiffness constant ρ_s. The values of those two parameters have to be determined from the microscopic Hamiltonian. The partition function looks like, $\mathcal{Z} = \int \mathcal{D}\hat{n}(x,\tau)\delta(\hat{n}^2 - 1) exp[-S_B - S_{\hat{n}}]$, where S_B is the Berry phase term and it is not important in the present context. For d-dimensional antiferromagnets $S_{\hat{n}} = \int d\tau d^d x [\frac{\chi_\perp}{2} (\overrightarrow{\bigtriangledown} \hat{n})^2 + \frac{\rho_s}{2} (\partial_\tau \hat{n})^2]$ and $c^2 = \frac{\rho_s}{\chi_\perp}$. One can choose $c = 1$ to set the scale and that leaves only one free parameter ρ_s. Hence all the physical quantities should be a function of ρ_s. Like the antiferromagnetic order parameter m_0^2(Eq. 2.16) can be calculated from this NLSM description as a function of ρ_s and can be fitted with the experimental/numerical results of m_0^2 to obtain the value of ρ_s for a particular microscopic system.

antiferromangeic chain (1DHAFC) is successful in describing the static and dynamic properties of several Mott insulating magnetic materials[58, 59, 60]. Studying the effect of non-magnetic impurity in 1DHAFC is very interesting as such a defect can be doped controllably in an experiment to modify magnetic properties of the ground state and excited states of such systems.

From the experimental side spin chains can be realized in chemical compounds which have a highly anisotropic coupling between magnetic ions due to their inherent lattice structure, such that the coupling is significantly stronger in one direction. Such examples of effective 1D spin $1/2$ chains are the compounds Sr_2CuO_3[58], $KCuF_3$ [59]. Typically a non-magnetic impurity impurity is doped in such samples by doping Pd in the Cu sites. As it is easy to see that presence of such non-magnetic impurities (at any amount, like even a single impurity) in one dimensional spin chain breaks the system into disconnected finite size segments and introduces extra booundaries or edges in the system. The magnetic response of such system constitutes a finite size "bulk" effect due to the finite sizer segments and a boundary effect leading to an alternating local magnetization near the edges. These effects can be calculated theoretically as well as observed in experiments, giving an understanding of the spin texture modification due to impurities.

Even though for $S - 1/2$ 1DHAFC, the thermodynamic properties can be exactly calculated in the ground state using Bethe Ansatz[14], such calculations are often too complicated to be useful in calculating correlation functions[15]. An alternative route to study this kind of problems is the bosonization approach, which is asymptotically exact in the limit of low energies and long wavelengths. With this tool it is possible to fully determine the system's zero temperature critical behavior. Using bosonization techniques $S = 1/2$ 1DHAFC can be mapped to a $1 + 1$ dimensional bosonic field theory with a 'sine-Gordon' action, which has a scale invariant free-field part perturbed by a non-linear cosine interaction[16]. The renormalization group (RG) analysis of the cosine interaction turns out to be an example of the treatment of 'marginally irrelevant' interactions in the neighborhood of a well-characterized scale free RG fixed point. It was shown by Eggert, Affleck and Takahashi[61] that the corrections due to the leading marginally irrelevant operator of the RG, leads to an logarithmically divergence in the finite temperature susceptibility as the system approaches the zero temperature. The results of this calculation was used to fit the susceptibility data and extract the effective exchange coupling constant J for Sr_2CuO_3 [58].

In chapter 6 of the thesis, we focus on marginally irrelevant interactions that can give rise to violations of scaling predictions at critical points due to the presence of logarithmic corrections that multiply the scaling predictions. The physics of the multiplicative correction for a marginal operator is quite general and applicable in other models like the textbook example of ϕ^4 theory. The importance of studying the same physics in the context of $S-1/2$ chain is that we can access the system by a number of numerical and exact methods. So it represents an ideal testing ground for this important result.

Another interesting example of similar multiplicative logarithmic violations of scaling have been

argued to exist[62, 17] at the critical point of a continuous quantum phase transition[18, 3] between the usual Néel ordered antiferromagnetic ground state and a spontaneously dimerized non-magnetic state with valence-bond order in a two dimensional $S = 1/2$ SLHAF. The underlying field theory[18] proposed for this transition predicts a second order critical point between Néel and VBS phases. Some of the numerical works to verify these field theory predictions support[3, 19] the generic continuous nature of this Néel-VBS transition. However, some numerical studies[19, 62, 20] find a deviation from this prediction about continuous nature. Numerical experiments[62, 20] focusing on bulk correlation functions in microscopic models, where Néel to VBS order transition is driven by the competition between multi-spin interaction and two spin exchange interaction, found a multiplicative logarithmic correction to the scaling prediction. In another work[17] which focuses on the impurity spin texture induced by a missing-spin defect on similar microscopic models, also reach to the same conclusion. The interpretation of this violation of scaling predictions as logarithmic corrections is not yet resolved as some other studies[21, 22] interpret the violation as a weak first order phase transition. From the current set of numerical experiments it is hard to resolve which one of the above scenarios is true.

However in chapter 6 of the thesis, our main goal is to understand the origin of similar multiplicative logarithmic corrections by studying the Néel ordered phase of an analytically and numerically tractable model in 1D. As a probe of the critical properties we use the missing site "impurity" induced spin texture in vicinity of the defect. On the analytical side, we work within the bosonization framework and use renormalization group (RG) improved perturbation theory to obtain predictions for the alternating part of the spin texture in this example. These predictions are compared with Quantum Monte-Carlo (QMC) data[1] for a one-dimensional chain with nearest neighbor Heisenberg exchange J and six-spin coupling $Q = 4qJ$; for $q < q_c$(in the Néel phase). We found a good agreement between the numerical data and our analytical results where we note that the strength of the log corrections is larger for q further away from the critical point, and vanishes for $q = q_c$, consistent with the bosonized field theory results.

Chapter 3

Random site dilution in particle-hole symmetric non-interacting fermionic system

In this chapter, we will discuss the details of our work on random dilution in bipartite fermion hopping Hamiltonian. In the introduction we have outlined our goal of this work as characterizing the behavior of density of states near zero energy for a randomly diluted fermion hopping problem defined on a bipartite graph with particle-hole symmetry. With this motivation in mind we will outline the plan of this chapter as follows: in section 3.1 we describe the model Hamiltonian and our scheme of introducing random dilution. Followed by that in section 3.2 we will describe the symmetries of the problem. In section 3.3 we will discuss a folk theorem known about the ground state of the BPRH Hamiltonian with site dilution and we will also discuss our scheme to implement those theorems in our search of the ground state. In section 3.4 we will discuss the results and in section 3.5 we discuss few possible direction of future research.

3.1 Models

The bipartite random hopping/dilution model is nothing but the simple tight binding model defined on a bipartite graph, with only nearest neighbor hopping. The Hamiltonian is given by ,

$$H = \sum_{\langle ij \rangle} \mathbb{M}_{ij} \mathbb{C}_i^\dagger \mathbb{C}_j \equiv \begin{pmatrix} c_{iA}^\dagger c_{iB}^\dagger \end{pmatrix} \begin{pmatrix} 0 & t_{ij} \\ -t_{ij}^\dagger & 0 \end{pmatrix} \begin{pmatrix} c_{jA} \\ c_{jB} \end{pmatrix} \tag{3.1}$$

where t_{ij} can take any non zero value but only if $i \in A$-sublattice and $j \in B$-sublattice, otherwise it is zero. Also the condition $\mathbb{M} = \mathbb{M}^\dagger$ has to be satisfied as because of Hermiticity . The model is defined on a two-dimensional brickwall graph (Fig. 3.2), which is topologically same as the familiar honeycomb lattice. We consider the simplest case i.e. t_{ij} is non zero only when i and j are indices of nearest neighbor sites; otherwise t_{ij} is uniform i.e. $t_{ij} = t$, we set the energy scale by putting $t_{ij} = 1$.

This simple model has a gapped and gapless phase. From Fig. 3.2 one can see that every lattice point has three bonds along which we can name the hopping parameter as t_x, t_y, t_z; we choose the t_z in the horizontal direction and t_x, t_y in the vertical up and down direction respectively. When t_x=t_y=t_z=t the model is gapless and when $t_z > t_x + t_y$ (and all permutations) it is gapped. We go from gapless to gapped phase by tuning a parameter as $\alpha = t_z/t_x$ while keeping $t_x = t_y$. By the above condition $\alpha = 1$ is the isotropic gapless point and as α is increased beyond 2 the model goes from gapless to gapped phase.

The random disorder in this model for BPRH (bipartite random hopping) class is introduced by drawing the values of t_{ij} from some random valued distribution. Here we are interested in BPRD (bipartite random dilution) class, for which we keep the all t_{ij} values fixed and randomly select a nearest neighbor pair $\langle ij \rangle$ to put $t_{ij} = 0$.

3.2 Symmetry properties of BPRH Hamiltonian

The bipartite random hopping Hamiltonian in 3.1 has three important symmetries, namely particle-hole symmetry, time-reversal symmetry and sublattice-symmetry. The particle-hole symmetry transformation leaves the Hamiltonian invariant under the following operation: $d_j \rightarrow (-1)^j c_j^\dagger$, $d_j^\dagger \rightarrow (-1)^j c_j$, here we dropped the sublattice index from the creation/annihilation operators: when j is even it is A-sublattice, otherwise it is B-sublattice. With this transformation applied on 3.1, the particle-hole symmetric Hamiltonian, the eigenvalues come in $\pm\epsilon_\mu$ pairs.

Since we are interested about the spectrum of this Hamiltonian matrix, just knowing one half of the eigenvalues ϵ_μ is enough as the other is half is just $-\epsilon_\mu$. Thus we note that it is advantageous to study the square of hopping matrix $\mathbb{M}^2$ $(= \begin{pmatrix} t_{ij}t_{ij}^\dagger & 0 \\ 0 & -t_{ij}^\dagger t_{ij} \end{pmatrix})$ instead of the hopping matrix $\mathbb{M}$ $(= \begin{pmatrix} 0 & t_{ij} \\ -t_{ij}^\dagger & 0 \end{pmatrix})$. For bipartite lattices in $\mathbb{M}^2$ the two sublattices are decoupled with same absolute values of eigenvalues (differing in sign), that reduces the size of the matrix to be considered to half of the original. Moreover, for very small numbers the $\mathbb{M}^2$ is more numerically stable.

3.3 Ground state properties of the free fermion problem

3.3.1 Ground state flux configuration

For a half-filled band of electrons hopping on a planar, bipartite graph Lieb's theorem puts a constraint on the magnetic flux confinement in each closed loop which minimizes the ground state energy. To state the theorem let's first define several notations as follows: For a generic fermion hopping problem on a lattice the hopping amplitude t_{ij} between sites i and j is a complex variable and can be generally written as $t_{ij} = |t_{ij}|exp(i\gamma_{ij})$ with $\gamma_{ij} = \gamma_{ij}$ due to Hermiticity. In zero temperature this theorem imposes a condition of the fluxes γ_{ij} which minimizes the total ground state energy. The condition is on the "magnetic flux" enclosed in a plaquette, defined as the quantity $\sum_{\langle ij \rangle, i,j \in loop} \gamma_{ij}$. With this

definition, the theorem states that the "magnetic flux" enclosed by a loop of size $4m$ is π, whereas the magnetic flux enclosing by a plaquette of size $4m + 2$ is 0(where m is an integer). The theorem was proved by Lieb [49] only for bipartite graphs which has a plane of reflection not overlapping with any nodes. When sites are removed in random locations (Fig. 3.2) that symmetry doesn't exist anymore. However Willans et. al.[38] have shown with the aid of perturbative and numerical calculation that the same plaquette flux configuration minimizes the energy even in the absence of those symmetries.

So in our calculation of the ground state density of state we use the same flux configuration which minimizes the ground state energy. Next we will discuss a convenient scheme for our specific problem to put in fluxes for each defective plaquette such that we always stay in the flux sector that conforms to expectations from Lieb (we've checked that this configuration has lower energy compared to other configurations even in the multi-impurity case).

Pure system To start with, in the pure sample on a brickwall lattice(topologically equivalent to the honeycomb lattice) with periodic boundary condition in both direction, the ground state is the one with zero flux in every closed hexagonal loop. One needs to be a little careful about the choice of boundary conditions here. To satisfy Lieb's theorem on a brickwall lattice, if one takes $2p$(p is an integer) unit cells in the closed direction, the boundary condition have to be antiperiodic. To see this , look at the Fig. 3.2: there are 4 bonds in each unit cell, so for a closed loop with $2p$ unit cells there will be a loop of size $8p$, which must enclose a flux π. Similarly for $2p + 1$ unit cells the choice of boundary condition must be periodic. Our calculations are all done with semi-open boundary conditions (for reasons explained in next subsection), for which we carefully implement the correct boundary condition in the closed direction for the pure system and check that this gives the lowest energy state.

System with defect When one site is deleted from a pure brickwall lattice, in joins three consecutive hexagonal loops to a bigger loop of size 12. We call such closed loops as defective plaquettes. Infact any closed loop made of more than 6 edges(except the boundary loops) can be called defect plaquettes. So for a system with multiple vacancies randomly located, it is possible to have all kinds of closed loops which needs to carry the correct fluxes. In addition the flux binding by a vacancy causes a flux string as it leaves a flux in the attaching hexagonal plaquette to the defective plaquette. Such a string can terminate in another such vacancy or to the open boundary.

We came up with a simple way to conveniently put such fluxes in the defective plaquettes, such that the ground state is always is minimum energy flux configuration. In our way we use open boundaries in y-direction and periodic (or antiperiodic depending on the number of unit cells) boundaries in the x-direction. For every impurity we start a flux string and take it to the open boundaries by flipping sign of a bond parallel to the the open boundary. If another impurity falls on the way of that flux string we simply flip the sign of bonds under the same scheme towards the open boundary. As a result the horizontal bonds to the open boundary, which are after the second vacancy gets double flipped in

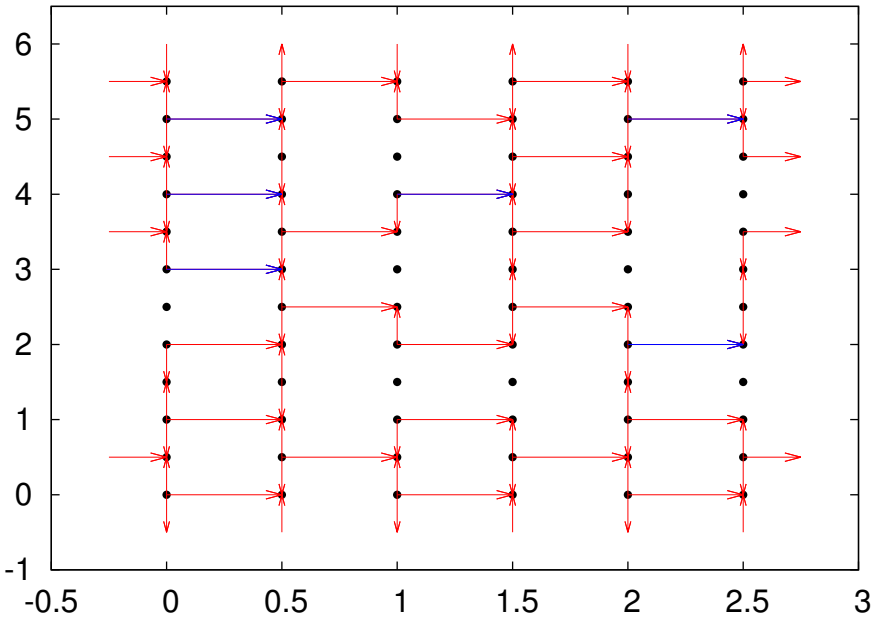

Figure 3.1: A sample with 72 sites and 4 vacancies on each of A and B-sublattice. Antiperiodic boundary condition in X-direction and open boundary condition in X-direction. We demonstrate the flux configuration consistent with Lieb's condition which is made by our ground state flux generator. Here sites are represented as black dots. An impurity is shown as a site with deleted bonds. The red bonds are the one with real hopping amplitude $+1$, the blue bonds are the one which have real hopping amplitude -1. Note that we flip one bond at the boundary usually the bond which links last unit cell with the first one(not shown in this picture) to satisfy Lieb's condition as discussed in the main text.

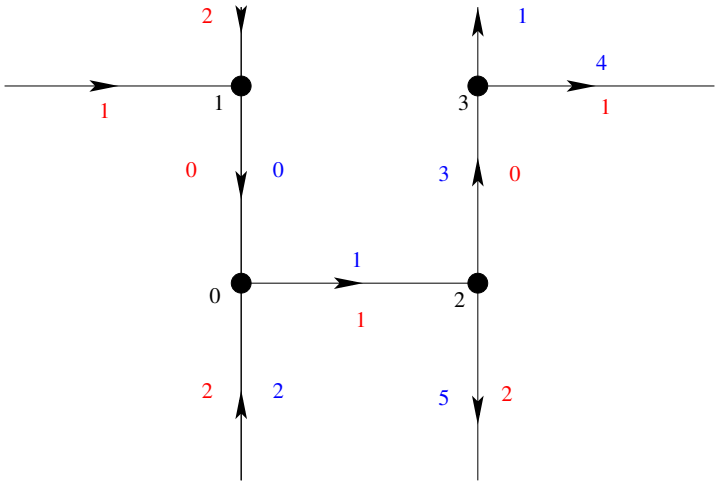

Figure 3.2: A picture of an unit cell of the brickwall lattice. In this figure the black numbers indicates site indices, blue numbers are for the bond indices. The red numbers denotes the bond type. For example take the site with index 0: the 0th neighbor of that site is the site with index 1, the 1st neighbor is site 2 and the 2nd neighbor is site 1 of another unit cell. Similarly the three bonds attached with the site 0 are numbered as following: 0th bond is bond number 0, 1st bond is bond number 1 and 2nd bond is bond number 2. Every bond links between two sites , to index that we take help of the arrows. Every arrowhead points from a B-sublattice site to an A-sublattice site. So, consider the bond with index 1, the 0th site connected with that is the site with index 2 and the 1th site connected is 0.

sign and the flux string terminates in the second vacancy. We check that our scheme always correctly generate the minimum energy flux configuration. As a demonstration in Fig. 3.1 we show a typical flux configuration in a diluted finite size sample.

3.4 Results

Before discussing the results, we will introduce a few notations and express all quantities in terms of them for convenience. I instead of energy E we will use the quantity $\Gamma = log(1/E)$ and instead of DOS we will plot integrated density of states (IDOS), $N(\Gamma)$. IDOS, being a monotonic function turns out to be a better representation of the spectral properties.

3.4.1 Gapped phase

Density of states We calculate the density of states using the methods discussed in Appendix-A. We observe that the behavior of integrated density of states(IDOS) goes through a crossover at a very low energy. In the energy range where Willans et. al. [38] studied IDOS, our results match theirs, and fit the "Dyson" form

$$N(\Gamma) \sim \Gamma^{-x} \tag{3.2}$$

with $x \sim 0.8$ (Willans et al[38] got a good fit with $x \sim 0.7$[38]).

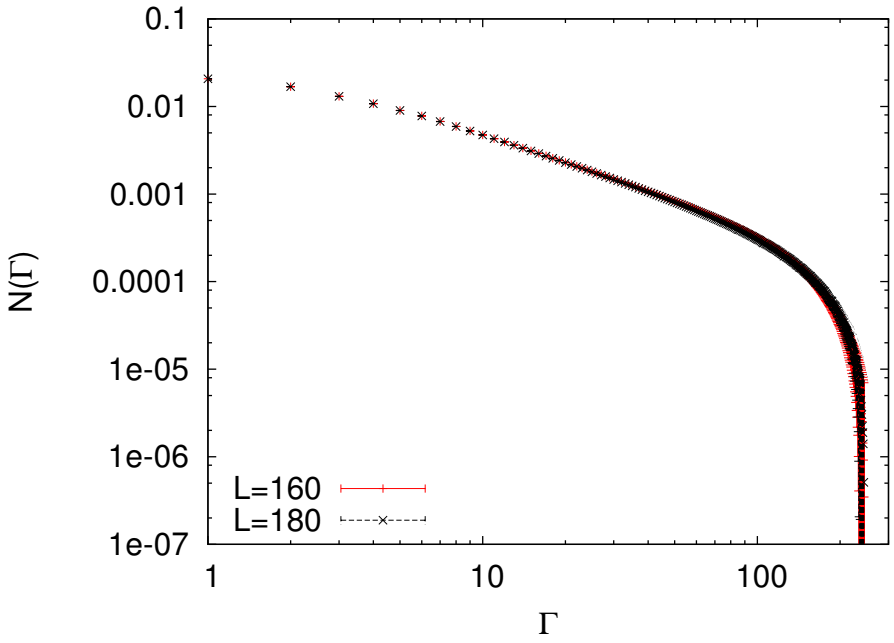

Figure 3.3: Integrated density of states $N(\Gamma)$ plotted against $\Gamma(=log(1/E))$ for the gapped phase of Kitaev's model on a honeycomb lattice with semiopen boundary condition. The parameter values used here $J_x = J_y = 1, J_z = 4(\alpha = J_z/J_x)$. In this figure we show the results for 5% impurity concentration, for samples of 51200 sites(L=160 unit cells in either direction) and 64800 sites(L=180 unit cells in either direction), averaged over 1000s of disorder realizations. This plots for size $L = 160$ and 180 overlaps till a large value of Γ, demonstrating the system size taken will not have finite size effects, till a large value of $\Gamma(= 100)$.

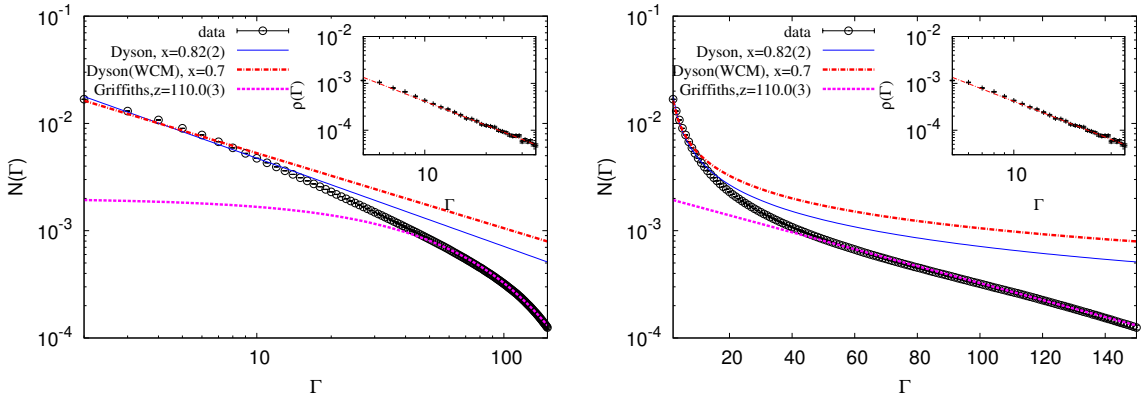

Figure 3.4: Integrated density of states $N(\Gamma)$ plotted against $\Gamma(=log(1/E))$ for the gapped phase of Kitaev's model on a honeycomb lattice with semiopen boundary condition. The parameter values used here $J_x = J_y = 1, J_z = 4(\alpha = J_z/J_x)$. In this figure we show the results for 5% impurity concentration, for sample of 64800 sites, averaged over 1000s of disorder realizations. The main plot shows a crossover from "Dyson" form to "Griffiths" or "modified Gade" (difficult to distinguish, see the figure 3.5 for a closer comparison) form in the behavior of low energy IDOS. Inset shows a zoomed portion in the higher energy range of the plot, to compare Willan's et al[38] (WCM) result. For comparison the inset plot is made for a sample with 3200 sites and 5% impurity concentration , same as Willans et al[38]. Here we show both log-log(left) and semi-log(right) plots for visual verification, as Dyson form is a straight line in log-log plot and Griffith's form is a straight line in semi-log plot. Here we see the $N(\Gamma)$ vs Γ plot has a crossover from straight in log-log plot tp straight in semi-log plot; giving a visual verification of our claim.

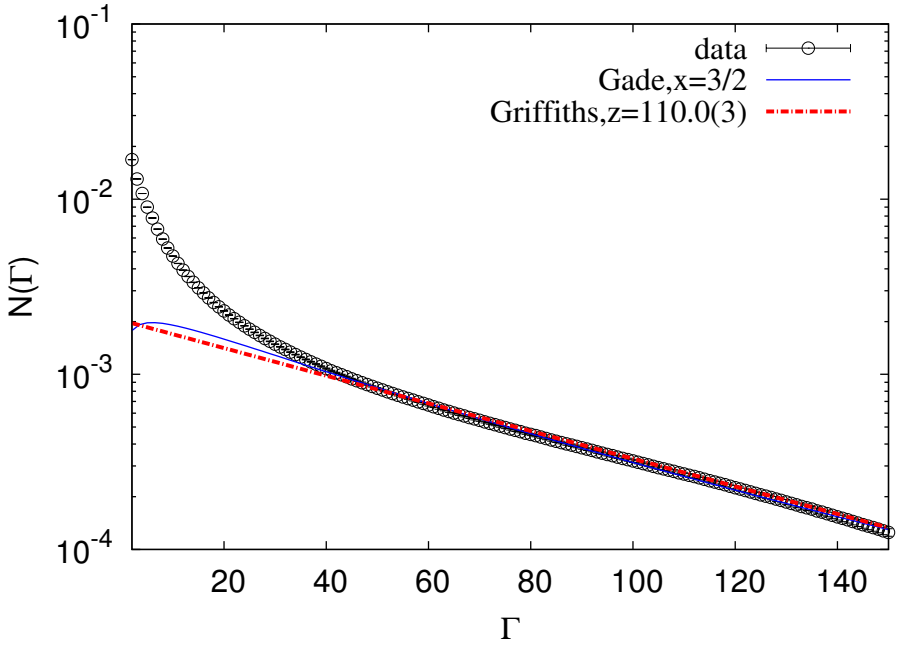

Figure 3.5: Integrated density of states $N(\Gamma)$ plotted against $\Gamma(=log(1/E))$ for the gapped phase of Kitaev's model on a honeycomb lattice with semiopen, boundary condition. The parameter values used here $J_x = J_y = 1, J_z = 4(\alpha = J_z/J_x)$. In this figure we show the results for 5% impurity concentration, for sample of 64800 sites, averaged over 1000s of disorder realizations. The plot shows a crossover from "Dyson" form to "Griffiths" or "modified Gade" form in the behavior of low energy IDOS. This plot demonstrates the fact: it is hard to decide that for high values of Γ, which of the two forms fits better with the data. The only thing we can say for sure that certainly the IDOS looks straighter than the "Dyson" form, so indeed there is a transition. The fits made here are within the range of $\Gamma = 40$ to 140. The z value fluctuates when we change the range. For example for the range of $\Gamma = 25$ to 80, z is 76.

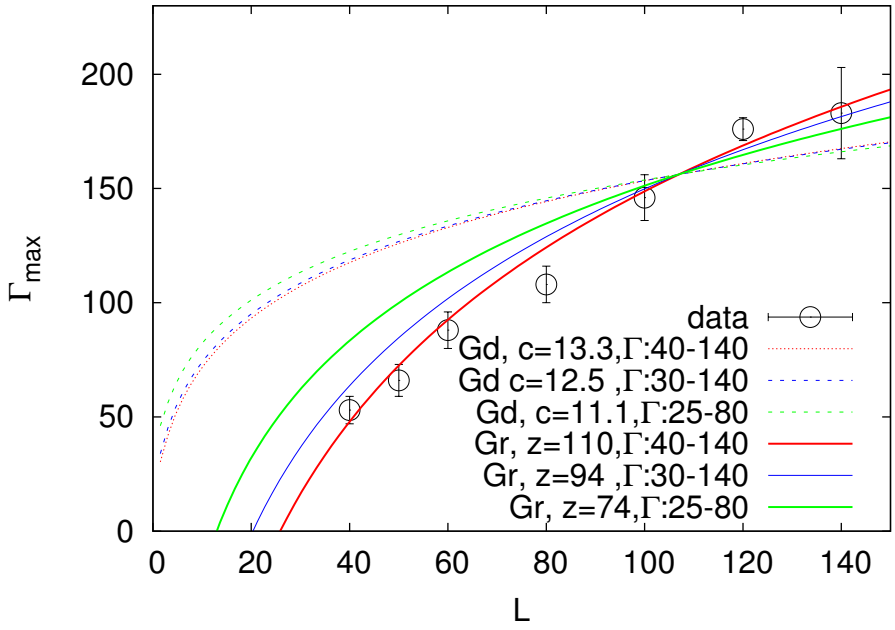

Figure 3.6: Mode of next to lowest non zero energy state plotted against L, for $\alpha = 4$. As a fit parameter we used the same values of c for "Gade" form as obtained from the density of states plots. And same value of z for the "Griffiths" form as obtained from DOS. The range of Γ shown in the plot indicates the range of Γ used for fitting in the Density of states plot. Here Gd: Modified Gade, and Gr: Griffith. The fit is made for large length scale above $L = 60$.

IDOS fits well to the "Dyson" form upto an energy $E \sim 10^{-20}$. At an energy lower than $E \sim 10^{-30}$, the behavior of IDOS deviates from "'Dyson" form as in Figures 3.8 and 3.5 we can see that. However from the IDOS plots it is almost impossible to say that whether for $\Gamma > 30$ the data fits better to Griffiths form with

$$N(\Gamma) \sim e^{-\frac{d}{z}\Gamma} \tag{3.3}$$

with a very high value of dynamical exponent ($z \sim 110$ when fitted from $\Gamma = 40$ to 140), or to "modified Gade" form with

$$N(\Gamma) \sim \Gamma^{1-\frac{1}{x}} e^{-c\Gamma^{\frac{1}{x}}} \tag{3.4}$$

with $x = 3/2$.

Lowest gap analysis One can define an energy dependent length scale $L(\Gamma)$ from the density of states such that $N(\Gamma) \equiv L^{-2}(\Gamma)$, then the "Modified Gade" form scales as $\Gamma \sim (logL)^{3/2}$ and the Griffith's form scales as $\Gamma \sim logL$. To check which scaling behavior works better we look at the scaling behavior of mode value of lowest non zero gap (Γ_{max})(over all the samples). However, because of the presence of zero modes (we discuss details about these modes in the 3.4.4), we look at the scaling of the next to lowest energy state. We plot Γ_{max} with the sample size(No. of unit cells in a direction, we call it L, here $N = L^2$) in Fig. 3.7. We show histogram for the distribution of next to lowest

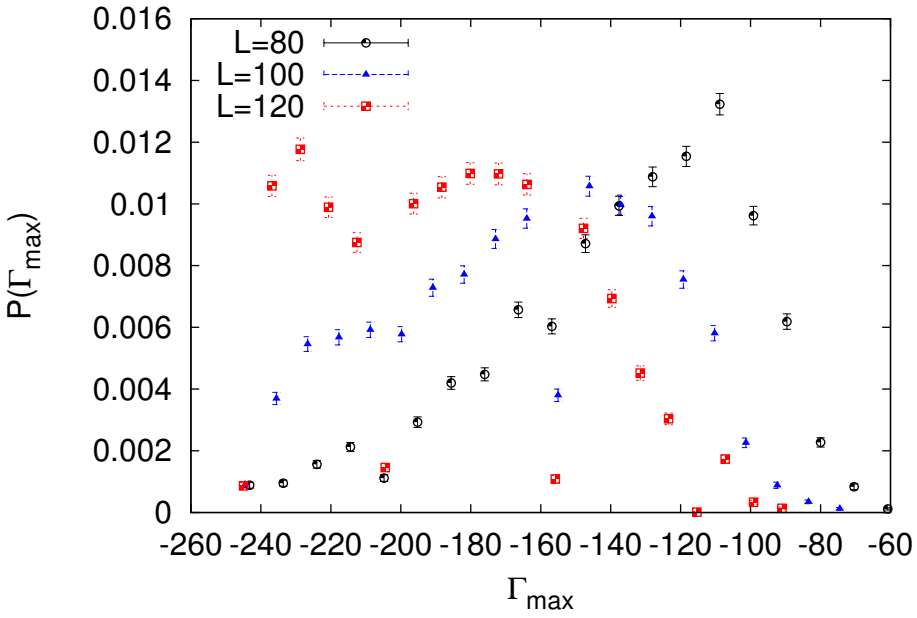

Figure 3.7: Histogram of next to lowest energy state over 5000 samples, for $\alpha = 4$

energy state for three representative sizes. And in Fig. 3.6 we show the scaling of the mode of that distribution. In Fig. 3.6 we can see that clearly "Griffiths" form fits better than "Gade' form, which is hard to distinguish from density of states plots.

A special feature in the histogram(Fig. 3.7) to notice is that, below a certain size ($L = 100$), the histogram has a single mode and with increase in size the histogram shows a bimodal character. We presume that such behavior might be a consequence of the the fact that in gapped phase there is a crossover from "Dyson" form to "Griffiths" form at a certain low energy scale ($\Gamma = 30 - 40$), the change in the number of modes of the histogram beyond a certain length scale (between $L = 80 - 100$), might be reflecting the same crossover behavior.

3.4.2 Gapless phase

We attempt to study the form of the density of states using the same direct calculation scheme described above. We calculate the integrated density of states in presence of finite number of vacancies upto very low energy($E_{min} = 10^{-55}$) and large size systems($N = 80000$) and contrast our result with the corresponding results of critical delocalized phase in the bipartite random hopping (BPRH) universality class[39]. In the delocalized phase the IDOS at low energy follows the "Gade" form

$$N(\Gamma) \sim \Gamma^{1-\frac{1}{x}} e^{-c\Gamma^{\frac{1}{x}}} \tag{3.5}$$

with $x = 3/2$(Fig 3.9, dubbed as "modified Gade" form to contrast with the original "Gade"[40] form with exponent 2. In Fig 3.10 we contrast the "modified Gade" form with the "Griffiths" form and from that plot we can see clearly the data is a better fit to the "modified Gade" form. However in the gapless

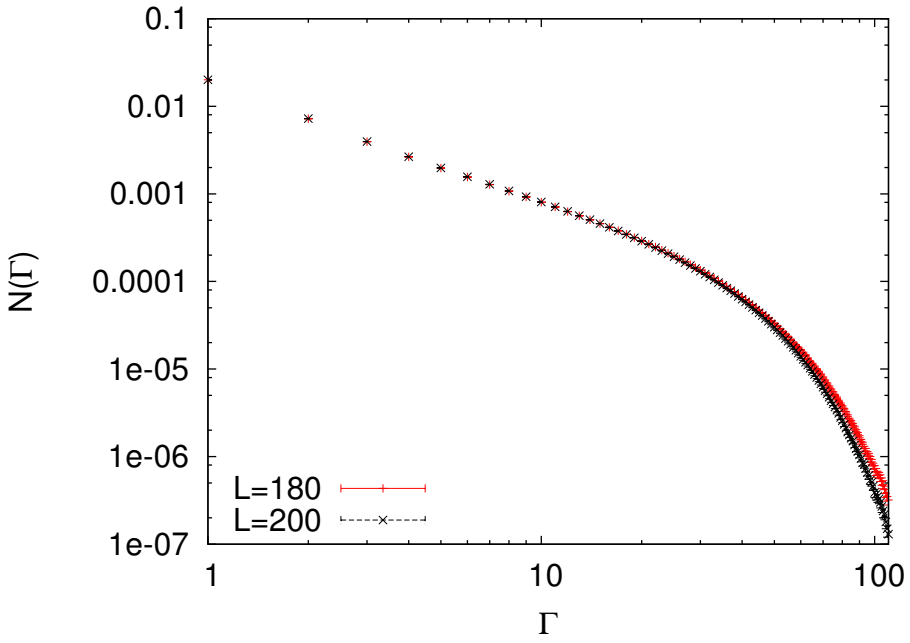

Figure 3.8: Integrated density of states $N(\Gamma)$ plotted against Γ(=$log(1/E)$) for the gapped phase of Kitaev's model on a honeycomb lattice with semiopen boundary condition. The parameter values used here $J_x = J_y = 1, J_z = 1(\alpha = J_z/J_x)$. In this figure we show the results for 5% impurity concentration, for samples of 64800 sites(L=180 unit cells in either direction) and 80000 sites(L=200 unit cells in either direction), averaged over 3000s of disorder realizations. This plots for size $L = 180$ and 200 overlaps till a large value of Γ, demonstrating the system size taken will not have finite size effects, till a large value of $\Gamma(= 50)$.

phase also at the the high energy (smaller Γ) the DOS takes a "Dyson" form, but at low energy the the Dyson form has a crossover to the "modified Gade" form 3.4.

Lowest gap analysis The corresponding lowest gap analysis for gapless was done in a similar manner. Here we don't see any peculiar bimodal character in the histogram and that is probably because we don't have a crossover behavior. The gapless phase IDOS is best described by the "modified Gade" form density of states data. From the scaling behavior of lowest non zero gap we can notice that whether the gapless phase is best described by "Griffiths" form or "Gade" form, is hard to decide. Also it depends a lot on the range of Γ used to fit in the DOS plot. Unfortunately in DOS plot we have clean data with good statistics only upto $\Gamma = 55$.

3.4.3 Tracking the transition

By analyzing the above results one can try to construct the following picture of the delocalization to localization (or metal-insulator) transition: the gapless phase($\alpha = 1$) is a completely delocalized state, located somewhere near the transition region and is nicely described by the "modified Gade"

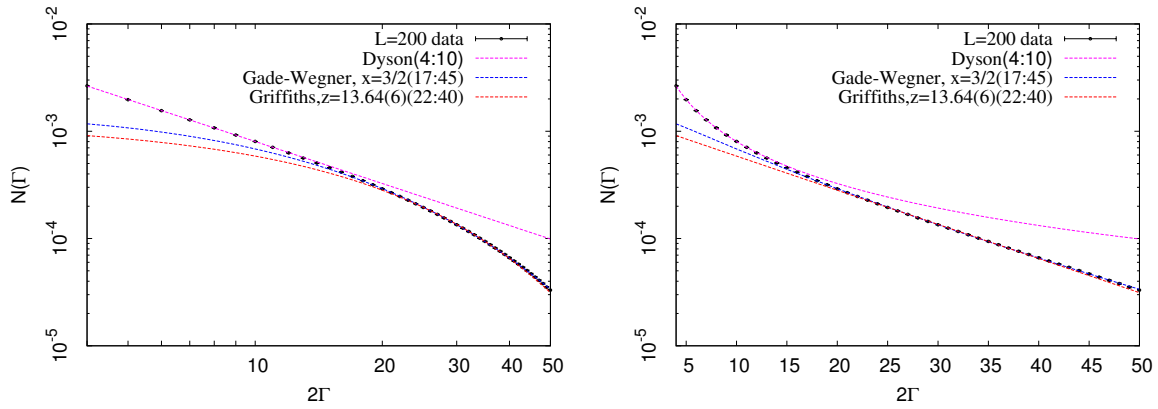

Figure 3.9: Integrated density of states $N(\Gamma)$ plotted against Γ for the gapless phase of bipartite hopping problem on a brickwall lattice with semiopen boundary condition. The parameter values used here $t_x = t_y = t_z = 1(\alpha = t_z/t_x)$. In this figure we show the results for 5% impurity concentration, of systems with 80000 sites, averaged over 3000s of disorder realizations. Like gapped phase, we also see here a crossover from "Dyson" form in small Γ to a weaker than "Dyson" form in large Γ. In this figure we compare between "modified Gade" form($x = 3/2$) and "Griffiths" form in the large Γ regime, and the figure above demonstrates that "modified Gade" form is a better fit to the data.

form at lower energy range. The gapped phase ($\alpha = 4$) is also located near the transition region from localized to delocalized phase. As a result one can see the "Dyson" form in the high energy IDOS as a signature of the critical point, which goes to "Griffiths"/"modified Gade" form as a property of localized/delocalized phase at lower energy. A schematic diagram of this picture is in Fig 3.13. So if this picture is true, by tuning the α is should be possible to see that with higher α the IDOS is more going towards the "Griffiths" form and the lower α is more going towards the "modified Gade" form - for that exponent "z" of "Griffiths" form must go higher and higher with increasing value α. To note here, for pure system the transition point is located at $\alpha = 2$.

In order to check this picture we did a quick analysis for a smaller size system in Fig. 3.14, 3.15. And from these figure this picture seems to be true. The supporting evidence for the picture in 3.13 is not enough with the analysis shown above.

3.4.4 Puzzle with zero modes

In our analysis, we carefully tried to avoid all known reasons of exact zero modes. One important feature of the bipartite hopping problem is that, it must have "graph zeroes" (zero energy eigenstates due to the geometry) equal in number to $|N_A - N_B|$, where N_A (N_B) are the number of $A(B)$ sublattice sites. For each of these, one needs to explicitly keep one Majorana mode. In our calculation, we avoid such zero modes by choosing $N_A = N_B$. Additionally we avoid any edge zero modes by choosing armchair boundary condition for the honeycomb model. We also carefully avoid any edge zero modes

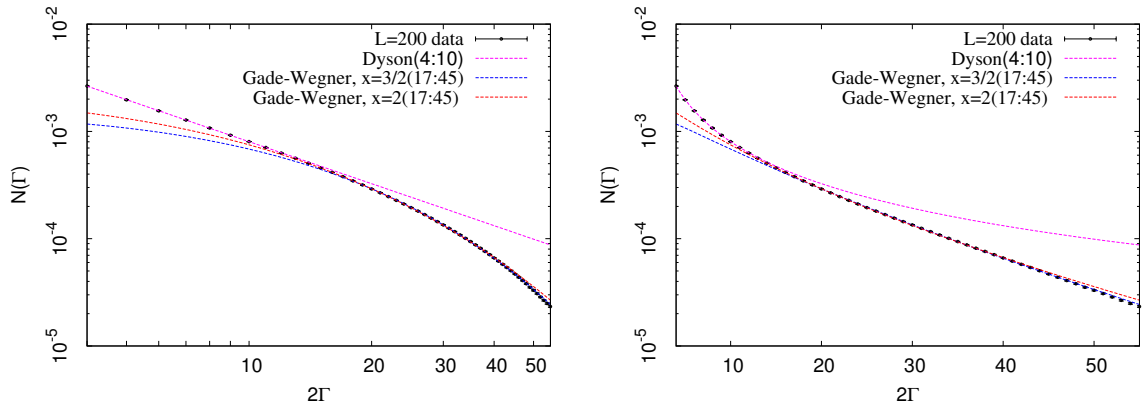

Figure 3.10: Integrated density of states $N(\Gamma)$ plotted against Γ for the gapless phase of bipartite hopping problem on a brickwall lattice with semiopen boundary condition. The parameter values used here $t_x = t_y = t_z = 1(\alpha = t_z/t_x)$. In this figure we show the results for 5% impurity concentration, of systems with 80000 sites, averaged over 3000s of disorder realizations. Like gapped phase, we also see here a crossover from "Dyson" form in small Γ to a weaker than "Dyson" form in large Γ. In this figure we compare between "modified Gade" form($x = 3/2$) and "Gade" form($x = 2$), and the figure demonstrates "Gade" is a better fit to the data for small Γ but as we go to the large Γ, namely the low energy limit modified Gade is a better fit. Thus from figures 3.9 and 3.10 we conclude in the gapless phase the true low energy behavior of the DOS follows the "modified Gade" form , reminiscent of the BPRH universality class.

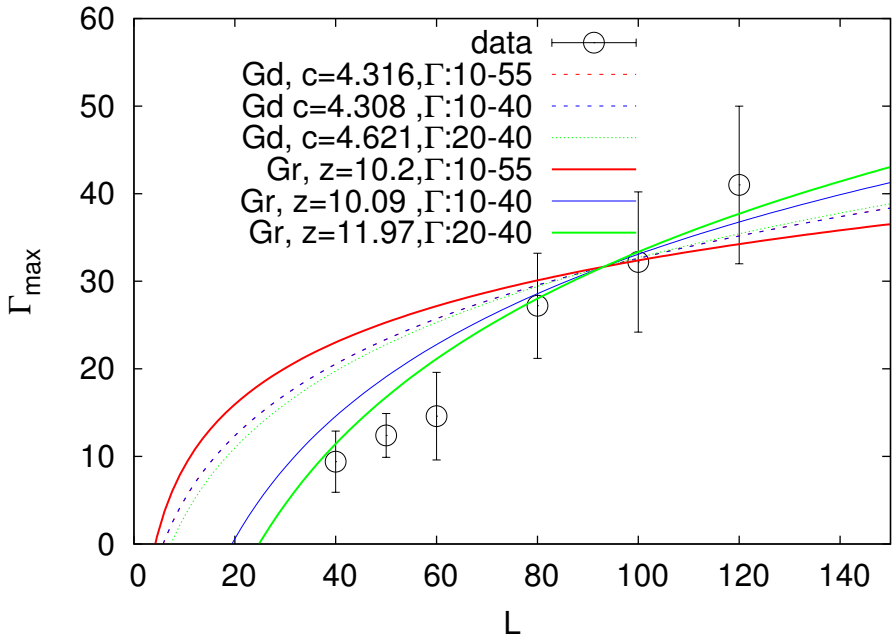

Figure 3.11: Mode of next to lowest non zero energy state plotted against L, for $\alpha = 1$. As a fit parameter we used the same values of c for "Gade" form as obtained from the density of states plots. And same value of z for the "Griffiths" form as obtained from DOS. The range of Γ shown in the plot indicates the range of Γ used for fitting in the Density of states plot Here Gd: Modified Gade, and Gr: Griffith.The fit is made for large length scale above $L = 60$.

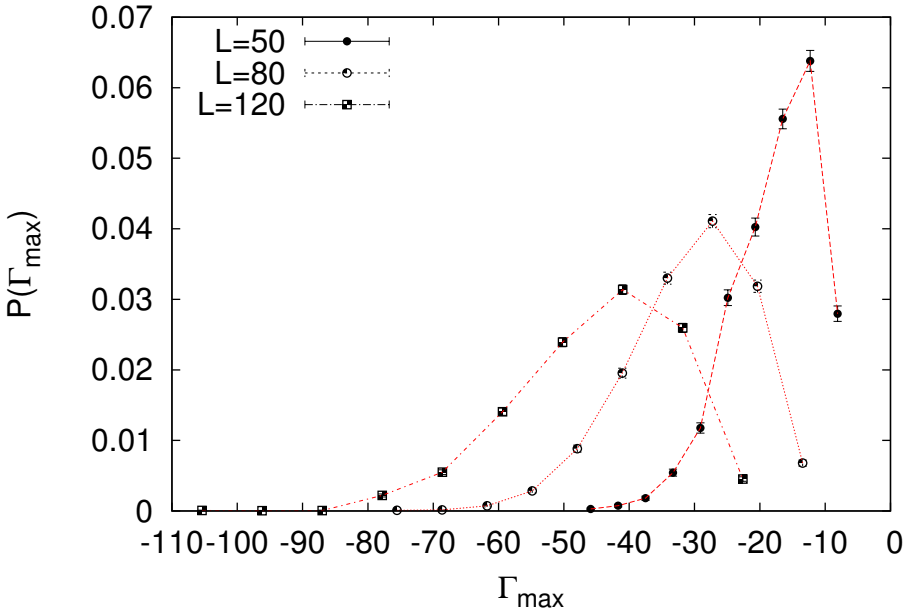

Figure 3.12: Histogram of next to lowest energy state over 5000 samples, for $\alpha = 1$

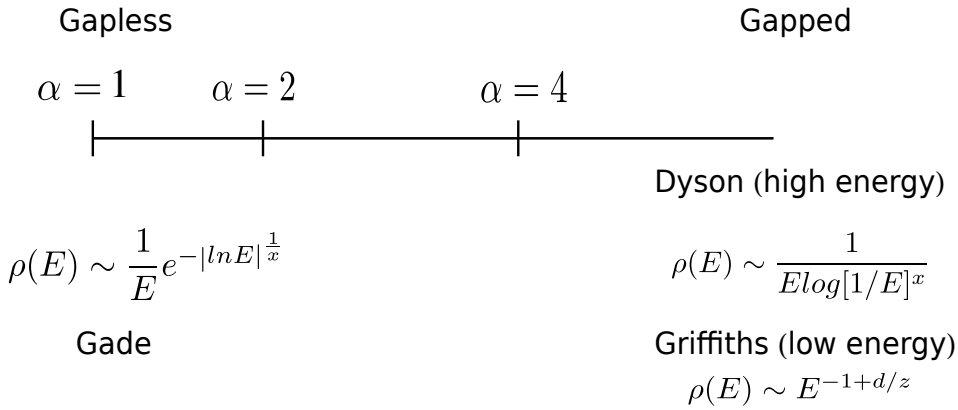

Figure 3.13: Schematic diagram of the conjectured phase transition. For pure system $\alpha = 1$ is the gapless phase and $\alpha > 2$ is the gapped phase. From this Figure one can guess the disordered system gapped to gapless transition point to be somewhere between $\alpha = 2$ and 3, provided the conjectured picture of the phase transition is correct.

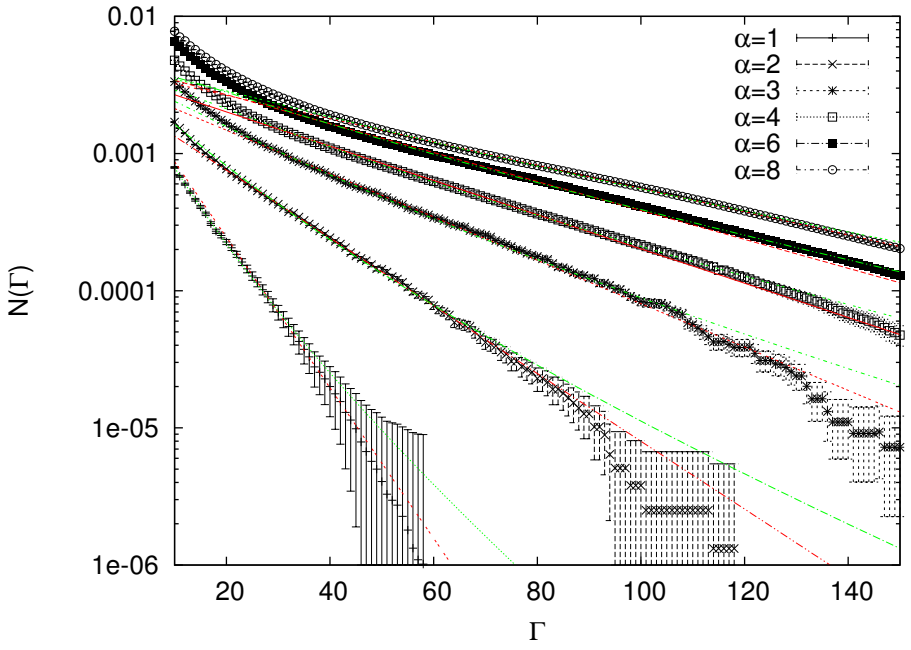

Figure 3.14: Integrated density of states $N(\Gamma)$ plotted against Γ for various values of α of of bipartite hopping problem on a brickwall lattice with semiopen boundary conditions. For pure system $\alpha = 1$ is the gapless phase and $\alpha > 2$ is the gapped phase.

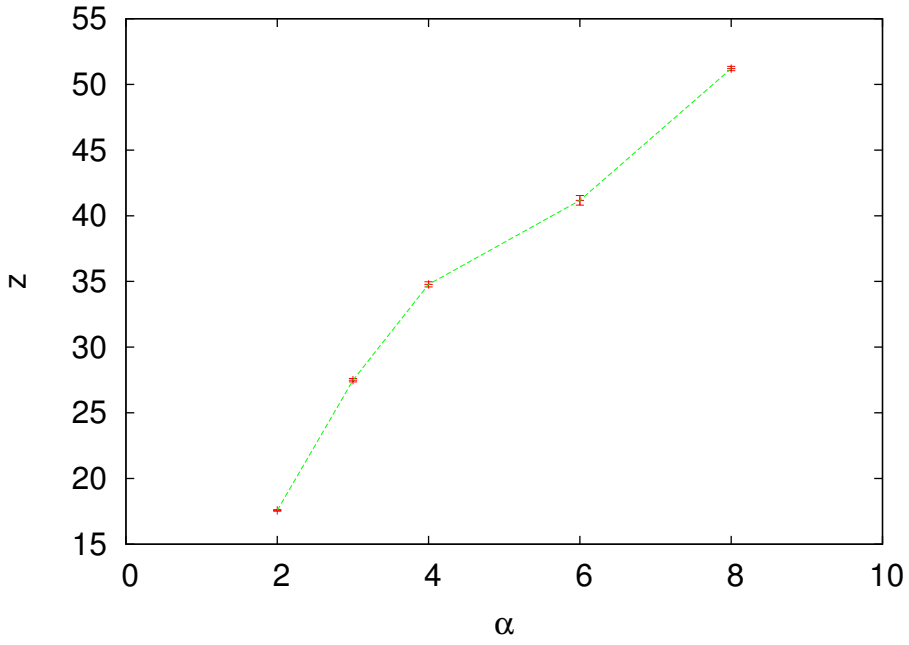

Figure 3.15: Exponent of Griffith's form 2.7 , by fitting $N(\Gamma)$ to Γ for various values of α. The trend in increasing z with α indicates that the system is more into the critical "Gade" phase.

due to vacancies sitting on the boundaries of the finite size samples by simply choosing not to put any vacancies on the boundaries.

Apart from these kind of zero modes, there can be some exact zero modes due to the location of vacancies on the graph e.g. such modes can occur if their is a disconnected or dangling part in the lattices. We carefully avoid such cases also in our calculations. This kind of zero modes are entirely "geometrical" and has nothing to do with the lattice structure or the phase properties. However in spite of eliminating all exact zero mode producing configurations of vacancies on the lattice, we find that in certain realizations of vacancies there are some very low energy modes, which we suspect as some exact zero modes. Such modes are possibly "geometric" in nature, as they do not depend on the system's phase properties. In an attempt to understand those zero modes we study the scaling properties of such zero modes for both $\alpha = 4$ and $\alpha = 1$ and note that the probability of a sample having a zero mode is almost 1 in the thermodynamic limit(Fig. 3.16). Whereas the number of such zero modes per sample per site also saturates to a constant value in the thermodynamic limit(Fig. 3.16).

As a further attempt to understand the zero modes we have a possible explanation of the origin of the same from Kasteleyn's theorem[1][63]. We know that the Kasteleyn weighting of a planar bipartite graph is a choice of sign for each undirected edge with the property that each face with $0mod4$ edges encloses a π flux and each face with $2mod4$ edges encloses as "0" flux. This condition is same as

[1]Kasteleyn's theorem provides provides an way to calculated the number of closed pack dimer covering on any graph. According to the theorem that number can be evaluated by calculating the Pffaffian of the Kasteleyn's matrix, which is nothing but the adjacency matrix of the graph with a weighting scheme known as Kasteleyn's weight as described in the main text.

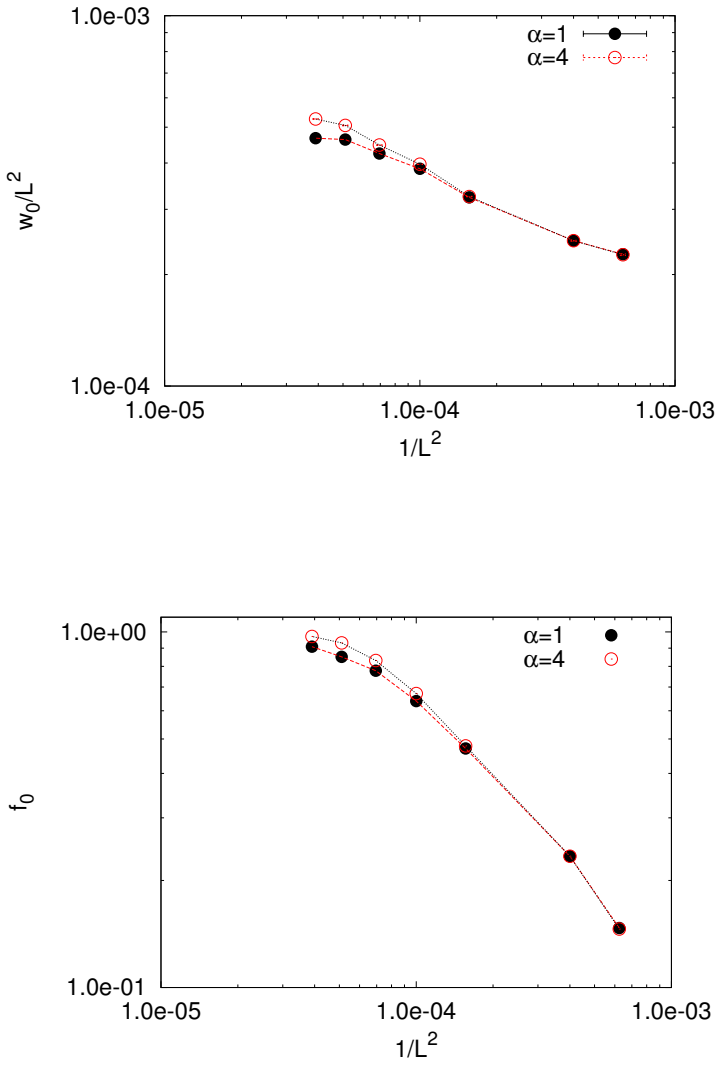

Figure 3.16: w_0 denotes the number of zero modes per sample and f_0 denotes the fraction of samples which have a zero mode. From the scaling of f_0 one can see that in thermodynamic limit the probability of finding a zero mode is almost 1. From the scaling of w_0 one can conclude that at thermodynamic limit the number of zero modes per sample per site almost converges towards a fixed value.

the Lieb's theorem [64] which was proven for bipartite graph with certain symmetries. However, with this Kasteleyn's weighting prescription one can construct the Kasteleyn's matrix(same as our hopping matrix with $\alpha = 1$) whose Pffaffian gives the number of possible ways of close pack dimer covering of a graph. So it might be possible to show that in the cases when we encounter a zero mode due to the presence of disorder, there is no way of finding a closed pack dimer covering of the disordered bipartite graph.

We show in Fig. 3.17 two configurations of impurity distributions on a small size sample; one of which has a zero mode and other doesn't. If we can show the the one with zero modes cannot have a closed pack dimer covering and in contrast the one without zero mode has a dimer covering, that will be an example supporting our guess of the origin of zero modes from Kasteleyn's theorem.

3.5 Discussion

In this work we tried to answer some questions regarding the nature of density of states in the localized and delocalized phases of randomly site diluted bipartite fermion hopping problem. We performed our detailed analysis for the gapless phase $\alpha = 1$ and noted the density of states to be of "modified Gade" form on the other hand in the gapped phase $\alpha = 4$ we note a crossover of from "Dyson" form to "Griffith's form" or "modified Gade". In the 3.4.3 we discussed in detail our interpretation of these observation and the need of more analysis to this unresolved issue. On the other hand another unresolved issue is these zero modes which we already discussed in the 3.4.4, at the end of that section we indicated the possible analysis required to fully understand that issue.

Even though random site dilution is a very different kind of disorder from random hopping as pointed out in the introduction, we see that the low energy DOS behavior of the former is localized and delocalized phases are very similar to that of later [39]. A physical RG type picture explaining the generation of many low energy states near $E = 0$ in the strong disorder limit was discussed by Motrunich et al[39] which we have reviewed briefly in the introduction. There is no reason for such a mechanism to work in this case of site dilution- in spite of the resemblance. This leaves a future direction of research to provide such a RG picture which will give the possible mechanism by which large number of states are generated near $E = 0$ and also to explain why these two kind of disorders leads to same form of DOS behavior at low energy.

There are a few more unanswered questions and possible extensions on this work which can be listed as follows:

- We understood the density of states behavior (Eq. 2.6) in the gapless phase quite unambiguously but in the gapped phase we don't have good enough results to distinguish between the Gade (Eq. 2.6)and Griffiths (Eq. 2.7 behavior. More data is required in this phase to know the correct behavior of density of states.

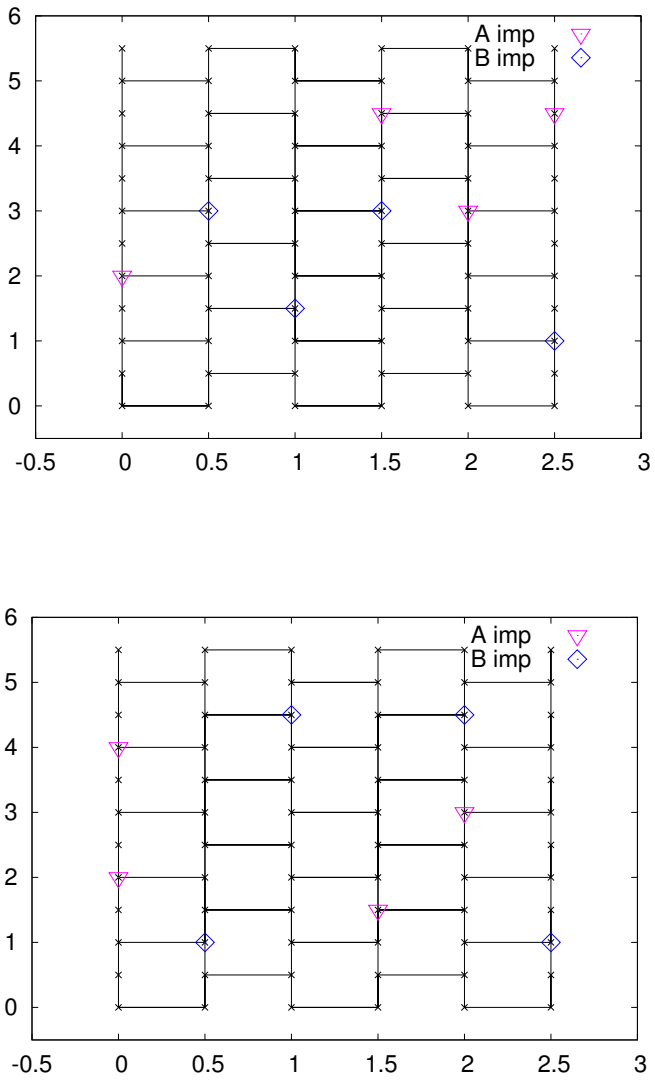

Figure 3.17: Both of the plots are made for samples with 72 sites and 8 impurities, with 4 on each sublattice. There is antiperiodic boundary condition in the X-direction and open boundaries in the Y-direction. The top one shows a configuration which has a zero mode and the bottom one shows a configuration which has no zero modes.

- We have empirical evidence supporting our conjecture about the origin of zero modes by lack of dimer covering. A proof or some sort of more detailed numerical analysis is required to be sure that is always the case.
- An extension of this work is possible by analyzing the same hopping problem on a non-bipartite graph. As it is known such a problem belongs to a different universality class; so it will be interesting to understand the behavior of such class of systems.

Chapter 4

Random site dilution in an $SU(2)$ symmetric interacting spin system

This chapter is about the effects of site dilution in the $SU(2)$ symmetric Yao-Lee spin model. In the introduction we have mentioned that this spin model can be mapped to a free lattice gas of fermions in the background of a static Z_2 gauge field, and thus the magnetic susceptibility of the spin system can be mapped to the compressibility of that Fermi gas. Using this connection we will analyze the susceptibility of the randomly diluted Yao-Lee spin model by the result of the density of states analysis of randomly diluted bipartite hopping problem of the last chapter. With this main agenda, this chapter is organized as follows: in section 4.1 we will discuss the relevant models to this chapter i.e. Kitaev's spin model and $SU(2)$ symmetric Yao-Lee model. Even though our main goal in this chapter is to study the later model, we will describe the Kitaev's model as it gets mapped to a very similar free fermion hopping problem as that of Yao-Lee's model and has same phase digram. In the section 4.2 of this chapter we will discuss this map in detail for the the Yao-Lee model and at the end we will briefly mention the similarities and difference of this model with Kitaev's model. Section 4.3 of this chapter will contain discussion about choice of basis to construct Fock space in the free fermion model such that it faithfully represents the spin model. In addition we will discuss the subtleties in mapping randomly site diluted spin model to the randomly diluted fermion hopping problem. In section 4.4 we will recall the results of the previous chapter on random dilution in free fermion hopping problem to characterize the magnetic susceptibility behavior of the metallic and insulator phases of Yao-Lee model, which is our main result of this chapter. In section 4.5 we end the chapter with a discussion on our interpretation of these results and some possible future direction of research.

4.1 Models

4.1.1 Kitaev's model

Kitaev's spin model is a very special kind of spin model which has anisotropic nearest neighbor spin interaction depending on the direction of the bonds in real space. Before defining the original model

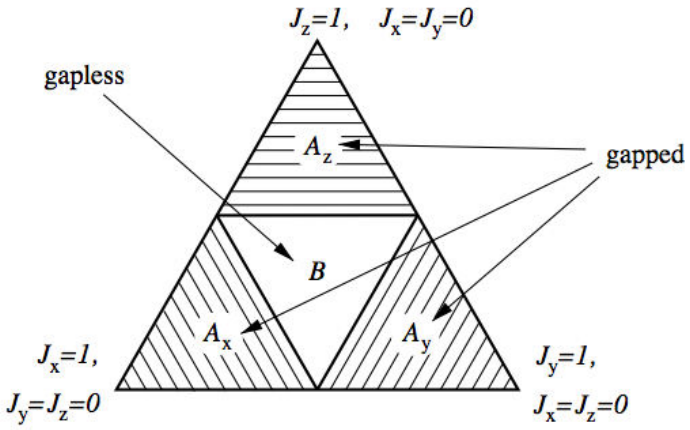

Figure 4.1: Phase diagram of Kitaev's model

on a honeycomb lattice let us introduce few notations as follows: a bond on the lattice (as in Fig. 4.1) between the nearest neighbor sites with labels j and k can be in one of the three orientations in physical space - labeled using the variable $\lambda(= x, y \text{ or } z)$. A spin degree of freedom with moment $1/2$ at site j is represented by the Pauli matrices σ_j^λ, where the superscript is the spin component. The exchange strength between spins at sites j and k in λ direction is denoted as $J_{\langle jk\rangle_\lambda}$. With this notations defined, the Hamiltonian is given by

$$H^K = -\sum_{\langle jk\rangle_\lambda} J_{\langle jk\rangle_\lambda} \sigma_j^\lambda \sigma_k^\lambda \,. \tag{4.1}$$

Ground state of Kitaev's honeycomb model has both gapped and gapless phases. In the parameter space with all $J_\lambda > 0$ there are three gapped phases ($J_z > J_x + J_y$ and its permutations) and one gapless phase around the point J_x=J_y=J_z=J, as shown in Fig. 4.1.

The ground state of Kitaev's spin model has quantum spin liquid like behavior in both gapped and gapless phase, as the two spin correlation function vanish identically beyond nearest neighbor sites for all values of the coupling constants.

4.1.2 Yao-Lee's model

Construction of an SU(2) symmetric extension of Kitaev's model requires a lattice with coordination number three and a tricolourability property for the links of the lattice. On such a lattice, each link can be assigned a type-label x, y or z such that every vertex has exactly one link of each type. Again our brickwall lattice in Fig. 3.2. satisfy those conditions. The Hamiltonian with same notations as before can be defined as,

$$H^{YL} = -\sum_{\langle jk\rangle_\lambda} J_{\langle jk\rangle_\lambda} (\tau_j^\lambda \tau_k^\lambda)(\sigma_j . \sigma_k). \tag{4.2}$$

The model has two different sets of spin degrees of freedom (τ and σ) at every site for SU(2) invariance. The phase diagram of this model is same as that of Kitaev's model. In next section we will point out the similarities of this model with Kitaev's model.

However one important difference of this model from Kitaev's one comes in the behavior of correlation functions. The gapped phase has exponentially decaying spin-spin correlation; but the gapless phase of this model has power law correlation with exponent four. As the model is $SU(2)$ spin rotation invariant, it has spinfull fermionic excitations.

4.2 Solving spin Hamiltonian by Majorana fermionization

Representing a spin degrees of freedom in terms of a fermionic or bosonic is often useful as it allows one to apply the powerful techniques developed to solve fermionic or bosonic system in obtaining a solution for the spin system. Such mappings doesn't always ease the solution as in most of the cases, like Jordan-Wigner fermionization of Heisenberg spin chain maps it to a interacting fermionic model. Similarly Schwinger bosonization [65] maps Heisenberg spin model into a non-linear interacting bosonic system which can be only solved perturbatively. On the other hand the well used Schwinger fermion representation comes with an additional, difficult to deal with, constraint equation to satisfy; such that the fermionic Hilbert space is a faithful representation of the spin model Hilbert space. There are attempts in literature to get rid of this constraint, such as "drone-fermion" representation: where one represents a spin operator in terms of a canonical complex fermionic operator and a Majorana fermion[1] operator.

Kitaev first time introduced a complete Majorana fermion representation of fermionic spins to map a two dimensional interacting spin model (known as Kitaev's model and described in Models section) into a non-interacting Majorana fermion system which is exactly solvable. In Kitaev's scheme every spin at a site is represented by four independent flavors of Majorana fermions. Given that two Majorana fermions are required to represent a canonical complex fermion and each Majorana fermion has a Hilbert space dimension $\sqrt{2}$, this doubles the Hilbert space dimension per spin from two to four. To project back in the physical Hilbert space Kitaev introduced a projection operator which commutes with the Hamiltonian.

Kitaev's model is not spin rotation symmetric and to explain some physical system (as discussed in 2.3.1) one requires a model with such symmetries. Yao-Lee extended Kitaev's scheme in solving an $SU(2)$ invariant spin (model described in models section) which has a spin liquid ground state. The Majorana fermionization of Kitaev is not spin-rotation symmetric and was simply extended to such a symmetric case by introducing another Majorana fermion representation similar to one introduced by Shastry-Sen [45] for one dimensional spin models. In this section we will discuss this Majorana fermionization in detail and we will also discuss the subtleties in extending the same in presence of site

[1] In 1937 Majorana [66] discovered that a modification of Dirac's equation in possible which includes a charge conjugated Dirac spinor and is completely written in terms of real numbers. This "real" Dirac equation has two solutions known as Majorana fermions, one being a charge neutral particle and the other being a charge neutral antiparticle with the special property of the particle being it's own antiparticle. Since then there are debates on whether there is a physical example of this mathematical solution.

However apart from that debate Majorana fermions are proven to be a useful mathematical tool in fermionizing interacting spin models, we discuss in detail such an use of Majorana fermion in this chapter.

dilution.

4.2.1 Mapping Yao-Lee's model to free Majorana fermions

As mentioned in the Models section, this model has two different sets of spin degrees of freedom at every site for SU(2) invariance. One set of spin degrees of freedom are expressed by the Pauli spin matrices (σ^λ,$\lambda = x, y, z$) which are represented by $SU(2)$ invariant Majorana fermion representation as

$$\begin{aligned} \sigma^x &= -ic^y c^z \\ \sigma^y &= -ic^z c^x \\ \sigma^z &= -ic^x c^y, \end{aligned} \tag{4.3}$$

where c^λ ($\lambda = x, y, z$) are Majorana fermions operators. The other spin degrees of freedom is represented by another set of Pauli spin operators (τ^λ,$\lambda = x, y, z$) at every site, which can be written by another set of Majorana operators $b^\lambda(\lambda = x, y, z)$ in a $SU(2)$ invariant way as

$$\begin{aligned} \tau^x &= -ib^y b^z \\ \tau^y &= -ib^z b^x \\ \tau^z &= -ib^x b^y. \end{aligned} \tag{4.4}$$

The Majorana fermion operators obey the commutation relation

$$\{c_i^\lambda, c_j^{\lambda'}\} = 2\delta_{\lambda\lambda'}\delta_{ij} \tag{4.5}$$

$$\{b_i^\lambda, b_j^{\lambda'}\} = 2\delta_{\lambda\lambda'}\delta_{ij}, \tag{4.6}$$

and all other commutations being zero. Note that any model with this kind of structure will look like a bilinear in both b and c. And now that we have two independent Pauli matrices as every site and we are writing each one of them by SU(2) symmetric representation of three Majorana fermions, we have double counted the single site Hilbert space, leading to 8-dimensional Hilbert space at each site. To get back to the original Hilbert space the typical choice[45] is

$$c^x c^y c^z b^x b^y b^z = i, \tag{4.7}$$

(or alternatively $c^x c^y c^z b^x b^y b^z = -i$). This allows us to write

$$\sigma^\alpha \tau^\beta = ic^\alpha b^\beta \tag{4.8}$$

(or alternatively $\sigma^\alpha \tau^\beta = -ic^\alpha b^\beta$), where α and β runs over x,y and z. Each of this basically represents a copy of the physical subspace, once a choice is made by choosing a constraint condition (as in Eqn.

4.7) the other copy becomes the "unphysical" sector. This is an interesting point about this model and Majorana representation, here the "unphysical sector" is not unphysical in true sense ($SU(2)$ algebra is satisfied in that sector as well) as it an equally faithful copy of the physical states and one can work with either copies [45].

The hopping Hamiltonian Using the Majorana mapping described above, the Hamiltonian in terms of the Majorana fermions is

$$H^{YL} = i\sum_{\langle jk\rangle} J_{\langle jk\rangle_\lambda} u_{\langle jk\rangle_\lambda} \left(\sum_{\alpha=x,y,z} c_j^\alpha c_k^\alpha \right). \tag{4.9}$$

Where the outer sum is over all three types of links $\langle jk\rangle$ ($\lambda = x, y, z$). The products $ib_j^\lambda b_k^\lambda$ on the λ type $\langle jk\rangle$ bonds become static Z_2 gauge fields $u_{\langle jk\rangle_\lambda}$ as $u_{\langle jk\rangle_\lambda}$ satisfy $\left[H, u_{\langle jk\rangle_\lambda}\right] = 0$ and $\left[u_{\langle j'k'\rangle_\lambda}, u_{\langle jk\rangle_\lambda}\right] = 0$; making $u_{\langle jk\rangle_\lambda}$ a good quantum number with eigenvalues ± 1. The Hamiltonian becomes a bilinear in c Majorana fermion operators which are coupled to static Z_2 gauge fields.

At this stage it will be useful to mention the difference between the hopping Hamiltonian of Yao-Lee model (Eq. 4.2) and that of the Kitaev's model (Eq. 4.1) as following: the Yao-Lee hopping Hamiltonian has three different flavors of c-fermions which means this has three copies of Kitaev's original solution with each of those fermion flavors being coupled with the same gauge field-which means all of this three copies have exactly the same spectrum. This Eq. 4 has a global $SO(3)$ rotational symmetry which rotate among the three flavour of Majorana fermions as a consequence of the $SU(2)$ symmetry of the Yao-Lee spin model it represents. Due this resemblance with the original Kitaev's model, the properties of this free Majorana fermion hopping problem of this $SU(2)$ symmetric Yao-Lee model, is same as that of Kitaev's original model.

4.3 Choice of basis for constructing Fock space of fermion operator

To make physical sense with Majorana fermions we need to construct the Hilbert space as the Fock space of pairs of Majorana fermions, combined to make the canonical complex fermion. We will do this first for a bipartite graph with equal number of A and B sublattice sites, then we will discuss the modifications when one and then many sites are removed from this system. Finally we will see the physical meaning of coupling a magnetic field with the spins of the original spin model in terms of those canonical fermions.

Pure system with even number of sites Consider a bipartite honeycomb lattice with even number of sites and let's choose a convenient pairing of two of the three Majorana fermions at each site to a complex canonical fermion as

$$z_j = (c_j^x + ic_j^y)/2. \tag{4.10}$$

This leads to

$$\sigma_j/2 = -(z_j^\dagger z_j - \frac{1}{2}), \tag{4.11}$$

where the z-fermions carry the conserved S^z quantum number. The other fermions can be paired in a convenient was as

$$f_p = (c^z_{p,A} + ic^z_{p,B})/2, \tag{4.12}$$

where A and B are sublattice sites for an unit cell p. One can think this as pair formation between sites coupled by a vertical bond in the honeycomb or horizontal bond in brickwall lattice, as in Fig (3.2). Similarly for the Z_2 gauge field u_{jk} the pairing can be symmetric as ,

$$\zeta_{\langle ij\rangle} = \frac{b_i^{\langle ij\rangle} + ib_j^{\langle ij\rangle}}{2}. \tag{4.13}$$

Thus the full Hamiltonian in terms of these complex fermions and the Z_2 gauge field is given by

$$\begin{aligned}
H^{YL} &= \sum_{\langle jk\rangle_\lambda} J_{\langle jk\rangle_\lambda} \left(2\zeta^\dagger_{\langle jk\rangle_\lambda}\zeta_{\langle jk\rangle_\lambda} - 1\right)\left[2i\left(z_j^\dagger z_k - z_k j^\dagger z_j\right) + ic_j^z c_k^z\right] \\
&= \sum_{\langle jk\rangle_\lambda} J_{\langle jk\rangle_\lambda} \left(2n_{\zeta_{\langle jk\rangle_\lambda}} - 1\right)\left[2i\left(z_j^\dagger z_k - z_k^\dagger z_j\right) + ic_j^z c_k^z\right]. \\
&= \sum_{\langle jk\rangle_\lambda} J_{\langle jk\rangle_\lambda} u_{\langle jk\rangle_\lambda}\left[2i\left(z_j^\dagger z_k - z_k^\dagger z_j\right)\right] + \sum_{\langle jk\rangle_\lambda} J_{\langle jk\rangle_\lambda} u_{\zeta_{\langle jk\rangle_\lambda}} ic_j^z c_k^z. \\
&= \sum_{\langle jk\rangle_\lambda} it_{\langle jk\rangle_\lambda}\left[\left(z_j^\dagger z_k - z_k^\dagger z_j\right)\right] + \sum_{\langle jk\rangle_\lambda} J_{\langle jk\rangle_\lambda} u_{\zeta_{\langle jk\rangle_\lambda}} ic_j^z c_k^z.
\end{aligned} \tag{4.14}$$

On a bipartite graph with sublattice A and B , $M_{ij} = t_{\langle jk\rangle_\lambda}$ and $M_S = \frac{1}{2}(M^T + M)$, $M_A = \frac{1}{2}(M^T - M)$.

$$H^{YL} = i\left(z_A^\dagger z_B^\dagger\right)\begin{pmatrix} 0 & M \\ -M^T & 0\end{pmatrix}\begin{pmatrix} z_A \\ z_B\end{pmatrix} + \left(f^\dagger f\right)\begin{pmatrix} M_A & M^S \\ -M_S & -M_A\end{pmatrix}\begin{pmatrix} f^\dagger \\ f\end{pmatrix} \tag{4.15}$$

Note that all this canonical fermions doesn't reside on the sites of the lattice, the f fermions reside on the 'z' bonds of the lattice and z-fermions resides on the sites of the lattice. The Z_2 static gauge field also resides on the bonds of the lattice, whose Z_2 character is clear from this equation as the bond fermion number on the bonds $n_{\zeta_{\langle jk\rangle_\lambda}}$ can be either zero or one. On the other hand we have a free canonical fermion (z-fermions) hopping Hamiltonian with hopping amplitude $t_{\langle jk\rangle_\lambda}(= u_{\langle jk\rangle_\lambda} J_{\langle jk\rangle_\lambda})$ between nearest neighbor sites j and k. In addition we have another set of canonical fermion hopping (f-fermions) Hamiltonian which can be physically interpreted as following: f_p fermions resides on the z bonds connecting two sites of an unit cell and when $p \equiv p'$ the f-fermion part of the Hamiltonian represents an on site potential term, otherwise it represents a superconductor Hamiltonian with a gap term ($f_p f_{p'} + f_p^\dagger f_{p'}$) of gap magnitude $t_{\langle jk\rangle_\lambda}$.

The $SU(2)$ invariance of the original problem is in the fact that the free fermion hopping problem and superconductor problem has exactly identical spectra.

Nature of Projection operators The nature of projection (4.7) is simpler to understand by writing in terms of the original Kitaev's projection (D_j) as follows:

$$\left(2n_j^z - 1\right) D_j = 1 \tag{4.16}$$

where

$$D_j = b_j^x b_j^y b_j^z c_j^z. \tag{4.17}$$

So the full projection operator becomes

$$P^{YL} = \prod_j \left(\frac{1 + \left(2n_j^z - 1\right) D_j}{2} \right). \tag{4.18}$$

The n_j^z operator only increase or decrease the number of z-fermions and that number is conserved in the system. Thus the P^{YL} operator should work very similar to the Kitaev's projection

$$P^K = \prod_j \left(\frac{1 + D_j}{2} \right). \tag{4.19}$$

Removing one site from the pure system To construct the Hilbert space when one site is removed from the pure system with even number of site needs some regularization scheme, as it is not obvious that in presence of such an abrupt disorder one can consistently carry out the calculation in the canonical fermion Hilbert space while keeping the faithful representation of the spins intact. A sensible way to do this regulation is by putting back the removed site by re-introducing three infinitesimal couplings δ to the bulk system.

For the z fermion part of the Fock space, this has a trivial effect i.e. to leading order, δ simply mixes the zero mode wavefunction of the diluted hopping problem with the trivial zero mode that lives on the single site that has been removed from the system. This splits these two zero modes to give two canonical fermion modes at energies $\sim \pm\delta$.

For the ζ fermion part of the Fock space, keeping this removed site in our description allows us to construct the Fock space exactly as in the pure system.

And for the f fermion part of the Fock space, putting the removed site back in is essential for making sense of the Majorana zero mode: To leading order, δ leads to a single canonical fermion eigenstate at energy $\sim |\delta|$ obtained by mixing the zero mode of the diluted hopping problem with the trivial zero mode on the site that is removed. In the $\delta \to 0$ limit, this becomes a genuine Majorana excitation.

Removing many sites from the pure system In a similar fashion one can argue removal of many sites from the system. As we have seen for removing each sites by the above regulated scheme, there will be a genuine zero energy Majorana mode localized at the removed site. The rest of the eigenstates of the hopping problem can be obtained by solving the single particle hopping problem (Eq. 4.15).

So the hopping problem is same as in Eq.1.27 of chapter 3 with $t_{\langle jk\rangle_\lambda}(=u_{\langle jk\rangle_\lambda}J_{\langle jk\rangle_\lambda})$. The ground state or energy minimizing flux sector of the hopping problem will be decided by the Lieb's theorem as discussed in the 3.3.

Thus the spectral properties obtained in the 3.4 for the bipartite hopping problem essentially represents the energy eigenstates of the fermionic hopping problem of Hamiltonian in Eqn. 4.9.

4.3.1 Coupling to external magnetic field and measuring susceptibility

After finding the spectrum of the fermion hopping problem now our task is to calculate the magnetic response of the system from those exact eigenvalues. For that consider a simple physical way to think about the two different spin degrees of freedom at every site in Yao-Lee's model can be interpreting the σs as spins and τs as orbital degrees of freedom. In that picture it is easy to add a Zeeman field B in the z direction as,

$$-B\sum_j \frac{\sigma_j^z}{2} = \frac{iB}{2}\sum_j c_j^x c_j^y = +B\sum_j \left(z_j^\dagger z_j - \frac{1}{2}\right). \tag{4.20}$$

Since this is a bilinear in c, this keeps the model exactly solvable. In our choice of basis in the fermionic Fock space, B maps to a chemical potential for non-interacting canonical (complex) fermions z coupled to a static gauge field, and susceptibility therefore maps to the compressibility of this fermion problem, since in presence of the magnetic field the hopping Hamiltonian becomes

$$H^{YL} = i\begin{pmatrix} z_A^\dagger z_B^\dagger \end{pmatrix}\begin{pmatrix} B & M \\ -M^T & B \end{pmatrix}\begin{pmatrix} z_A \\ z_B \end{pmatrix} + \begin{pmatrix} f^\dagger f \end{pmatrix}\begin{pmatrix} M_A & M^S \\ -M_S & -M_A \end{pmatrix}\begin{pmatrix} f^\dagger \\ f \end{pmatrix} \tag{4.21}$$

Thus, the z-fermions carry the S^z quantum number which is conserved in the presence of the field $B\hat{z}$. As a result we have

$$\langle S_{tot}^z\rangle = \sum_\mu \left(\frac{1}{2} - \frac{1}{e^{(\epsilon_\mu+B)/T}+1}\right) \tag{4.22}$$

and correspondingly the uniform linear susceptibility

$$\chi_{tot}(T) = \sum_\mu \frac{e^{\frac{\epsilon^\mu}{T}}}{T\left(e^{\frac{\epsilon^\mu}{T}}+1\right)^2}. \tag{4.23}$$

A physical picture of magnetization can be the following: As we already know that the DOS is going to diverge at low energy, the spins with energy $E < B$ will be completely polarized and the one with $E > B$ will be completely unpolarized. Thus as one turn on the temperature T , the leading order terms in susceptibility dominated by canonical fermions with energy $E < T$ will be free and will give a Curie response. Rest of the fermions with $E > T$ will have a very small response and will give a sub leading contribution. So the susceptibility at finite T for finite density of diluted sites can be expressed as,

$$\chi(T) \sim \int_0^T \frac{e^{\frac{\epsilon^\mu}{T}}}{T\left(e^{\frac{\epsilon^\mu}{T}}+1\right)^2}\rho(\epsilon)d\epsilon. \tag{4.24}$$

4.4 Site dilution effects

With that physical connection clear, let us look at the effects of site dilution on the magnetic susceptibility of the spin problem.

Contribution of single zero mode Consider a situation in which there is a single zero mode (corresponding to a missing site) in an otherwise gapped spectrum, then susceptibility acquires a Curie tail in the low temperature limit as (expanding Eqn. 4.23)

$$\chi_{tot}(T) = \frac{1}{4T} + ... \tag{4.25}$$

So, the zero mode corresponds to a free spin-half object. In the case where the pure spectrum is gapped, the regular terms are exponentially small at low temperature, as is the susceptibility of the pure problem. Thus, the impurity susceptibility (conventionally defined to be the difference in the susceptibility of the system with defect and the pure system) is given in the low temperature limit as

$$\chi_{imp}(T) = \frac{1}{4T} + ... \tag{4.26}$$

Thus, the missing site gives rise to an impurity spin-half i.e an orphan spin and the zero mode wavefunction essentially defines the orphan spin texture in these problems since this Curie tail is associated with a magnetization pattern $\langle S_j^z \rangle$ controlled by $|\Phi_j^{\mu_0}|^2$ where μ_0 is the zero mode.

Mixing of zero modes Two zero modes mix with each other and develop non- zero energies in the bipartite hopping problems only if they correspond to vacancies on opposite sublattices. As a result, if sites of one sublattice are preferentially diluted in the bipartite problems, one can end up in a situation with $n = |N_A - N_B|$ zero modes that survive this mixing between zero modes. In this case, we would obtain

$$\chi_{imp}(T) = \frac{n}{4T} + ... \tag{4.27}$$

However for finite vacancy density we always consider $N_A = N_B$, so we never encounter this contribution in our case.

Finite vacancy density As discussed before, we can appeal to the density of states results for random site dilution in bipartite hopping problem (Eq. 2.6,2.72.9) to obtain the magnetic susceptibility in the randomly diluted Yao-Lee Hamiltonian using Eq. 4.24. Notice that in both gapped and gapless phases the low temperature susceptibility behaves as

$$\begin{aligned} \chi(T) &\sim \int_0^T \frac{e^{\frac{\epsilon\mu}{T}}}{T\left(e^{\frac{\epsilon\mu}{T}}+1\right)^2}\rho(\epsilon)d\epsilon. \\ &\sim \rho(T) \\ &\sim \frac{1}{T}h(log(1/T)) \end{aligned} \tag{4.28}$$

induced by a finite density of vacancies (equal in number in opposite sublattices) where h is some decreasing function of its argument that makes this density states integrable. This is the form of the susceptibility in a Random-Singlet or Bhatt-Lee type phase as we have seen in the introduction. So it seems from the behavior of low temperature susceptibility that the nature of delocalization-localization transition is very similar in nature as that one obtained for randomly disordered Heisenberg antiferromagnet (Eq. 2.14).

4.5 Discussion

Let us summarize the conclusion and point out some immediate questions which are not answered with some possible extensions of this work.

- We have shown an example of $SU(2)$ symmetric spin model in two dimension where in presence of random dilution the susceptibility shows the "random-singlet" phase like behavior in both of the gapped and gapless phase. We reached at this conclusion by exact numerical solution of the model at very low energy i.e. $E \sim 10^{-150}$ (setting exchange coupling $J = 1$) and since we see such a "random singlet" like behavior at this low energy we conclude that probably this phase is the true low energy phase of the system.

- A physical way to connect the random dilution effects with the random singlet physics can be as follows: The mixing between two zero modes with index, say 1 and 2 kills the Curie terms associated with each and gives rise to a susceptibility which falls of exponentially below an energy scale Δ_{12} . Δ_{12} can therefore be thought of as a renormalized exchange constant which is antiferromagnetic in sign. This is very similar to the real space decimation RG picture of Dasgupta-Ma [42] and it is presumable, since there is a close relationship between the strong disorder RG picture of Ref [39] for low energy states of such bipartite and pure-imaginary random hopping problems, and the strong disorder RG ideas, which is the motivation of the random-singlet description of Bhatt-Lee [44, 52]. However in spite of this connection we don't have a complete physical understanding of the mechanism behind generation of the low energy states. So one need to develop some strong disorder RG picture of the model we study for the same.

- Even though we see the "random singlet" like magnetic susceptibility in both metal and insulator phase, the exact functional form of the same is not clear from this work and the nature of ambiguity is discussed in details in last 3.5. In addition also the precise tracking of the transition point is lacking from this work.

- In this thesis we have only considered the randomly diluted spin model on a bipartite lattice, a very interesting extension of this study could be on a non-bipartite lattice. Random dilution on a non-bipartite lattice is completely different universality class (Discussed in 3.5). So it will be interesting to know the true low temperature behavior for such a system by similar analysis.

Chapter 5

Ground state properties of randomly diluted 2D Heisenberg antiferromagnets

In this chapter, we will discuss our work on the doublet ground state properties of two dimensional Néel ordered Heisenberg antiferromagnet. In the introduction we have briefly mentioned that in this work we characterized an universal relation between the staggered component of doublet ground state magnetization ($\equiv n^z_\uparrow$, Eq. 2.17) with the standard magnetization density of a singlet ground state ($\equiv m$, Eq. 2.16). The universal relation was obtained empirically from numerical experiments on various deformations of $S = 1/2$ SLHAF. Here we provide a detailed characterization of the relationship between $n^z_\uparrow$ and m using spin wave analysis. We also provide two effective low energy models for the understanding of the same namely the sublattice spin mean filed model and quantum rotor model.

Here we will give the details of our study in subsequent sections with the following plan: In first Section 5.1 we define four deformations of the square lattice $S = 1/2$ Heisenberg antiferromagnet relevant to our study. In Section 5.2 we review the empirical results obtained from available numerical data for $n^z_\uparrow$ as well as the full spin texture $\Phi^z(\vec{r})$, focusing on the universal properties alluded to earlier. In Section 5.4, we outline the analytical approaches to the relationship between $n^z_\uparrow$ and m. The first is a large-S spinwave expansion, within which we calculate the ground state spin texture $\Phi^z(\vec{r})$ and its antiferromagnetic Fourier component $n^z_\uparrow$ to leading $\mathcal{O}(1/S)$ order, and demonstrate that such a calculation also yields the universality properties summarized earlier, but does not provide a quantitatively accurate account of the numerical results for $\Phi^z(\vec{r})$ or $n^z_\uparrow(m)$. The second is a mean-field theory formulated in terms of the total spin of each sublattice. And the third approach is in terms of a quantum rotor Hamiltonian which is expected to correctly describe the low-energy tower of states for odd $N_{\rm tot}$. In Section 5.5, we conclude with some speculations about a possible effective field theory approach to the calculation of $\Phi^z(\vec{r})$, as a possible future direction of research.

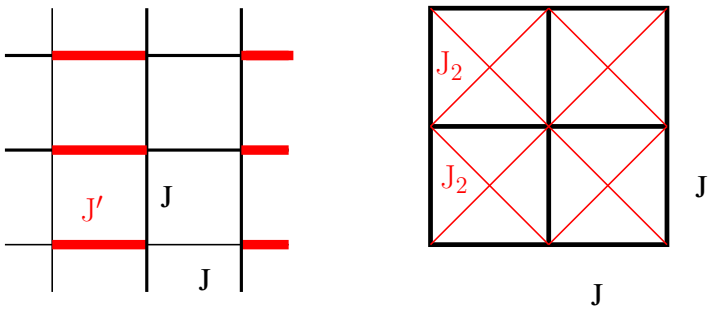

Figure 5.1: An illustration of the interactions present in the JJ' (left panel) and JJ_2 (right panel) model Hamiltonians. In this illustration, black bonds denote exchange interaction strength of J, while a red bond represents exchange strength of J' (J_2) in the left (right) panel

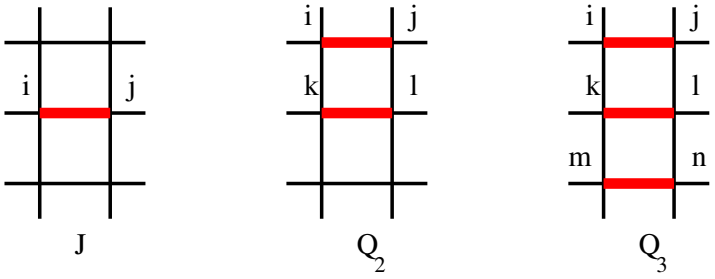

Figure 5.2: Bond and plaquette operators in JQ model Hamiltonians. A thick bond denotes a bipartite projector acting on that bond. All possible orientations of these bond and plaquette operators are allowed.

5.1 Models

Apart from the standard Heisenberg model with nearest neighbor antiferromagnetic interactions, we consider two deformations of the $S = 1/2$ SLHAF in our spin wave analysis study, namely the JJ' and JJ_2 model. The numerical data with which we compare our results considers JJ_2 and two other models called JQ_2 and JQ_3 model. In this section we will explain all four models in detail. However, all of them retain the full $SU(2)$ spin rotation symmetry of the original model.

Heisenberg model with nearest-neighbor interaction We first study the standard Heisenberg model on a square lattice with nearest neighbor interaction,

$$H = J \sum_{\langle i,j \rangle} \mathbf{S}_i . \mathbf{S}_j . \tag{5.1}$$

JJ' **model** The first of these deformed Heisenberg models is the coupled-dimer antiferromagnet, in which there are two kinds of nearest neighbor interactions J and J', as shown in Fig. 5.1 (left panel), where the ratio $\alpha = J'/J$ can be tuned from $\alpha = 1$ to $\alpha = \alpha_c \approx 1.90$ at which collinear

antiferromagnetic order is lost.[34] The Hamiltonian for this system reads:

$$H_{JJ'} = J \sum_{\langle ij \rangle} \mathbf{S}_i \cdot \mathbf{S}_j + J' \sum_{\langle ij \rangle'} \mathbf{S}_i \cdot \mathbf{S}_j, \tag{5.2}$$

where $\langle ij \rangle$ ($\langle ij \rangle'$) denotes a pair of nearest neighbor sites connected by a black (red) bond (see Fig. 5.1).

$J J_2$ model Another deformation of the Heisenberg model, the $J J_2$ model, has additional next nearest neighbor Heisenberg exchange interactions J_2, as shown in Fig. 5.1 (right panel). The Hamiltonian reads

$$H_{JJ_2} = J \sum_{\langle ij \rangle} \mathbf{S}_i \cdot \mathbf{S}_j + J_2 \sum_{\langle\langle ij \rangle\rangle} \mathbf{S}_i \cdot \mathbf{S}_j, \tag{5.3}$$

where $\langle\langle ij \rangle\rangle$ denotes a pair of next nearest neighbor sites. Both these are amenable to straightforward spin-wave theory analyses, and the coupled dimer model can also be studied numerically to obtain numerically exact results even for very large sizes due to the absence of any sign problems in Quantum Monte Carlo studies. However, exact numerical results on the $J J_2$ model are restricted to small sizes since Quantum Monte Carlo methods encounter a sign problem when dealing with next-nearest neighbor interactions on the square lattice.

JQ-models In addition to the $J J_2$ model the numerical observations were studied on two more deformations that involve additional multispin interactions; the "JQ" models.[62, 67] Of these, the JQ_2 model has 4-spin interactions in addition to the usual Heisenberg exchange terms, and is defined by the Hamiltonian

$$H_{JQ_2} = -J \sum_{\langle ij \rangle} P_{ij} - Q_2 \sum_{\langle ij,kl \rangle} P_{ij} P_{kl}, \tag{5.4}$$

where the plaquette interaction Q_2 involves two adjacent parallel bonds on the square lattice as shown in Fig. 5.2 (middle panel) and

$$P_{ij} = \frac{1}{4} - \mathbf{S}_i \cdot \mathbf{S}_j \tag{5.5}$$

is a bipartite singlet projector. The first term in Eq. 5.4 is just the standard Heisenberg exchange.

Similarly, the JQ_3 model has 6-spin interactions and is defined by the Hamiltonian

$$H_{JQ_3} = -J \sum_{\langle ij \rangle} P_{ij} - Q_3 \sum_{\langle ij,kl,nm \rangle} P_{ij} P_{kl} P_{nm}, \tag{5.6}$$

where the plaquette interactions now involve three adjacent parallel bonds on the square lattice, as shown in Fig. 5.2 (right panel). The products of singlet projectors making up the Q_2 and Q_3 terms tend to reduce the Néel order of the ground state, and, when sufficiently strong, lead to a quantum phase transition into a valence-bond-solid state.[62, 67] The numerical results were obtained by staying within the Néel state in both models, and the universal aspects of this state was studied as the Néel order is weakened.

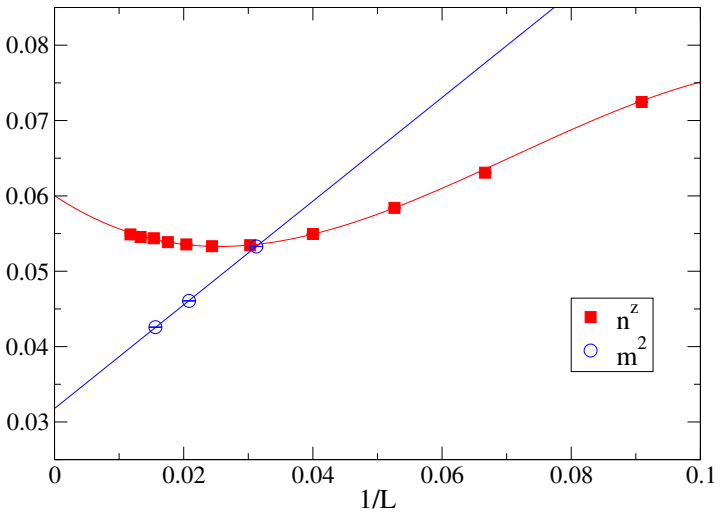

Figure 5.3: An illustrative example of finite size corrections of $n^z_\uparrow$ and m^2, observed in the antiferromagnetic phase of the JJ' model($J' = 1.8$). Note the non-monotonic behavior of finite size corrections for $n^z_\uparrow$, which is fitted to a cubic polynomial. In contrast, finite size data for m^2 is well described by a linear dependence on $1/L$.

5.2 Review of numerical results

The available numerical results for this systems were obtained by total spin-$1/2$ sector version [68] of the valence-bond basis projector QMC method [69, 70] to study $L \times L$ samples with L odd and free boundary conditions. By that method $\Phi^z(\vec{r})$ and $n^z_\uparrow$ were computed in such samples for the JJ' model and JQ models in their antiferromagnetic phase. On the other hand the same models on $L \times L$ lattices with L even and periodic boundary conditions, were studied using the original singlet sector valence bond projector QMC method. In next two paragraphs we will highlight the two main features observed from numerical experiments i.e. non monotonicity in finite size scaling, the universality relation between $n^z_\uparrow$ and m described before and the spin texture.

Finite size scaling : The finite size scaling data for $n^z_\uparrow$ from a sequence of $L \times L$ systems with L odd, shows that $n^z_\uparrow$ extrapolates to a finite value in the $L \to \infty$ limit as long as the system is in the antiferromagnetic phase. However, we noted from the numerical data that the approach of this observable to the thermodynamic limit has a non-monotonic behavior. To obtain accurate extrapolations to infinite size, it is therefore necessary to fit the finite size data to a third-order polynomial in $1/L$. We find that the coefficient for the leading $1/L$ term in this polynomial is rather small; this is true for all the models studied here, as long as they remain in the antiferromagnetic phase. In Fig. 5.3 and Fig. 5.4, we show examples of this behavior of the finite size corrections in $n^z_\uparrow$. In these figures, we also show the approach to the thermodynamic limit for m, as measured in a sequence of periodic $L \times L$ systems with L even. We find that in complete contrast to the behavior of $n^z_\uparrow$, m extrapolates monotonically to the thermodynamic limit, with a dominant $1/L$ dependence—this is consistent with previous studies of the

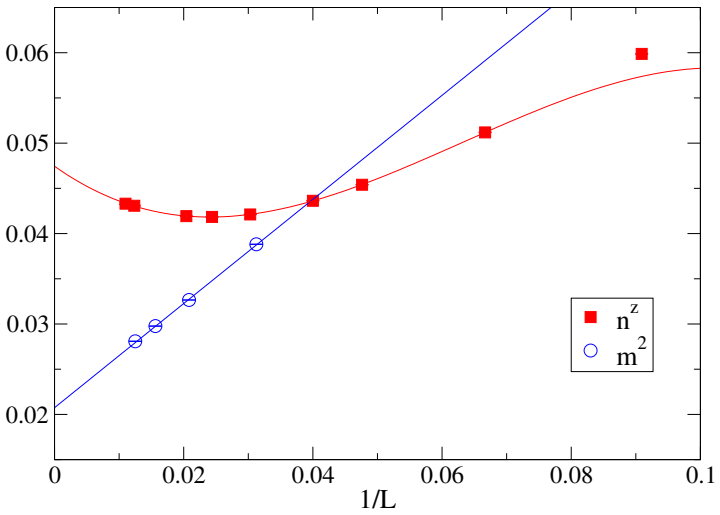

Figure 5.4: Another illustrative example of finite size corrections of $n^z_\uparrow$ and m^2, observed in the antiferromagnetic phase of JQ_2 model at $Q_2 = 1.0$. Again, note the non-monotonic behavior of finite size corrections for $n^z_\uparrow$, which is fitted to a cubic polynomial (only $L > 20$ data used in the fit). In contrast, finite size data for m^2 is well described by a linear dependence on $1/L$.

structure factor in square lattice antiferromagnets [70] (however, with spatially anisotropic couplings, one can also observe strong non-monotonicity in m[71]). In section 5.4 on our spin wave analysis of this problem, we will provide a more detailed characterization of this non-monotonic behavior of finite size scaling.

Universal relation between $n^z_\uparrow$ and m : The non-zero value of $n^z_\uparrow$ in the thermodynamic limit clearly reflects the long-range antiferromagnetic order present in the system and a partial breaking of the SU(2) symmetry (due to the fact that we study only one member of the doublet ground state). For periodic systems, the same long range antiferromagnetic order is captured by the non-zero value of m in the large L limit—and a calculation of m (through $\langle m^2 \rangle$) for the odd-L systems with periodic boundaries would of course lead to the same value. However, since $m_0 \neq n^z_\uparrow$, the full staggered magnetization is not forced to lie along the z spin axis, so it could be interesting to understand the relationship between these two measures of antiferromagnetic order.

To empirically characterize this relation, the numerical data is plotted as $n^z_\uparrow$ versus m in the thermodynamic limit of the JJ', JQ_2 and JQ_3 models in Fig. 5.5. In that figure, *each* point represents the result of a careful extrapolation similar to the examples shown in Fig. 5.3 and Fig. 5.4, and provides an accurate estimate of the corresponding thermodynamic limits for $n^z_\uparrow$ and m. So from this figure the conclusion is that $n^z_\uparrow$ is a universal function of m_0 independent of the microscopic structure of the Hamiltonian. To model this universal function, we use a polynomial fit that is constrained to ensure that $n^z_\uparrow \to \frac{m_0}{3}$ when $m_0 \to \frac{1}{2}$; the rationale for this constraint will become clear in Sec. 5.4. We find

(Fig. 5.5) that the QMC results for $n^z_\uparrow(m_0)$ are fit well by the following functional form:

$$n^z_\uparrow(m) = (\frac{1}{3} - \frac{a}{2} - \frac{b}{4})m_0 + am_0^2 + bm_0^3 \,, \tag{5.7}$$

with $a \approx 0.288$ and $b \approx -0.306$.

Spin texture : As discussed in the introduction, one can think this universal relationship as being a property of the underlying low energy effective field theory of the antiferromagnetic phase, one is led to expect that the full spatial structure of the spin texture $\Phi^z(\vec{r})$ should also be universal. More precisely, one is led to expect $\widetilde{\Phi}^z(\vec{q})$, the Fourier transformation of $\Phi^z(\vec{r})$ should be peaked at the antiferromagnetic vector $\mathbf{Q} = (\pi, \pi)$, with a universal shape near the peak.

To test this, we compare the spin texture in the JJ' model and the JQ_3 model, choosing the strengths of the J' interaction and the Q_3 interaction so that both have the same value of m_0, and therefore the same value of $n^z_\uparrow$. This is shown in Fig. 5.6, which shows that these very different microscopic Hamiltonians have spin-textures whose Fourier transform falls on top of each other at and around the antiferromagnetic wavevector.

5.3 Analytical approach to the problem

We now present three distinct analytical approaches to understanding these numerical results presented in the previous section: First, we develop a spin-wave expansion that becomes asymptotically exact for large S[35]. Second, we explore a mean-field theory written in terms of the total spin of each sublattice. Third, we describe an alternative approach in which the low-energy antiferromagnetic tower of states of a spin-$1/2$ antiferromagnet is described by a phenomenological rotor model[36] adapted to the case of a system with odd $N_{\rm tot}$.

5.4 Spin-wave expansion

In this subsection we will first set up the general framework for spin wave calculations, followed by that we will discuss the subtleties of the spin-wave calculation with open boundaries in a odd sized sample, next we will describe the method of our calculation and finally the results. The standard spin wave calculations for systems with even size and periodic boundaries are presented in appendix-3. The leading order spin-wave calculation proceeds as usual by using an approximate representation of spin operators in terms of Holstein-Primakoff bosons. The resulting bosonic Hamiltonian is truncated to leading (quadratic) order in boson operators to obtain the first quantum corrections to the classical energy of the system.

General framework of spin-wave theory As is standard in the spin wave theory of Néel ordered states, we start with the classical Néel ordered configuration with the Néel vector pointing along the $\hat{z}$ axis, which corresponds to $S^z_{\vec{r}} = \eta_{\vec{r}} S$(as before, $\eta_{\vec{r}}$ is $+1$ for sites belonging to the A sublattice,

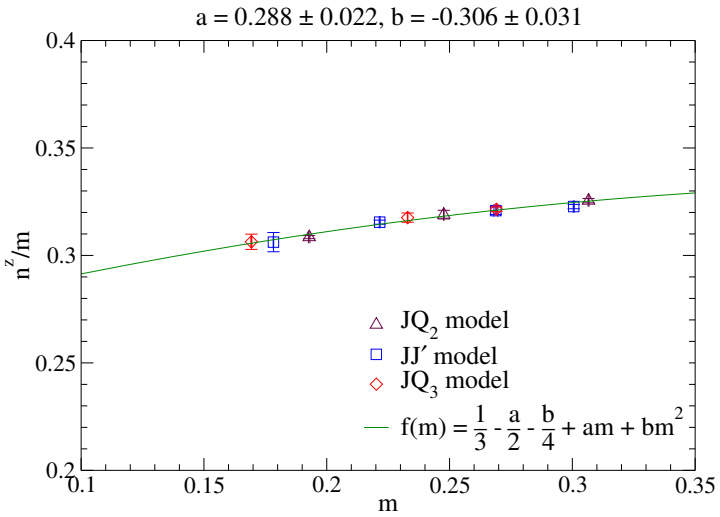

Figure 5.5: Extrapolated thermodynamic values of $n^z_\uparrow$ for three different models of antiferromagnets on an open lattice, plotted as function of staggered magnetization m_0 for the same models on periodic lattices. The former is clearly an universal function of the later. This universal function can be well approximated by a polynomial fit constrained to ensure that $n^z_\uparrow(m_0) \to m_0/3$ in the limit of $m_0 \to \frac{1}{2}$: $n^z_\uparrow \approx (1/3 - a/2 - b/4)m_0 + am_0^2 + bm_0^3$, with $a \approx 0.288$ and $b \approx -0.306$.

and -1 for sites belonging to the B sublattice). We then represent the spin operators at a site $\vec{r}$ of the square lattice in terms of canonical bosons to leading order in S as follows: For sites $\vec{r}$ belonging to the A sublattice we write

$$S^+_{\vec{r}} = \sqrt{2S} b_{\vec{r}}\,; \;\; S^z_{\vec{r}} = S - b^\dagger_{\vec{r}} b_{\vec{r}}\,, \tag{5.8}$$

while on sites $\vec{r}$ belonging to the B sublattice we write

$$S^-_{\vec{r}} = \sqrt{2S} b_{\vec{r}}\,; \;\; S^z_{\vec{r}} = -S + b^\dagger_{\vec{r}} b_{\vec{r}}\,. \tag{5.9}$$

The number of bosons at each site thus represents the effect of quantum fluctuations away from the classical Néel ordered configuration.

To quadratic order in the boson operators, this expansion yields the following spin wave Hamiltonian in the general case (with arbitrary two-spin exchange couplings):

$$\begin{aligned} H^{sw} &= \epsilon_{cl} S^2 + \frac{S}{2} \mathbf{b}^\dagger M \mathbf{b}\,, \text{ with} \\ & M_{\vec{r}\vec{r}'} = \begin{pmatrix} A_{\vec{r}\vec{r}'} & B_{\vec{r}\vec{r}'} \\ B_{\vec{r}\vec{r}'} & A_{\vec{r}\vec{r}'} \end{pmatrix} \\ & \mathbf{b}_{\vec{r}} = \begin{pmatrix} b_{\vec{r}} \\ b^\dagger_{\vec{r}} \end{pmatrix}\,. \end{aligned} \tag{5.10}$$

Here $\epsilon_{cl} S^2$ is the classical energy of the Néel state, M in the first line is a $2N_{\rm tot}$ dimensional matrix specified in terms of $N_{\rm tot}$ dimensional blocks A and B, and $\mathbf{b}$ is a $2N_{\rm tot}$ dimensional column vector as indicated above. Elements of A and B can be written explicitly as

$$A_{\vec{r}\vec{r}'} = (Z^U_{\vec{r}} - Z^F_{\vec{r}})\delta_{\vec{r}\vec{r}'} + J^F_{\vec{r}\vec{r}'}, \tag{5.11}$$

$$B_{\vec{r}\vec{r}'} = J^U_{\vec{r}\vec{r}'}. \tag{5.12}$$

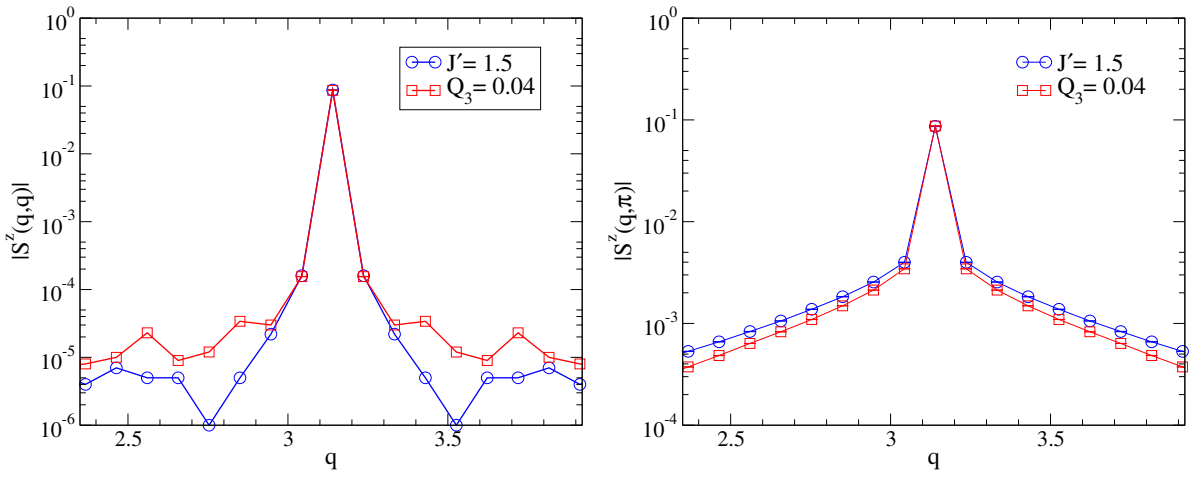

Figure 5.6: Fourier transform (with antiperiodic boundary conditions assumed for convenience) of the numerically computed (for JJ' and JQ_3 model with $L = 65$, $S = 1/2$) $\Phi^z(\vec{r})$ along cuts passing through the antiferromagnetic wavevector (π, π). Note the universality of the results in the neighborhood of the antiferromagnetic wavevector, which in any case accounts for most of the weight in Fourier space.

In the above, $J^F_{\vec{r}\vec{r}'}$ are Heisenberg exchange couplings between two sites $\vec{r}$ and $\vec{r}'$ belonging to the same sub-lattice, $J^U_{\vec{r}\vec{r}'}$ are the Heisenberg exchange couplings between sites belonging to different sublattices, and

$$Z^U_{\vec{r}} = \sum_{\vec{r}'} J^U_{\vec{r}\vec{r}'}, \tag{5.13}$$

$$Z^F_{\vec{r}} = \sum_{\vec{r}'} J^F_{\vec{r}\vec{r}'}. \tag{5.14}$$

The effects of quantum fluctuations on the classical Néel state can now be calculated by diagonalizing this Hamiltonian by a canonical Bogoliuov transformation $\mathbb{S}$ which relates the Holstein-Primakoff bosons b to the bosonic operators γ corresponding to spin-wave eigenstates

$$\mathbf{b} = \mathbb{S}\Gamma, \quad \Gamma_\mu = \begin{pmatrix} \gamma_\mu \\ \gamma^\dagger_\mu \end{pmatrix}, \tag{5.15}$$

where $\mathbb{S}$ is a $2N_{\rm tot}$ dimensional matrix that transforms from $\mathbf{b}$ which creates and destroys bosons at specific lattice sites $\vec{r}$ to Γ which creates and destroys spin-wave quanta in specific spin-wave modes μ. We want H^{sw} be *diagonal* in this new basis. We represent this diagonal form as

$$H^{sw} = \epsilon_{cl} S^2 + \frac{S}{2} \Gamma^\dagger D \Gamma \,, \tag{5.16}$$

where

$$D = \begin{pmatrix} \Lambda & 0 \\ 0 & \Lambda \end{pmatrix}, \tag{5.17}$$

with Λ denoting the diagonal matrix with the $N_{\rm tot}$ positive spin wave frequencies λ_μ on its diagonal.

To construct a $\mathbb{S}$ that diagonalizes H^{sw} in the Γ basis, we look for $2N_{\rm tot}$ dimensional column vectors

$$y^{\mu} = \begin{pmatrix} u^{\mu} \\ v^{\mu} \end{pmatrix} , \tag{5.18}$$

which satisfy the equation

$$My^{\mu} = \epsilon_{\mu} \mathcal{I} y^{\mu} \tag{5.19}$$

with *positive* values of ϵ_{μ} equal to the positive spin-wave frequencies λ_{μ} for $\mu = 1, 2, 3 \ldots N_{\rm tot}$. Here u^{μ} and v^{μ} are $N_{\rm tot}$ dimensional vectors,

$$\mathcal{I} = \begin{pmatrix} \mathbf{1} & \mathbf{0} \\ \mathbf{0} & -\mathbf{1} \end{pmatrix} , \tag{5.20}$$

and $\mathbf{1}$ is the $N_{\rm tot} \times N_{\rm tot}$ identity matrix. With these y^{μ} in hand, one may obtain $N_{\rm tot}$ additional solutions to Eq. 5.19, this time with *negative* $\epsilon_{N_{\rm tot}+\mu} = -\lambda_{\mu}$ by interchanging the roles of the $N_{\rm tot}$ dimensional vectors u_{μ} and v_{μ} in this construction. In other words, we have

$$y^{N_{\rm tot}+\mu} = \begin{pmatrix} v^{\mu} \\ u^{\mu} \end{pmatrix} , \tag{5.21}$$

with $\mu = 1, 2, 3 \ldots N_{\rm tot}$.

We now construct $\mathbb{S}$ by using these y^{μ} (with $\mu = 1, 2, 3 \ldots 2N_{\rm tot}$) as its $2N_{\rm tot}$ columns:

$$\mathbb{S} = \left(y^1, y^2, y^3 \ldots y^{2N_{\rm tot}} \right) . \tag{5.22}$$

Clearly, this choice of $\mathbb{S}$ satisfies the equation

$$M\mathbb{S} = \mathcal{I}\mathbb{S}\mathcal{I}D \tag{5.23}$$

Furthermore, the requirement that the Bogoliuov transformed operators γ obey the same canonical bosonic commutation relations as the b operators implies that $\mathbb{S}$ must satisfy

$$\mathbb{S}^{\dagger}\mathcal{I}\mathbb{S} = \mathcal{I} , \tag{5.24}$$

This constraint is equivalent to "symplectic" orthonormalization conditions:

$$\begin{aligned} (u^{\mu})^{\dagger} u^{\nu} - (v^{\mu})^{\dagger} v^{\nu} &= \delta_{\mu\nu} , \\ (u^{\mu})^{\dagger} v^{\nu} - (v^{\mu})^{\dagger} u^{\nu} &= 0 , \end{aligned} \tag{5.25}$$

for $\mu, \nu = 1, 2, 3 \ldots N_{\rm tot}$. It is now easy to see that Eq. 5.23 and Eq. 5.24 guarantee that H^{sw} is indeed diagonal in the new basis, since

$$\mathbf{b}^{\dagger} M \mathbf{b} = \Gamma^{\dagger}\mathbb{S}^{\dagger} M \mathbb{S}\Gamma = \Gamma^{\dagger}\mathbb{S}^{\dagger}\mathcal{I}\mathbb{S}\mathcal{I}D\Gamma = \Gamma^{\dagger} D \Gamma . \tag{5.26}$$

For periodic samples, it is possible to exploit the translational invariance of the problem and work in Fourier space to obtain these spin-wave modes and their wavefunctions and calculate $m_0 = S - \Delta^{'}$ correct to leading order in the spin-wave expansion—these results are standard[33], they are provided in details on Appendix-2. On the other hand, the corresponding results for $L \times L$ samples with free boundary conditions and $N_A = N_B + 1$ do not seem to be available in the literature, and our discussion below focuses on this case.

Odd sized samples with free boundary We begin by noting that the non-zero entries in A only connect two sites belonging to the same sublattice, while those in B always connect sites belonging to opposite sublattices. As a result of this, the solutions to the equation for y^μ can also be expressed in terms of a single function $f_\mu(\vec{r})$ defined on sites of the lattice.

To demonstrate this, we consider an auxiliary problem of finding $\tilde{\epsilon}_\mu$ such that the operator $A - B - \tilde{\epsilon}_\mu \eta_{\vec{r}}$ has a zero mode $f_\mu(\vec{r})$. This auxiliary problem has $N_{\rm tot}$ solutions corresponding to the $N_{\rm tot}$ roots $\tilde{\epsilon}_\mu$ of the polynomial equation $\det(A - B - \tilde{\epsilon}_\mu \eta_{\vec{r}}) = 0$; these $\tilde{\epsilon}_\mu$ can be of either sign. To make the correspondence with the *positive* ϵ_μ solutions (u^μ, v^μ) (with $\mu = 1, 2 ... N_{\rm tot}$) of the original equation $My^\mu = \epsilon_\mu \mathcal{I} y^\mu$, we now note that

$$\langle f_\mu | A - B | f_\mu \rangle = \tilde{\epsilon}_\mu N_\mu \tag{5.27}$$

where

$$N_\mu \equiv \sum_{r_A} |f_\mu(r_A)|^2 - \sum_{r_B} |f_\mu(r_B)|^2. \tag{5.28}$$

Since $A - B$ is a positive (but not positive definite) operator, this implies that $\tilde{\epsilon}_\mu$ has the same sign as N_μ for all non-zero $\tilde{\epsilon}_\mu$. To make the correspondence with the positive $\epsilon_\mu \equiv \lambda_\mu$ solutions ($\mu = 1, 2 \ldots N_{\rm tot}$) of the original problem, we can therefore make the ansatz

$$\begin{aligned} u^\mu_{\vec{r}_A} &= f_\mu(r_A)/\sqrt{N_\mu}, u^\mu_{r_B} = 0 \\ v^\mu_{r_B} &= -f_\mu(r_B)/\sqrt{N_\mu}, v^\mu_{r_A} = 0 \end{aligned} \tag{5.29}$$

if $N_\mu > 0$, or the alternative ansatz

$$\begin{aligned} u^\mu_{r_B} &= -f_\mu(r_B)/\sqrt{-N_\mu}, u^\mu_{r_A} = 0 \\ v^\mu_{r_A} &= f_\mu(r_A)/\sqrt{-N_\mu}, v^\mu_{r_B} = 0 \end{aligned} \tag{5.30}$$

if $N_\mu < 0$. Here, r_A (r_B) denotes sites belonging to the A (B) sublattice of the square lattice. This ansatz clearly ensures that the y^μ (with $\mu = 1, 2..N_{\rm tot}$) obtained in this manner satisfy the original equation with positive $\epsilon_\mu \equiv \lambda_\mu$ and are appropriately normalized.

Treatment of zero modes The above approach we took for demonstration purpose is not the one we use in our actual computations (see below), but it provides a useful framework within which we may discuss possible zero frequency spin-wave modes, *i.e* $\lambda_{\mu_0} = 0$ for some μ_0: A mode μ_0 with $\lambda_{\mu_0} = 0$ clearly corresponds to a putative zero eigenvalue of the operator $A - B$. From the specific

form of $A-B$ in our problem, it is clear that such a zero eigenvalue does indeed exist, and $f_{\mu_0}(\vec{r})$, the corresponding eigenvector of $A-B$, can be written down explicitly as

$$f_{\mu_0}(\vec{r}) = 1 \tag{5.31}$$

Since this corresponds to the root $\tilde{\epsilon}_{\mu_0} = 0$ of the auxiliary problem, it can *in principle* be used to obtain a *pair* of zero frequency modes ϵ_{μ_0} and $\epsilon_{\mu_0+N_{\rm tot}}$ for the original problem of finding ϵ_μ and y^μ that satisfy $My^\mu = \epsilon_\mu \mathcal{I} y^\mu$.

However, we need to ensure that the symplectic orthonormalization conditions (Eq. 5.26) are satisfied by our construction of the corresponding y^{μ_0} and $y^{\mu_0+N_{\rm tot}}$. This is where the restriction to a $N_{\rm tot} = L \times L$ lattice with $N_A = N_B + 1$ enters our discussion. For this case, $N_{\mu_0} = N_A - N_B = 1$, and we are thus in a position to write down properly normalized zero-mode wavefunctions:

$$\begin{aligned} u^{\mu_0}_{\vec{r}_A} = f_{\mu_0}(r_A), u^{\mu_0}_{r_B} = 0 \\ v^{\mu_0}_{r_B} = -f_{\mu_0}(r_B), v^{\mu_0}_{r_A} = 0 \ , \end{aligned} \tag{5.32}$$

and

$$\begin{aligned} u_r^{N_{\rm tot}+\mu_0} = v_r^{\mu_0}, \\ v_r^{N_{\rm tot}+\mu_0} = u_r^{\mu_0} \ . \end{aligned} \tag{5.33}$$

[Parenthetically, we note that the question of zero frequency spinwave modes for the more familiar case with $N_A = N_B$ and periodic boundary conditions has been discussed earlier in the literature[35] and will not be considered here.]

Thus, the equation $My^\mu = \epsilon_\mu \mathcal{I} y^\mu$ has a pair of zero modes related to each other by interchange of the u and v components of the mode, and it becomes necessary to regulate intermediate steps of the calculation with a staggered magnetic field $\hat{z}\epsilon_h \eta_{\vec{r}}$ with infinitesimal magnitude $\epsilon_h > 0$ in the $\hat{z}$ direction. Denoting the corresponding A by A^{ϵ_h}, we see that $A^{\epsilon_h} - B$ is now a positive definite operator and does not have a zero eigenvalue. Indeed, it is easy to see from the foregoing that the corresponding eigenvalue now becomes non-zero, yielding a positive spin-wave frequency $\lambda^{\epsilon_h}_{\mu_0} = N_{\rm tot}\epsilon_h$. One can also calculate the $\mathcal{O}(\epsilon_h)$ term of $f^{\epsilon_h}_{\mu_0}(\vec{r})$ and check that $f^{\epsilon_h}_{\mu_0}$ tends to $f_{\mu_0}(\vec{r})$ in a non-singular way as $\epsilon_h \to 0$, from which one can obtain the corresponding $y^{\mu_0}(\epsilon_h)$ analytically in this limit. Thus, the contribution of the zero mode to all physical quantities can be obtained in the presence of a small $\epsilon_h > 0$, and the $\epsilon_h \to 0$ limit of this contribution can then be taken smoothly and analytically at the end of the calculation.

Treatment of non-zero modes In our actual calculations, we use this analytical understanding of the zero frequency spin wave mode to analytically obtain the properly regularized zero mode contribution to various physical quantities, while using a computationally convenient approach to numerically calculate the contribution of the non-zero spin wave modes. To do this, we rewrite Eq. 5.19 for

$\mu = 1, 2, 3 \ldots N_{\rm tot}$ as

$$\begin{aligned} (A+B)\phi^\mu &= \lambda_\mu \psi^\mu \\ (A-B)\psi^\mu &= \lambda_\mu \phi^\mu \end{aligned} \tag{5.34}$$

where

$$\begin{aligned} \phi^\mu &= u^\mu + v^\mu \\ \psi^\mu &= u^\mu - v^\mu. \end{aligned} \tag{5.35}$$

This implies

$$(A-B)(A+B)\phi^\mu = \lambda_\mu (A-B)\psi^\mu = \lambda_\mu^2 \phi^\mu \tag{5.36}$$

$$(A+B)(A-B)\psi^\mu = \lambda_\mu (A+B)\phi^\mu = \lambda_\mu^2 \psi_\mu \tag{5.37}$$

We now decompose

$$A - B = K^\dagger K. \tag{5.38}$$

where

$$K = \sqrt{\omega} U. \tag{5.39}$$

with ω the diagonal matrix with diagonal entries given by eigenvalues of the real symmetric matrix $A - B$, and U the matrix whose rows are made up of the corresponding eigenvectors.

With this decomposition, we multiply Eq 5.37 by K from the left to obtain

$$K(A+B)K^\dagger \chi^\mu = \lambda_\mu^2 \chi^\mu. \tag{5.40}$$

with $\chi^\mu = K\psi^\mu$. From the solution to this equation, we may obtain the ϕ as

$$\phi^\mu = (K^\dagger)\chi^\mu / \lambda_\mu. \tag{5.41}$$

and thence obtain ψ^μ using Eq. 5.35. In order to ensure the correct normalization of the resulting u^μ, v^μ, we impose the normalization condition

$$(\chi^\mu)^\dagger \chi^\mu = \lambda_\mu. \tag{5.42}$$

Thus our computational strategy consists of obtaining eigenvalues of the symmetric operator $K(A+B)K^\dagger$, and using this information to calculate the y^μ and thence the Bogoliuov transform matrix $\mathbb{S}$. Notwithstanding the normalization used in Eq. 5.42, the zero mode with $\lambda_{\mu_0} = 0$ causes no difficulties in this approach, since we work in practice with the projection of $K(A+B)K^\dagger$ in the space orthogonal to the zero mode. This is possible because we already have an analytic expression correct to $\mathcal{O}(\epsilon_h)$ for $y^{\mu_0}(\epsilon_h)$ and $y^{N_{\rm tot}+\mu_0}(\epsilon_h)$ corresponding to this zero mode, and do *not* need to determine these two columns of $\mathbb{S}$ by this computational method.

Putting all modes together, to the final expression of $n_\uparrow^z$ We use this procedure to calculate the zero temperature boson density as

$$\langle b_{\vec{r}}^\dagger b_{\vec{r}} \rangle = \lim_{\epsilon_h \to 0} \sum_{\mu=1}^{N_{\rm tot}} \left(v_{\vec{r}}^{\mu}(\epsilon_h) \right)^2 . \tag{5.43}$$

In this expression, one may use the numerical procedure outlined above to obtain the contribution of all $\mu \neq \mu_0$ *directly at* $\epsilon_h = 0$, while being careful to use our analytical results for $v^{\mu_0}(\epsilon_h)$ to obtain the limiting value of the contribution from $\mu = \mu_0$. This gives

$$\langle b_{\vec{r}_A}^\dagger b_{\vec{r}_A} \rangle = \sum_{\mu \neq \mu_0} (v_{\vec{r}_A}^{\mu})^2 \tag{5.44}$$

$$\langle b_{iB}^\dagger b_{iB} \rangle = 1 + \sum_{\mu \neq \mu_0} (v_{\vec{r}_B}^{\mu})^2 \tag{5.45}$$

Here, the distinction between sites on the A and B sublattices arises in this final result because $\lim_{\epsilon_h \to 0} v_{\vec{r}}^{\mu_0}(\epsilon_h) = -1$ for $\vec{r}$ belonging to the B sublattice, while $\lim_{\epsilon_h \to 0} v_{\vec{r}}^{\mu_0}(\epsilon_h) = 0$ for $\vec{r}$ belonging to the A sublattice.

Knowing the average boson number at each site gives us the first quantum corrections to the ground state expectation value $\langle S^z(\vec{r}) \rangle$:

$$\langle S^z(\vec{r}) \rangle = \eta_{\vec{r}} (S - \langle b_{\vec{r}}^\dagger b_{\vec{r}} \rangle) \tag{5.46}$$

This result for the spin-wave corrections to the ground state spin texture then allows us to write $n_\uparrow^z = \lim_{L \to \infty} (\sum_{\vec{r}} \eta_{\vec{r}} \langle S^z(\vec{r}) \rangle)/N_{\rm tot}$ as

$$n_\uparrow^z = S - \Delta \tag{5.47}$$

where Δ represents the leading spin-wave correction to the classical value for $n_\uparrow^z$.

Finite size scaling from spin wave theory

In order to obtain $n_\uparrow^z$ reliably in this manner, it is important to understand the finite size scaling properties of Δ for various values of $J^{'}/J$ in the striped interaction model and J_2/J in the model with next-nearest neighbor interactions. In addition we also want to understand the surprising non-monotonicity in scaling behavior from the spin-wave theory. In Fig. 5.7, we show a typical example of this size dependence. As is clear, we find that Δ has a non monotonic dependence on L: Δ initially increases rapidly with size, and, after a certain crossover size L^*, it starts decreasing slowly to finally saturate to its asymptotic value. This non-monotonic behavior is qualitatively similar to that observed in the finite size extrapolations of $n_\uparrow^z$ from our QMC data earlier. To explore this unusual size dependence further and reliably extrapolate to the thermodynamic limit, we analyze the contributions to Δ from the spin-wave spectrum in the following way: We note that there is always a monotonically and rapidly convergent $\mathcal{O}(1)$ contribution to Δ from the lowest frequency spin-wave mode, whose spin-wave frequency scales to zero as $1/N_{\rm tot}$ (for any finite $N_{\rm tot}$, this is *not* an exact zero mode of the system). We dub this the 'delta-function contribution' and its thermodynamic limit is easy to reliably extrapolate

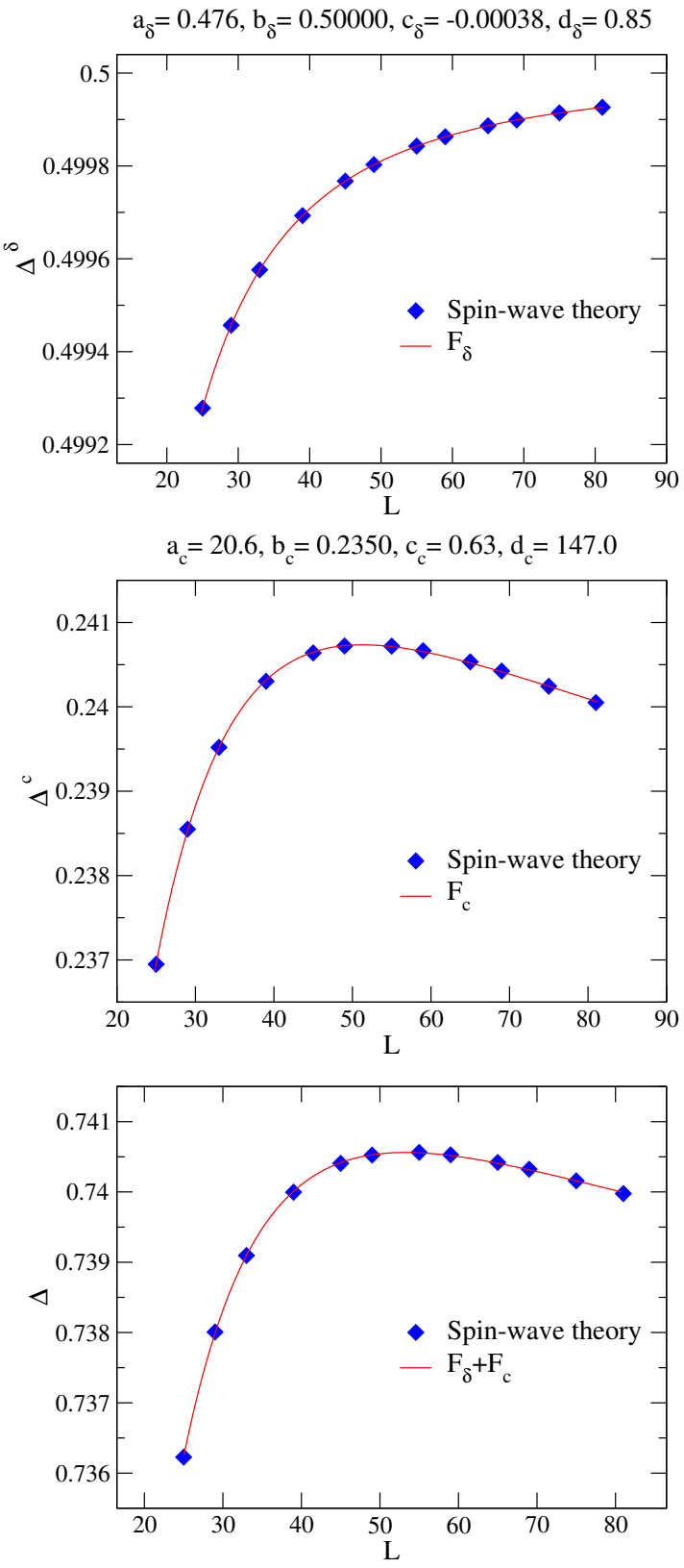

Figure 5.7: A typical example of the finite size scaling of the delta-function and continuum contributions to Δ. Note the monotonically increasing size dependence of the delta-function contribution, and the non-monotonic and more slowly converging nature of the continuum contribution. Due to this difference in their behavior, we find it more accurate to separately fit each of these contributions to a polynomial in $1/L$ and use this to obtain the thermodynamic limit of the total Δ. Here $F_{\delta/c}(L) = b_{\delta/c} + c_{\delta/c}/L - a_{\delta/c}/L^2 + d_{\delta/c}/L^3$.

to. In addition, there is a 'continuum contribution' coming from all the other spin-wave modes, each of which contributes an amount of order $\mathcal{O}(1/N_{\rm tot})$. This contribution converges less rapidly to the thermodynamic limit, and also happens to be non-monotonic: it first increases quickly with increasing size, and then starts decreasing slowly to finally saturate to the thermodynamic limit.

The delta-function contribution can be fit best to a functional form

$$F_\delta(L) = b_\delta + \frac{c_\delta}{L} - \frac{a_\delta}{L^2} + \frac{d_\delta}{L^3}, \tag{5.48}$$

with the dominant $1/L^2$ term accounting for the monotonic increase with L, while the continuum contribution is fit to

$$F_c(L) = b_c + \frac{c_c}{L} - \frac{a_c}{L^2} + \frac{d_c}{L^3}, \tag{5.49}$$

whereby the size dependence is predominantly determined by the competition between the term proportional to $1/L$ which decreases with increasing L, and the term proportional to $1/L^2$ which increases with increasing L. This gives rise to non-monotonic behavior whereby the continuum contribution first increases rapidly and then decreases slowly beyond a crossover length L^* to finally saturate to its infinite volume limit. We also find that the length L^* gets larger as we deform away from the pure square lattice antiferromagnet, making it harder to obtain reliable extrapolations to the thermodynamic limit.

5.4.1 Universality from spin wave theory

Using such careful finite-size extrapolations to obtain Δ for various values of J_2/J and $J^{'}/J$, we compare the result with Δ' calculated analytically. Specifically, we now ask if the universality seen in our QMC results is reflected in these semiclassical spin-wave corrections to $n^z_\uparrow$ and m_0. The answer is provided by Fig. 5.8, which shows that the numerically obtained spin-wave corrections apparently satisfy a universal linear relationship

$$\Delta - \Delta' \approx 1.003 + 0.013\Delta' \tag{5.50}$$

as one deforms away from the pure square lattice antiferromagnet in various ways.

What does this imply for $n^z_\uparrow(m_0)$ to leading order in $1/S$? To answer this, we note that

$$\frac{n^z_\uparrow}{m_0} = 1 - \frac{\Delta - \Delta'}{S} + \mathcal{O}(S^{-2}) \tag{5.51}$$

Using our numerically established universal result to relate $\Delta - \Delta'$ to Δ' and thence to m_0 itself, we obtain the universal relationship (upto leading order in $1/S$),

$$n^z_\uparrow = \alpha m_0 + \beta m_0^2 \tag{5.52}$$

with $\alpha \approx 0.987 - 1.003/S$ and $\beta \approx 0.013/S$. However, being a large-S expansion, spin-wave theory is unable to give a quantitatively correct prediction for $n^z_\uparrow(m_0)$ for the $S = 1/2$ case.

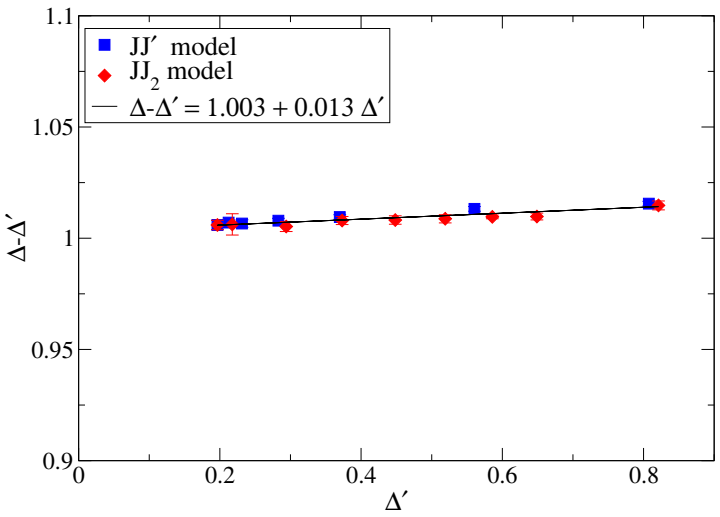

Figure 5.8: $\Delta - \Delta'$, the difference between the leading spin wave corrections to $n_{\uparrow}^{z}$ and m_0, plotted against the leading spin-wave corrections Δ' to m_0 for the $JJ^{'}$ and JJ_2 models described in the text.

Spin texture from spin-wave theory Finally, we use our spin-wave predictions for the ground-state spin texture to look at the Fourier transform of the spin-texture for various deformations of the pure antiferromagnet. The results are shown in Fig. 5.9, which demonstrates that spin-wave theory also predicts that the Fourier transform of the spin-texture near the antiferromagnetic wave-vector is a universal function of the wavevector; this provides some rationalization for the observed universality of the Fourier transformed spin texture seen in our QMC numerics.

5.4.2 Sublattice-spin mean-field theory

We now turn to a simple mean-field picture in terms of the dynamics of the total spins $\vec{L}_A$ and $\vec{L}_B$ of the A and B sublattices respectively, for an antiferromagnet composed of spin-S moments at every site. The idea of this mean-field theory is to approximately model the true low-energy spectrum of the spin-S antiferromagnet by that of a model in which the N_A, A-sublattice spins form a giant moment $\vec{L}_A$, coupling antiferromagnetically with a similar giant moment $\vec{L}_B$ formed by the N_B, B-sublattice spins. At the end of this section, we will see the limitations and scopes of such a simple picture.

Now in our case with $N_A = N_B + 1$, it is clearly appropriate to assume that the total spin quantum number of $\vec{L}_B$ as $S_B \equiv SN_B$ while the total spin quantum number of $\vec{L}_A$ should be taken to be $S_A \equiv SN_A = S_B + S$. In this mean-field treatment, we assume the following low-energy effective Hamiltonian describes the dynamics of $\vec{L}_A$ and $\vec{L}_A$,

$$H_{MF} = J_{MF}\vec{S}_A \cdot \vec{S}_B \tag{5.53}$$

with $J_{MF} > 0$. Within this mean-field treatment, the $S_{\rm tot} = S$ ground-state multiplate expected from the Lieb-Mattis theorem for an odd sized sample is thus modeled by the $S_{\rm tot} = S$ multiplate obtained by the quantum mechanical addition of angular momenta $S_B \equiv SN_B$ and $S_A = S_B + 1/2$. Within

this mean-field theory, $n^z_\uparrow$ is modeled as the expectation value of $(L^z_A - L^z_B)$ in the $S^z_{\rm tot} = S$ state of this multiplate.

$$n^z_\uparrow = \lim_{N_B\to\infty} \frac{1}{N_{tot}} \langle S_{tot} = S, S^z_{tot} = S; S_B; S_A | \left(L^z_A - L^z_B\right) | S_{tot} = S, S^z_{tot} = S; S_B; S_A\rangle \tag{5.54}$$

Which can be readily obtained in closed form using the following standard result for the minimum angular momentum state $|J = j_1 - j_2, m_J\rangle$ state obtained by the addition of angular momenta j_1 and j_2 (with $j_1 \geq j_2$):

$$\langle j_1, m_1; j_2, m_2 | J, m_J\rangle = \rho_J c^{J,m_J}_{m_1,m_2} \tag{5.55}$$

with

$$\rho_J = \sqrt{\frac{(2J+1)!(2j_2)!}{(2j_1+1)!}} \tag{5.56}$$

and

$$c^{J,m_J}_{m_1,m_2} = (-1)^{j_2+m_2} \left[(j_1+m_1)!((j_1-m_1)!\right]^{1/2} \left[(j_2+m_2)!(j_2-m_2)!(J+m_J)!(J-m_J)!\right]^{1/2} \tag{5.57}$$

for $m_1 + m_2 = m_J$ and $c^{J,m_J}_{m_1,m_2} = 0$ otherwise. In our case, $j_1 = S_B + S$, $j_2 = S_B$, $J = S$, $m_J = S$, and $n^z_\uparrow = \langle m_1 - m_2\rangle_{J,m_J}/N_{\rm tot}$ can therefore be readily calculated to obtain,

$$n^z_\uparrow = \lim_{N_B\to\infty} \frac{2S+1}{2N_B+1} \times \sum_{m=-(S_B-S)}^{S_A} \frac{(2m-S)\Gamma(2S_B+1)\Gamma(S_A+m+1)}{\Gamma(2S_A+2)\Gamma(S_B+m+1-S)}, \tag{5.58}$$

using $\Gamma(n) = (n-1)!$, where n is an integer. Surprisingly this sum can be carried out to the following closed form expression

$$n^z_\uparrow = \lim_{N_B\to\infty} \frac{1}{2N_B+1}\left(S + \frac{2S}{S+1}S_B\right). \tag{5.59}$$

On the other hand, we may also calculate m_0^2 defined as

$$m_0^2 = \langle (\vec{L}_A - \vec{L}_B)^2\rangle_{J=0}/N^2_{\rm tot}, \tag{5.60}$$

where the average is taken in the $S_{tot} = 0$ singlet state (note the suffix). Like before this is obtained by quantum-mechanics addition of $\vec{L}_A$ and $\vec{L}_B$ where the two sublattice angular momenta are equal: $S_B = S_A = SN_{tot}/2$ for sample with even number of sites N_{tot}. This leads to,

$$m_0^2 = \lim_{N_{tot}\to\infty} \frac{1}{N_{tot}} 2\sqrt{S_B(S_B+1)}\,. \tag{5.61}$$

This allows us to compute the ratio $n^z_\uparrow/m_0$ in the thermodynamic limit:

$$n^z_\uparrow/m_0 = \lim_{N_{tot}\to\infty} \left[\frac{S}{S+1}m_0 + \mathcal{O}\left(\frac{1}{N_{\rm tot}}\right)\right] \tag{5.62}$$

Is there a limit in which this sublattice-spin mean-field theory is expected to give exact results? The sublattice-spin model represents the Hamiltonian of an infinite-range model in which *every* A sublattice-spin interacts with *every* B sublattice-spin via a *constant* (independent of distance) antiferromagnetic exchange coupling J_{MF}. In this limit, we also expect $m_0 \to 1/2$, and thus, our mean field theory predicts that $n^z_\uparrow \to m_0/3$ when $m_0 \to 1/2$. This is the constraint that we built into our choice of polynomial fit for $n^z_\uparrow(m_0)$ in section. 5.2.

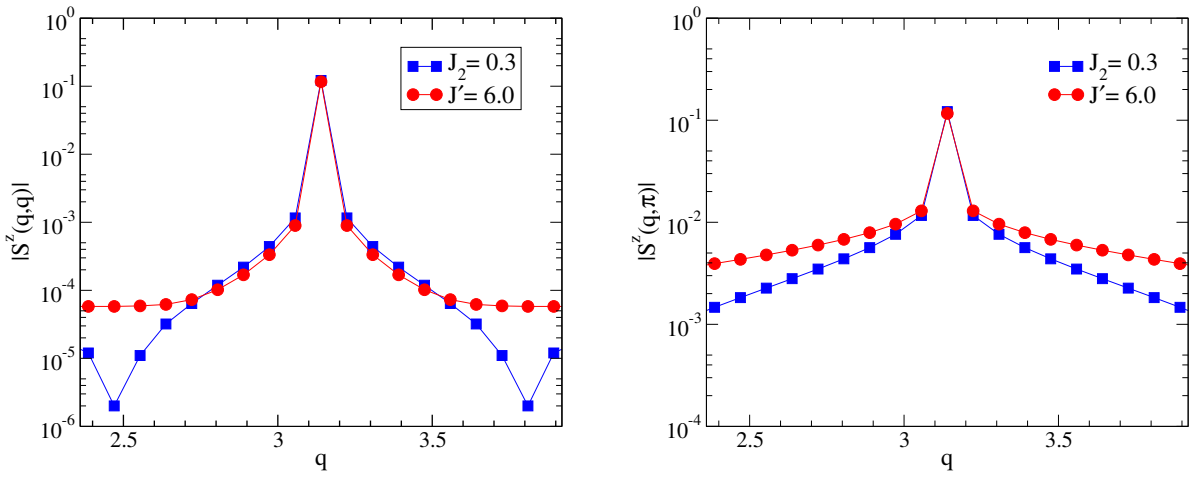

Figure 5.9: Fourier transform (with antiperiodic boundary conditions assumed for convenience) of the spin-wave result for $\Phi^z(\vec{r})$ (assuming $S = 3/2$ and calculated using $L = 75$ for JJ_2 and JJ' model) along cuts passing through the antiferromagnetic wavevector (π, π). Note the nearly universal nature of the results in the neighborhood of the antiferromagnetic wavevector, which in any case accounts for most of the weight of the transformed signal.

For further understanding of this sublattice-spin model as a low energy effective model, consider Heisenberg model on a square lattice with nearest neighbor interaction (Eq. 5.1). We go to the reciprocal space by Fourier transforming the spin operators as,

$$\mathbf{S_Q} = \frac{1}{\sqrt{N_{\text{tot}}}} \sum_i \mathbf{S}_i exp(-i\mathbf{Q}.\mathbf{r}_i). \tag{5.63}$$

In the last expression $\mathbf{r}_i$ is the coordinate of spin i and $\mathbf{Q}$ runs on the reciprocal space points in first Brillouin zone (BZ). On a lattice with N_{tot} sites and periodic boundary condition this leads to the following expression of Hamiltonian in reciprocal space,

$$H = J \sum_{\mathbf{Q} \in BZ} \zeta_{\mathbf{Q}} \mathbf{S_Q}.\mathbf{S_{-Q}} \tag{5.64}$$

The lattice structure factor is denoted as $\zeta_{\mathbf{Q}}$, for a square lattice that reads,

$$\zeta_{\mathbf{Q}} = \frac{1}{2} \sum_{i=1,2} \cos(\mathbf{Q}.\mathbf{a}_i), \tag{5.65}$$

with a_i $(i = 1, 2)$, the unit vectors of a square lattice. On this lattice the Néel state is invariant by translations associated to wavevectors $\mathbf{Q}_0 \equiv (0, 0)$ and $\mathbf{Q}_N = (\pi, \pi)$. One can breakdown the Hamiltonian H in two components, H_0 containing the $\mathbf{Q}_0$ and $\mathbf{Q}_N$ momentum terms and H_1 containing all other momentum terms.

$$H = H_0 + H_1 \tag{5.66}$$

where

$$H_0 = J(\mathbf{S}_0^2 - \mathbf{S}_{\mathbf{Q}_N} \mathbf{S}_{-\mathbf{Q}_N}) \tag{5.67}$$

and

$$H_1 = J \sum_{\mathbf{Q} \in BZ - \{\mathbf{Q}_0, \mathbf{Q}_N\}} \zeta_{\mathbf{Q}} \mathbf{S}_{\mathbf{Q}} \mathbf{S}_{\text{-}\mathbf{Q}}. \tag{5.68}$$

From the expression 5.63 one can easily show

$$H_0 = \frac{2J}{N_{tot}} \left(\mathbf{S}_{tot}^2 - \mathbf{S}_A^2 - \mathbf{S}_B^2 \right), \tag{5.69}$$

$$H_0 = \frac{4J}{N_{tot}} \left(\mathbf{S}_A . \mathbf{S}_B \right), \tag{5.70}$$

where $\mathbf{S}_{tot} \equiv SN_{tot}$ is the total spin of the system and $S_B \equiv SN_B$,$S_B \equiv SN_A$ are respectively the total spin of A and B sublattices. This is the model we-called sublattice mean-field model(Eq. 5.53) by writing $J_{MF} = \frac{4J}{N_{tot}}$. The model is exactly solvable as H_0 is an $SU(2)$ invariant Hamiltonian commuting with $\mathbf{S}_{tot}^2$,$\mathbf{S}_{tot}^z$ and $\mathbf{S}_{A(B)}^2$. Also from the above discussion we can see that it is the true low energy description (in the thermodynamic limit) of the 'classical' Néel ordered antiferromagnetic phase, when only the wavevectors corresponding to Néel order($\mathbf{Q}_0$ and $\mathbf{Q}_N$) is contributing. In such a limit the $n_\uparrow^z/m_0$ ratio in Eq. 5.62 will be exact. Since numerical and spin wave results both show clear deviations from this results(Eq. 5.7 and Eq.5.52), we conclude the other such non-zero wavevector modes are essential for a correct calculation of the universal function $n_\uparrow^z(m_0)$; as is evident from Fig. 5.6.

5.4.3 Quantum rotor Hamiltonian

The other approach we take in understanding effective low energy behavior of antiferromagnetic phase is in terms of a quantum rotor picture. Consider SLHAF, which is a bipartite system with N_{tot}(even) number of sites; the ground state of the same is a Néel ordered state ($|\psi_N\rangle$) with quantum fluctuations. As we know the classical Néel state ($|\psi_N\rangle$) is not an eigenstate of the spin operator and explicitly breaks the $SU(2)$ symmetry of the Heisenberg Hamiltonian. However, for a finite size system with $N_A = N_B$, the ground state is always singlet($S_{tot} = 0$) by Lieb-Mattis [30] theorem, which means that the true ground state has no preferred direction in spin space, restoring the $SU(2)$ symmetry. The solution of this apparent puzzle was suggested by Anderson by noticing that the $|\psi_N\rangle$ can be thought of quantum superposition of all possible eigenstates of the Heisenberg spin model(Eq. 5.1). As shown by Anderson, those eigenstates are characterized by finite total angular momentum sectors from $L_{tot} = 0$ to $L_{tot} = SN_{tot}$(as the Hamiltonian is $SU(2)$ symmetric) and the rotational symmetry can be restored by the precession of the Néel state vector in all those spin sectors. Anderson also argued, the Néel state is a superposition of many effectively degenerate states, they are truly degenerate in the thermodynamic limit. These states for finite size system is knowns as "Anderson's tower of states", which collapses to the degenerate state in thermodynamic limit. The vector representing Néel order(Néel vector $\vec{n}$) precesses between those angular momentum sectors due to the quantum fluctuations, but the rate of precessing is $\mathcal{O}\left(\frac{1}{N_{\text{tot}}}\right)$, so in the thermodynamic limit one can think of it as a stationary or infinitely heavy degrees of freedom. This idea is in par with the concept of "spontaneous symmetry breaking", as we know when any continuous symmetry is broken, the corresponding order parameter variable

becomes very "heavy" in a well-defined sense.[35] The long-time, slow dynamics of this heavy nearly classical variable is controlled by an effective "mass" that diverges in the thermodynamic limit.

Neuberger and Ziman [26] approached to model the low energy spectrum of a finite system (the "tower of states") by constructing an effective Hamiltonian which respects the $SU(2)$ symmetry of the original Heisenberg Hamiltonian. By the discussion above the Néel vector can be thought of as a angular momentum degree of freedom, which is made by quantum addition of spin angular moments of the system. The angular momentum variable is precessing very slowly about some axis for some large value of N_{tot}, and thus it can be mapped to a model for a rigid rotor. In the usual case of an antiferromagnet with an even number of spin-S moments, the low-energy effective Hamiltonian that controls the orientation dynamics of the Néel vector $\vec{n}$ is

$$H_{rotor} = \frac{\vec{L}_{tot} \cdot \vec{L}_{tot}}{2\chi N_{\rm tot}} \tag{5.71}$$

where $\vec{L}_{tot}$ is the angular momentum conjugate to the "quantum rotor" coordinate $\hat{n} \equiv \vec{n}/|\vec{n}|$, χ is the uniform susceptibility per spin, and $N_{\rm tot}$ is the total number of spins. The effective moment of inertia of the rotor being an extensive quantity is given by $I = N_{tot}\chi$ (intuitively the rotor is heavier as the N_{tot} and χ increases). The eigenstates of H_{rotor} will be

$$E_{rotor} = \frac{L_{tot}(L_{tot}+1)}{2\chi N_{\rm tot}}. \tag{5.72}$$

Now we generalize this to our case of $N_A = N_B + 1$ and an odd number of spins $N_{\rm tot} = 2N_B + 1$. Following earlier work on quantum rotor descriptions of insulating antiferromagnets doped with a single mobile charge-carrier[36], we postulate that the correct rotor description of our problem is in terms of a rotor Hamiltonian in which $\vec{L}$ is replaced by the angular momentum operator $\vec{L}'$ conjugate to a quantum rotor coordinate $\hat{n}$ that now parametrizes a unit-sphere with a fundamental magnetic monopole at its origin.[37] In other words, we postulate a low-energy effective Hamiltonian

$$H^S_{rotor} = \frac{\vec{L}'_{tot} \cdot \vec{L}'_{tot}}{2\chi N_{\rm tot}} \tag{5.73}$$

where the superscript reminds us that the lowest allowed angular momentum quantum number l of the modified angular momentum operator $\vec{L}'_{tot}$ is $l = S$. The angular wavefunction[37] of the $|l = S, m_l = S\rangle$ ground state of this modified rotor Hamiltonian is the *monopole harmonic* $Y_{-S,S,S}(\theta,\phi)$. To calculate $n^z_\uparrow/m_0$ we calculate $\langle n^z_\uparrow\rangle_\uparrow$ i.e. the expectation value of $\hat{n}^z \equiv \cos(\theta)$ in this monopole harmonic wave function on the unit sphere. Since $|Y_{-S,S,\pm S}(\theta,\phi)|^2 \propto (1 \pm \cos\theta)^{2S}$, it leads to

$$\langle n^z_\uparrow\rangle_\uparrow = \frac{S}{S+1} m_0, \tag{5.74}$$

which is exactly the same expression we got from sublattice mean-field theory.

Connection between two-sublattice mean field theory and quantum rotor model The question one can ask here is: why do we get the same relation (Eq. 5.62 and Eq. 5.74) from two apparently

different low energy approximations of the antiferromagnetic phase ? The rotor model is a more general phenomenological approach than the sublattice mean-field theory which doesn't take into account any nonzero wave vector modes or the amplitude fluctuations of the Néel order parameter, also the model makes no assumptions about any long range interactions. It still reproduces the sublattice mean-field theory results which is asymptotically exact in the limit of innite-range unfrustrated interactions. This seems to be consistent with Andersons analysis of the low-energy tower of states in an antiferromagnet which used a picture in terms of the total spin of each sublattice to arrive at a rotor description. To illustrate that statement let us look at the Eq. (5.69), the eigenvalues of H_0, will be

$$E = \frac{4J}{N_{tot}} \left[S_{tot}(S_{tot}+1) - S_A(S_A+1) - S_B(S_B+1) \right]. \tag{5.75}$$

Where both S_A and S_B can span over the values $0, 1, ..., \frac{N_{tot}S}{2}$ and for a given S_A, S_B , S_{tot} can span $0, 1, ..., N_{tot}S$. Which leads to the ground state energy in each S_{tot} sector as,

$$E_G(S_{tot}) = -\frac{J}{2}(N_{tot}+4) + \frac{4J}{N_{tot}} \left[S(S+1) \right]. \tag{5.76}$$

As by Lieb-Mattis theorem, for even N_{tot} and classical Néel state, $S_A = S_B = N_{tot}S/2$. This corresponds to the rotor spectrum in Eq. 5.72 and that tower of states in finite size also collapse to the ground state as $\mathcal{O}(1/N_{tot})$. This gives us a reason why we should expect same result from this two apparently different effective low energy models.

Thus, a more general phenomenological approach that goes beyond sublattice-spin mean-field theory but ignores all non-zero wavevector modes also gives

$$n^z_\uparrow = \frac{m_0}{3}, \tag{5.77}$$

for $S = 1/2$. Since our QMC data show clear deviations from this result[Fig 5.6], like before we conclude that such non-zero wavevector modes are essential for a correct calculation of the universal function $n^z_\uparrow(m_0)$.

5.5 Discussion

We conclude this chapter with some questions not answered in this work. A natural question that arises from our results is whether the universal ground state spin texture we have found here can be successfully described using an effective field theory approach of the type used recently by Eggert and collaborators for studying universal aspects of the alternating order induced by missing spins in two dimensional $S = 1/2$ antiferromagnets[72]. This approach uses a non-linear sigma-model description of the local antiferromagnetic order parameter, with lattice scale physics only entering via the values of the stiffness constant ρ_s and the transverse susceptibility $\chi_\perp$, and the presence of the vacancy captured by a local term in the action. An analogous treatment for our situation would need two things—one is a way of restricting attention to averages in the $S_{\rm tot} = 1/2$ component $|G\rangle_\uparrow$ of the ground state doublet,

and the other is an understanding of the right boundary conditions or boundary terms in the action, so as to correctly reflect that fact that our finite sample has open boundaries. This can be an interesting direction for future work, which may shed some light on the role of non-zero wavevector modes that were left out of the rotor description of the earlier section.

Chapter 6

Single impurity in one dimensional antiferromagnetic spin chain

In this chapter we will focus on understanding the origin of multiplicative logarithmic corrections on the impurity spin texture in Néel ordered phase of an one dimensional Heisenberg antiferromagnet. With the motivation as outlined in introduction, the plan of the chapter is as follows: in the section 6.1, we will describe the models studied in this problem. In section 6.2, we will briefly review some facts known from the numerical studies on the spin texture around the impurity in this system. In section 6.3 we will show with the help of bosonization that the low energy theory of one dimensional Heisenberg antigerromagnet is a "sine-Gordan" model, which has a bosonic free Gaussian term and a cosine interaction term; we will also discuss the effect of vacancy in spin chain on the "sine-Gordan" model. In section 6.4 we will use renormalization group (RG) improved perturbation theory from the bosonization framework to obtain predictions for the alternating part of the spin texture in this example; at the end of this section we will write down our field theory prediction for the same in a closed form. In the section 6.5 we will compare the numerical results to our field theory results, keeping careful track of the effects of the marginal cosine interaction term using one loop RG improved perturbation theory. In section 6.6 we will end the chapter with a discussion on the possible future research directions relevant to this work.

6.1 Models

For analytical studies, we consider simple Heisenberg antiferromagnet with nearest neighbor interaction in one dimension. The numerical data with which we compare our analytical results are obtained from a model called JQ_3 model.

6.1.1 Model studied in analytical work

The pure Heisenberg model (Eq.6.1) on an one dimensional ring with $N+1$ spins (indexed 0 to N, with periodic boundary condition) is given by,

$$H = J \sum_{i=0}^{N} \mathbf{S}_i . \mathbf{S}_{i+1}. \tag{6.1}$$

To treat this interacting spin model perturbatively, we introduce an exchange anisotropy in the z direction, the model with such anisotropy is called an XXZ Heisenberg spin chain (Eq.6.3). For perturbative treatment we will consider J_z as the small parameter, later we will show how to restore the effective low energy theory of usual isotropic Heisenberg model with $SU(2)$ symmetry from the low energy theory of XXZ model.

$$\begin{aligned} H &= H_{xx} + H_z \\ &= \sum_{i=0}^{N} \frac{J}{2} \left[S_i^+ S_{i+1}^- + S_i^- S_{i+1}^+ \right] + J_z S_i^z S_{i+1}^z, \end{aligned} \tag{6.2}$$

here J is positive, S_i s represent the usual spin operators.

6.1.2 Model studied in numerical work

The microscopic model here is an one-dimensional spin chain with nearest neighbor Heisenberg exchange J and six-spin coupling $Q = 4qJ$. The Hamiltonian for this model (known as 'JQ_3 model') is:

$$H = -J \sum_{i=0}^{N} P_{i,i+1} - Q \sum_{i} P_{i,i+1} P_{i+2,i+3} P_{i+4,i+5} \tag{6.3}$$

where $P_{ij} \equiv (\frac{1}{4} - \vec{S}_i \cdot \vec{S}_j)$ is the projector to the singlet state of the two spin-half variables at sites i and j. Both J and Q are positive, and periodic boundary conditions were imposed by placing the system on a ring so that site $N+1+k$ is identified with site k (the total number of spins $N+1$ is taken even).

6.2 Review on relevant numerical studies

The JQ_3 model was studied previously using the singlet sector valence-bond projection method[70], which shows that the Q term (in Eq.) drives a transition to a valence-bond solid phase at $q_c \approx 0.04$; so that the system is power-law Neel ordered for $q < q_c$ and VBS ordered for $q > q_c$. Such a transition is more well studied in the case where the transition is driven by next-nearest neighbor Heisenberg antiferromagnetic exchange couplings. But the JQ_3 model is more interesting to study because unlike the former it does not have a sign problem in standard non-zero temperature QMC calculations (as well as in the ground state projector QMC approach), and can therefore be studied at larger length scales and greater precision.

Now to introduce a vacancy in the JQ_3 spin chain, one can remove the spin at site 0 by deleting all interactions that involve the site 0 from the Hamiltonian (Eq.6.2). Since N is odd, the ground state of

the chain with a missing spin becomes a doublet with $S_{tot} = 1/2$. Focusing on $|G_\uparrow\rangle$, the $S^z_{tot} = 1/2$ component of this doublet, the spin texture $\Phi(r) = \langle S^z(r)\rangle_\uparrow$ can be obtained in this ground state for various values of q. This spin texture can be decomposed as $\Phi(r) = \Phi_u(r) + (-1)^{r/a} N_z(r)$, where alternating part $N_z(r)$ and a uniform part $\Phi_u(r)$ can be obtained from the numerical data [17] by a suitable coarse-graining procedure. That calculation of spin-texture was performed by Banerjee et al [17], using a recently developed spin-half sector generalization [68] of the valence-bond projector QMC algorithm.[70]

We postpone further discussion on those numerical results for $N_z(r)$ till the Section (6.5), where we compare the numerical results with our field theory results.

6.3 Effective low energy theory of spin $1/2$ chain

A spin $1/2$ antiferromagnetic chain can be modeled as a collection of bosonic harmonic oscillators in the low energy limit by the bosonization technique. In this Section we will review the details of that procedure. Then we will take care of a single site removal in the spin chain in the bosonization framework and represent the spin operators in terms of bosonic degrees of freedoms.

6.3.1 Spin chain to Harmonic oscillators

Fermionization of the spin chain

The first step of bosonizing a spin $1/2$ chain is: mapping the spin chain to a system of spin-less fermions($\equiv \psi$). That is performed by the standard Jordon-Wigner transformation which faithfully represents spin degrees of freedom to spin-less fermionic degrees of freedom in one dimension. The transformation is given by,

$$\begin{aligned} S^z_i &= \psi^\dagger_i \psi_i - \frac{1}{2} \\ S^+_i &= \psi_i \exp\left[i\pi \sum_{j=0}^{N} \psi^\dagger_j \psi_j \right]. \end{aligned} \tag{6.4}$$

Using Eq.(6.5), the spin Hamiltonian (6.3) is mapped into the fermionic Hamiltonian as

$$H_{XX} = \sum_{i=0}^{N} \left[\frac{J}{2} \left(\psi^\dagger_i \psi_{i+1} + \psi^\dagger_{i+1} \psi_i \right) \right] \tag{6.5}$$

and

$$H_Z = \sum_{i=0}^{N} J_z \left(\psi^\dagger_i \psi_i - \frac{1}{2} \right) \left(\psi^\dagger_{i+1} \psi_{i+1} - \frac{1}{2} \right) \tag{6.6}$$

The lattice fermionic operators satisfying the standard fermionic anitcommutation relations $\{\psi_i, \psi^\dagger_i\} = \delta_{ij}$ and $\{\psi_i, \psi_i\} = 0$. XXZ model recovers the full $SU(2)$ symmetry of Heisenberg model in the limit $J_z = \pm J$. In the limit $J_z = 0$ this Hamiltonian is exactly solvable as the problem reduces to a problem

of free spin-less fermion hopping problem. In that limit, the dispersion relation is $\cos(ak)$ (setting lattice units as a), with Fermi level at $k_F = \pm\pi/2a$. So the ground state is a half-filled band filled upto the Fermi level. Now the problem can be approached for small J_z by perturbative expansion around this ground state. Thus considering only very low energy fermionic excitations around this ground state, i.e. $|k \pm k_F| \leq \Lambda$ ($\Lambda \ll k_F$ is an UV cutoff), the fermionic operator can be written as:

$$\psi(x) \approx \sqrt{a}\left(e^{-ik_F x}\psi_R(x) + e^{ik_F x}\psi_L(x)\right). \tag{6.7}$$

Where ψ_L and ψ_R are left propagating and right propagating modes respectively, containing only slowly varying (compared to lattice scale a) Fourier modes. Now taking the continuum limit for H_{XX},

$$H_{XX} = v\int dx\left[:\psi_R^\dagger\left(i\frac{d\psi_R}{dx}\right): + \psi_L^\dagger\left(-i\frac{d\psi_L}{dx}\right):\right] \tag{6.8}$$

with $v = Ja$, the Fermi velocity.

Next we consider the H_Z term of the Hamiltonian (Eq.6.6). Note that near the Fermi level,

$$e^{-2ik_F x} \approx e^{-i\pi x} = (-1)^{j/a}. \tag{6.9}$$

With this one can see that S_j^z will have one smooth part and one rapidly oscillating part as

$$\begin{aligned} S_i^z &= :\psi_i^\dagger\psi_i: \\ &\equiv :\psi_R^\dagger(x)\psi_R(x) + \psi_L^\dagger(x)\psi_L(x): + e^{-2ik_F x}\psi_R^\dagger(x)\psi_L(x) + h.c. \\ &= :\psi_R^\dagger(x)\psi_R(x) + \psi_L^\dagger(x)\psi_L(x): + (-1)^{j/a}\,\psi_R^\dagger(x)\psi_L(x) + h.c. \end{aligned} \tag{6.10}$$

The H_Z term contains four different low energy processes near the Fermi level, we will discuss them one by one. Re-writing the four fermion interaction term with J_z interaction in terms of fermionic current operators as $J_L =: \psi_L^\dagger\psi_L :$ $J_R =: \psi_R^\dagger\psi_R :$, the J_z interaction term in the continuum limit becomes

$$\begin{aligned} H_Z &\approx J_z\sum_{i=0}^{N} S_i^z S_{i+1}^z = \sum_{i=0}^{N} :\psi_i^\dagger\psi_i::\psi_{i+1}^\dagger\psi_{i+1}: \\ &= J_z :\left[J_L + J_R + (-1)^{j/a}\,\psi_R^\dagger\psi_L + h.c.\right]::\left[J_L + J_R + (-1)^{j+1/a}\,\psi_R^\dagger\psi_L + h.c.\right]: \\ &= J_z\int dx\left[:J_L^2: + :J_R^2: + 4:J_L J_R: - \{(:\psi_L^\dagger\psi_R:)^2 + h.c.\}\right]. \end{aligned} \tag{6.11}$$

The First two terms in this expression represents a low energy process which breaks Lorentz invariance. Applying Wick's formula upto first order (restoring the Lorentz symmetry) on those two terms leads to a free fermion Hamiltonian as follows:

$$\begin{aligned} J_L(x)J_L(x) &= \lim_{a\to 0} J_L(x)J_L(x+a) \\ &\approx :J_L(x)J_L(x): + \frac{i}{2\pi a}\left[\psi_L^\dagger(x+a)\psi_L(x) - \psi_L^\dagger(x)\psi_L(x+a)\right] + constant \\ &\approx -\frac{i}{\pi}\psi_L^\dagger\frac{d}{dx}\psi_L + constant. \end{aligned} \tag{6.12}$$

Similarly,

$$J_R(x)J_R(x) \approx \frac{i}{\pi}\psi_R^\dagger \frac{d}{dx}\psi_R + constant. \tag{6.13}$$

Thus the only effect of this Lorenz symmetry breaking terms in Eq.(6.12) is to renormalizes the Fermi velocity as $u = a(J + \frac{J_z}{\pi})$ (Eq.6.8,6.13,6.13).

The third interaction term in Eq.(6.12) represents a Lorentz symmetry preserving process and we will keep that term as it is. The fourth term represents a process called "Umklapp" process and that is the only term which can generate a gap as we will see in the following discussion. We will call that term as H_1 (Eq.6.14) and the combination of all other massless terms as H_0. So H_0 expressed in terms of spin-less Fermion current with renormalized Fermi velocity is :

$$H_0 = u\pi \int dx \left[J_R^2 + J_L^2 + \frac{4J_z}{\pi u} J_L J_R \right]. \tag{6.14}$$

And the "Umklapp" part of the Hamiltonian is given by

$$H_1 = -J_z \int dx \{ (: \psi_L^\dagger \psi_R :)^2 + h.c. \}. \tag{6.15}$$

Bosonization of the spin-less fermionic Hamiltonian Next we appeal to the standard bosonization dictionary (see Appendix-A for a brief review on bosonization) to convert the fermionic fields(ψ) to bosonic fields (ϕ) as follows:

$$\begin{aligned} J_L &= \frac{1}{\sqrt{4\pi a}} (\Pi - \partial_x \phi) \\ J_R &= -\frac{1}{\sqrt{4\pi a}} (\Pi + \partial_x \phi) \\ \psi_L &= \frac{1}{\sqrt{2\pi a}} exp(-i\sqrt{4\pi}\phi_L) \\ \psi_R &= -\frac{1}{\sqrt{2\pi a}} exp(i\sqrt{4\pi}\phi_R), \end{aligned} \tag{6.16}$$

the prefactors depend on the UV cut-off (lattice constant a) and here Π is conjugate momentum to the bosonic field ϕ. We first take on H_0 (Eq.6.14) and then H_1 (Eq.6.15). Bosonized H_0 is given by

$$H_0 = \frac{u}{2} \left[\left(1 - \frac{2J_z}{u} \right) (\partial_x \phi)^2 + \left(1 + \frac{2J_z}{u} \right) (\partial_x \Pi)^2 \right]. \tag{6.17}$$

Where ϕ_L and ϕ_R are respectively left and right propagating parts of the ϕ which can be rewritten as

$$\begin{aligned} \phi_L(x) &= \frac{1}{2} \left[\phi(x) - \int_{-\infty}^{x} dy \Pi(y) \right] \\ \phi_R(x) &= \frac{1}{2} \left[\phi(x) + \int_{-\infty}^{x} dy \Pi(y) \right]. \end{aligned} \tag{6.18}$$

Introducing a dual field $\widetilde{\phi} = -\int_{-\infty}^{x} dy \Pi(y)$ the Hamiltonian (Eq.6.17) can be rewritten as

$$H = \frac{u}{2} \left[\left(1 - \frac{2J_z}{u} \right) (\partial_x \phi)^2 + \left(1 + \frac{2J_z}{u} \right) \left(\partial_x \widetilde{\phi} \right)^2 \right] \tag{6.19}$$

For convenience one can define a rescaling factor

$$R^2 = \frac{1}{4\pi}\left(\frac{1+\frac{2J_z}{u}}{1-\frac{2J_z}{u}}\right)^{\frac{1}{2}} \approx \frac{1}{4\pi}\left(1+\frac{2J_z}{\pi v}\right), \tag{6.20}$$

to rescale ϕ and $\widetilde{\phi}$ in an opposite way such that the canonical commutation relations are preserved.

$$\begin{aligned} \phi &\to \frac{\phi}{\sqrt{4\pi}R} \\ \widetilde{\phi} &\to \sqrt{4\pi}R\widetilde{\phi}. \end{aligned} \tag{6.21}$$

This gives the free boson Hamiltonian

$$H_0 = \frac{u}{2}\int_0^L dx \left[\left(\frac{d\phi}{dx}\right)^2 + \left(\frac{d\widetilde{\phi}}{dx}\right)^2\right] \tag{6.22}$$

Now let's turn to H_1 (Eq.6.15); one can expand it using the bosonization dictionary,

$$\begin{aligned} (:\psi_L(x)^\dagger\psi_R(x):)^2 &= \lim_{a\to 0} :\psi_L(x)^\dagger\psi_R(x)\psi_L(x+a)^\dagger\psi_R(x+a): \\ &= \frac{1}{4\pi^2a^2}\lim_{a\to 0} : e^{\frac{i\phi_L(x)^\dagger}{R}} e^{\frac{i\phi_R(x)}{R}} e^{\frac{i\phi_L(x+a)^\dagger}{R}} e^{\frac{i\phi_R(x+a)}{R}} : \\ &= \frac{1}{4\pi^2a^2}\lim_{a\to 0}\left(: e^{\frac{i\phi(x)}{R}} :: e^{\frac{2i\phi(x+a)}{R}} : + ...\right). \end{aligned} \tag{6.23}$$

Here "..." represents the derivative terms. In the weak-coupling limit $J_z \to 0$, where $R \approx \frac{1}{\sqrt{4\pi}}$, the operator $e^{\frac{2i\phi(x)}{R}}$ is irrelevant and can be dropped. With increasing R it becomes more relevant and the term H_1 takes the form

$$\begin{aligned} H_1 &= -J_z\int dx\{(:\psi_L^\dagger\psi_R:)^2 + h.c.\} \\ &= -\frac{J_z}{2\pi^2a^2}\int dx\cos\left(\frac{2\phi(x)}{R}\right). \end{aligned} \tag{6.24}$$

For convenience we choose to represent the coefficient in a dimensionless form as $\epsilon_0 = \frac{J_z}{2\pi^2 u}$, leading to

$$H_1 = -\frac{u\epsilon_0}{a^2}\int_0^L dx\cos\left(\frac{2\phi(x)}{R}\right). \tag{6.25}$$

Thus the full continuum Hamiltonian is of the form,

$$\begin{aligned} H &= H_0 + H_1 \\ &= \frac{u}{2}\int_0^L dx\left[\left(\frac{d\phi}{dx}\right)^2 + \left(\frac{d\widetilde{\phi}}{dx}\right)^2\right] - \frac{u\epsilon_0}{r_0^2}\int_0^L dx\cos\left(\frac{2\phi(x)}{R}\right). \end{aligned} \tag{6.26}$$

For generalization let us write the UV regulator as r_0, here we have always chosen $r_0 = a$. This Hamiltonian (Eq.6.27) is well known in the literature as the "sine-Gordan" model.

Note that all physical operators if this Bosonic theory are symmetric under a transformation

$$\begin{aligned} \phi &\equiv \phi + 2\pi R \\ \widetilde{\phi} &\equiv \widetilde{\phi} + \frac{1}{R}. \end{aligned} \tag{6.27}$$

This leads to an interpretation of the boson field ϕ as a periodic variable measuring the arc length on a circle of radius R, which was introduced as a scaling parameter for the fields ϕ and $\widetilde{\phi}$.

Comparing bosonization parameters with exact results

As mentioned in the introduction, the advantage of analyzing this spin-$1/2$ model in 1-dimension is that the field theory results can be compared with exact results. The scaling introduced via parameter R so far is valid only for small values of J_z and by this token it is not possible to know the true relations of the scale parameter R and the renormalized velocity u. By exact calculation using Bethe ansatz that can be determined analytically and it provides useful checks for the field theory results. With a new variable $\cos\theta \equiv \frac{J_z}{J}$ those quantities from Bethe ansatz calculations are known as

$$u = \frac{J\pi \sin\theta}{2\theta} \tag{6.28}$$

and

$$R = \sqrt{\left[\frac{1}{2\pi} - \frac{\theta}{2\pi^2}\right]}. \tag{6.29}$$

Thus at small J_z, $R \sim \frac{1}{\sqrt{4\pi}}\left(1 + \frac{J_z}{\pi J}\right)$ as we have seen previously from the perturbation theory in Eq. 6.20. And at the isotropic point ($J_z = J$) $R = \frac{1}{\sqrt{2\pi}}$, as expected from the $SU(2)$ symmetry at this value of R from Eq. 6.28.

6.3.2 Removing a site from the spin chain

Finally we impose the condition that we have a vacancy at the site at location zero i.e. the spin at site with index "0" is missing and the system is made of spins at sites indexed from 1 to N. This is equivalent to imposing an open boundary condition between sites with index 1 and N. To impose open boundaries assume two ghost sites with index 0 and $N+1$ and demand $\mathbf{S}(0) = \mathbf{S}(N+1) = \mathbf{0}$. That translates to following conditions for bosonic fields $\phi(r)$,

$$\begin{aligned} \phi(0) &= 0 \\ \phi(N+1) &= 2\pi R S^z_{tot}. \end{aligned} \tag{6.30}$$

Where $S^z_{tot} = \sum_{i=1}^{N} S^z_i$ is the total magnetization in z direction and the boundary condition is in par with the symmetry condition in Eq.6.28. With this boundary condition the mode expansion is given by,

$$\begin{aligned} \phi(r) &= \pi R + \frac{\pi R}{L} r + \sum_{n=1}^{\infty} \frac{\sin\left(\frac{n\pi r}{L}\right)(a_n + a_n^\dagger)}{\sqrt{\pi n}} \\ \widetilde{\phi}(r) &= \widetilde{\phi}_0 + i\sum_{n=1}^{\infty} \frac{\cos\left(\frac{n\pi r}{L}\right)(a_n - a_n^\dagger)}{\sqrt{\pi n}}. \end{aligned} \tag{6.31}$$

Here πR is actually eigenvalue of the zero mode represented by vacuum of bosons q_0. Such that $q_0|gnd\rangle \equiv q_0|0\rangle \equiv \pi R|0\rangle$ (actually $2\pi R S^z_{tot}$, but here $S^z_{tot} = 1/2$). The non zero commutation relations are $\left[\widetilde{\phi}(0), q_0\right] = i, \left[a_m, an^\dagger\right] = \delta_{mn}$.

The spin operators represented in terms of this bosonic operators with this open boundary conditions are given by,

$$
\begin{aligned}
S^z(r) &= \frac{a}{2\pi R}\frac{d\phi}{dr} + \frac{\mathcal{A}}{\sqrt{r_0}}(-1)^{\frac{r}{a}}\sin\left(\frac{\phi(r)}{R}\right) \\
S^-(r) &= e^{-i2\pi R\tilde{\phi}}\left[\mathcal{B}(-1)^{\frac{r}{a}} + \mathcal{C}\sin\left(\frac{\phi(r)}{R}\right)\right]
\end{aligned}
\tag{6.32}
$$

Where $\mathcal{A}$,$\mathcal{B}$,$\mathcal{C}$ are coefficients dependent on the microscopic details of the Hamiltonian, from the effective theory standpoint they are determined as free parameters of the theory by fitting with the experimental or numerical data.

So all the quantities for spin chain with a vacancy will be evaluated with these expressions of mode expansion(Eq.6.32) and magnetization(Eq.6.33).

6.3.3 RG analysis of sine-Gordon model

The "sine-Gordon" model is analyzed in various context as it is related to a variety of other models like the spin-$1/2$ XYZ chain, One dimensional fermionic system with backward scattering, two-dimensional Coulomb gas problem etc. Now we will briefly review the low energy behavior of "sine-Gordon" model from RG point view.

The three free parameters in this model given by u,ϵ and R, this effectively reduces to two as u is just an overall factor. The other two $\epsilon(L)$ and $R(L)$ can be thought of as dependent on the the energy/length scale. We want to know the stable low energy fixed point(or collection of points i.e. a fixed line) of the system in terms of RG flow, given a starting point $(\epsilon(L_0), R(L_0))$. The flow equation in the $\epsilon - R$ plane is determined by splitting the fields as fast(above momentum cutoff Λe^L) and slow(between momentum cutoff Λe^L and UV cutoff Λ) and then by generating the effective coupling of the slow field terms for H_1 in first two orders of ϵ and ϵ^2, obtained by integrating out the fast modes. This leads to the following flow equations,

$$
\begin{aligned}
\frac{d\epsilon(L)}{dL} &= 2\epsilon(L)\left(\frac{1}{2\pi R^2(L)} - 1\right) + \frac{\pi^2\epsilon^3}{2R^2(L)} \\
\frac{dR(L)}{dL} &= -\pi\epsilon^2(L).
\end{aligned}
\tag{6.33}
$$

The solution of this coupled first order differential equation upto second order in ϵ will give us the flow-trajectory as the hyperbolic equation,

$$
\left(1 - \frac{1}{2\pi R^2}\right)^2 - \pi^2\epsilon^2 = Const. \tag{6.34}
$$

The phase diagram of the "sine-Gordan "model is given by all possible paths $(\epsilon(L), R(L))$ satisfying Eq.6.34 in the $\epsilon - R$ plane. Each of those paths with an arrow direction denotes the flow of an initial point $(\epsilon(L_0), R(L_0))$ where the observable start at $L = L_0$ and flows towards the arrow direction at lower L (as in Fig "to be made"). The three different phases in this flow-trajectory diagrams are as follows,

- **Asymptotic freedom region**

  In the regime where $R \leq \frac{1}{\sqrt{2\pi}}$ and $\epsilon \geq \frac{1}{\sqrt{\pi}}\left(\frac{1}{2\pi R^2} - 1\right)$, the flow is towards the fixed line $\epsilon = 0, R \leq \frac{1}{\sqrt{2\pi}}$. This line is described as free Gaussian theory. In the corresponding spin problem the corresponding parameter range is $-1 < \frac{J_z}{J} \leq +1$. In this critical regime the ground state is singlet with $\langle S^z \rangle = 0$ with power law correlations. This phase is known as the "Tomonaga-Luttinger liquid" (TLL) phase.

- **Strong coupling**

  In the regime where $R \leq \frac{1}{\sqrt{2\pi}}, \epsilon < 0$ and $R > \frac{1}{\sqrt{2\pi}}, \epsilon > \frac{1}{\sqrt{\pi}}\left(\frac{1}{2\pi R^2} - 1\right)$, the flow is towards $\epsilon \to -\infty$.

  In the regime where $R \leq \frac{1}{\sqrt{2\pi}}, \epsilon > 0$ and $R > \frac{1}{\sqrt{2\pi}}, \epsilon < \frac{1}{\sqrt{\pi}}\left(\frac{1}{2\pi R^2} - 1\right)$, the flow is towards $\epsilon \to \infty$.

  As it is evident, in both of these two cases the cosine term in the Hamiltonian becomes very significant. The corresponding parameter regime in the spin chain for the first case can show staggered two point correlations as the signature of "spin Pierl's order". For the second case the spin problem shows Neel order with staggered magnetization.

- **crossover**

  The special line marking crossover from asymptotic freedom region to strong coupling region at $\epsilon = \frac{1}{\sqrt{\pi}}\left(\frac{1}{2\pi R^2} - 1\right)$. This line is in the TLL phase with $J_z = J$ and is of our interest here as it retains the $SU(2)$ symmetry of Eq.6.1, with symmetric two point correlators in all directions of same spin components. We discuss further about this regime below.

6.3.4 Low energy theory of isotropic Heisenberg model

The original model we want to study is the Heisenberg spin model with isotropic exchange interaction i.e. $J = J_z$ in Eq.6.1, but to handle interaction perturbatively we introduced an anisotropy in z direction by making $J_z \ll J$. This means our bosonic Hamiltonian doesn't have any $SU(2)$ symmetric phase representing the isotropic Heisenberg model. Nevertheless the effective low energy theory of the $SU(2)$ symmetric Heisenberg model can be recovered at the point ($\epsilon = 0$, $R = \frac{1}{\sqrt{2\pi}}$). To see how is that possible, one can calculate[1] the correlators $\langle S_z(x) S_z(x') \rangle$,$\langle S^+(x) S^-(x') \rangle$ from equations (6.32, 6.33) and notice that at leading order those two correlators decay with same power law exponent at the point ($\epsilon = 0, R = \frac{1}{\sqrt{2\pi}}$), manifesting $SU(2)$ symmetry. The renormalization group should always respect the symmetry of the Hamiltonian, so all the points flowing into and out from the $SU(2)$ symmetric point should posses $SU(2)$ symmetry. From the renormalization flow Eq. 6.34 and the

[1] For that calculation see Reference [73].

relations 6.34, 6.20 one can therefore conclude that on the line

$$\frac{1}{2\pi R^2} = 1 - \pi\epsilon_0, \tag{6.35}$$

the low energy theory is $SU(2)$ symmetric in a RG sense. Thus on that critical line(Eq. 6.36), at low energy the $SU(2)$ symmetry appears by the renormalization which does not exist in the original microscopic Hamiltonian corresponding this low energy theory(Eq. 6.1). So one can say the "sine-Gordan" model is the correct low energy model of the $SU(2)$ symmetric isotropic Heisenberg model (Eq. 6.1) on the critical line[23]. The well-known Kosterlitz-Thouless renormalization group theory[74] is applicable on the $SU(2)$ symmetric line yielding the flow equation (using Eq.(6.36) on Eq.(6.34)),

$$\frac{d\epsilon}{d\ln L} = \beta_\epsilon(\epsilon(L)) \tag{6.36}$$

with the one loop expression for the beta function being given by[25]

$$\beta_\epsilon(\epsilon(L)) = 2\pi\epsilon^2(L) - \frac{1}{2}(2\pi)^2\epsilon^3(L)\ . \tag{6.37}$$

This equation can be solved to obtain the running coupling constant $\epsilon(L)$ at scale L as[25]

$$\frac{1}{\epsilon(L)} - \frac{1}{\epsilon_0} = -2\pi\left\{\log\left(\frac{L}{r_0}\right) + \frac{1}{2}\log\left(\log\left(\frac{L}{r_0}\right)\right)\right\} + O(1). \tag{6.38}$$

Note that ϵ_0 is *negative* in the power-law ordered antiferromagnetic phase in the present sign convention.

Obtaining alternating part of the spin texture from bosonization framework

Within this bosonized formulation, the magnetization or spin-texture operator $S^z(r)$ at site $r = ja$ is represented as in Eq.(6.33). The alternating part of the spin texture is given by the operator $\frac{1}{\sqrt{r_0}}\sin\left(\frac{\phi(r)}{R}\right)$. The expectation value of that i.e. the one-point function $S = \langle\frac{1}{\sqrt{r_0}}\sin\left(\frac{\phi(r)}{R}\right)\rangle_\uparrow$ can be thought of as a function of L and the running coupling $\epsilon(L)$ for fixed bare coupling ϵ_0 and fixed r/L ($S = S\left(L, \epsilon(L)/\epsilon_0, \frac{r}{L}\right)$). So it will be useful to recall that one-point function must obey the Callan-Symanzik type RG flow equation[25]

$$\left(\frac{\partial}{\partial\ln L} + \beta_\epsilon(\epsilon)\frac{\partial}{\partial\epsilon} + \gamma(\epsilon)\right) S\left(L, \epsilon(L)/\epsilon_0, \frac{r}{L}\right) = 0. \tag{6.39}$$

with the anomalous dimension having the expansion

$$\gamma(\epsilon) = \frac{1}{2} + \left(\frac{\pi}{2}\right)\epsilon(L) \tag{6.40}$$

in terms of the running coupling ϵ. As is well-known, this can be solved to leading order in $\epsilon(L)$ to give the following scaling law for S

$$S\left(L, \epsilon(L)/\epsilon_0, \frac{r}{L}\right) \cong \frac{F_0}{\sqrt{L}}\left(\frac{\epsilon_0}{\epsilon(L)}\right)^{\frac{1}{4}}(1 + \epsilon(L)R)\ , \tag{6.41}$$

where $F_0\left(\frac{r}{L}\right)$ and $R\left(\frac{r}{L}\right)$ are some functions of the ratio $\frac{r}{L}$ and the key point about this formal expression for S is that all dependence on the ultraviolet regulator r_0 has been traded in for a dependence on $\epsilon(L)$, the running coupling at scale L for a flow that starts with bare coupling ϵ_0 at scale r_0.

6.4 Results for alternating part of spin-texture

With these preliminaries out of the way, we now outline the strategy we took to calculate the alternating part of $\langle S^z(r)\rangle_\uparrow$ (we defined it as $N_z(r)$). The basic idea is to begin by calculating the result for this alternating part using the bosonized part of the alternating spin density and bare perturbation theory to first order in ϵ_0 for a finite system of length L. As we shall see below, this bare perturbation theory result will turn out to depend logarithmically on the value of the ultraviolet cutoff r_0 via a logarithmic ultraviolet divergence arising from a first order perturbation theory contribution proportional to $\epsilon_0 \log \frac{L}{r_0}$. This logarithmic divergence makes bare perturbation theory suspect, since a notionally small $\mathcal{O}(\epsilon_0)$ correction turns out to have a logarithmically diverging coefficient.

To extract useful information from the bare perturbation theory, it is therefore necessary to appeal to the Callan-Symanzik equation for the one point function S, and use the fact that S is expected to have the general form as in Eq.6.41. In order to make contact with our bare perturbation theory result (for details of that calculation go to Appendix-B), we expand this renormalization group prediction to first order in the bare coupling constant:

$$\begin{aligned} S &= \frac{F_0\left(\frac{r}{L}\right)}{\sqrt{L}}\left(1-\frac{\pi}{2}\epsilon_0\log\frac{L}{r_0}+....\right)\left(1+\epsilon_0 R(\frac{r}{L})+....\right) \\ &\cong \frac{F_0(\frac{r}{L})}{\sqrt{L}}\left(1-\frac{\pi}{2}\epsilon_0\log\frac{L}{r_0}+\epsilon_0 R(\frac{r}{L})+....\right). \end{aligned} \tag{6.42}$$

By comparing with the result of our first order perturbation theory in ϵ_0, it becomes possible to fix the functions F_0 and R. This strategy gives us the one-loop RG improved result for the alternating part of $\langle S^z(r)\rangle_\uparrow$

$$N_z(r) = c\sqrt{a}\frac{F_0}{\sqrt{L}}\left(\frac{\epsilon_0}{\epsilon(L)}\right)^{\frac{1}{4}}(1+\epsilon(L)R)\ , \tag{6.43}$$

with

$$F_0(\frac{r}{L}) = -\sqrt{\frac{\pi\sin\theta_r}{2}}\ , \tag{6.44}$$

and

$$R(\frac{r}{L}) = \frac{\pi}{2}\log\frac{2\pi}{\sin\theta_r} + 2\left(\int_0^{\theta_r}+\int_0^{\pi-\theta_r}\right)\phi\cot\phi d\phi\ , \tag{6.45}$$

with $\theta_r \equiv \frac{\pi r}{L}$.

In order to cast this expression into an explicitly useful form for comparison with numerical results on a chain of N sites with lattice spacing a, we rewrite the prefactor as

$$\left(\frac{\epsilon_0}{\epsilon(L)}\right)^{\frac{1}{4}} \approx \left(1+2\pi|\epsilon_0|\left\{\log\left(\frac{L}{r_0}\right)+\frac{1}{2}\log\left(\log\left(\frac{L}{r_0}\right)\right)\right\}\right)^{1/4}.$$

Express $\epsilon(L)$ as

$$\epsilon(L) = -\frac{|\epsilon_0|}{1+2\pi|\epsilon_0|\left\{\log\left(\frac{L}{r_0}\right)+\frac{1}{2}\log\left(\log\left(\frac{L}{r_0}\right)\right)\right\}}\ . \tag{6.46}$$

As mentioned before, we choose the short-distance cutoff as $r_0 = a$ and set the length L to $L = (N+1)a$ (see Appendix B). Eqns (6.43),(6.44), (6.45) with these inputs constitutes a theoretical prediction

with two free parameters (the overall amplitude c, and the bare coupling ϵ_0 at the lattice scale), and we find (Section 6.5) that this provides an extremely good two-parameter fit of our numerical data in the power-law ordered antiferromagnetic phase of the one dimensional JQ_3 model. In addition, the spin texture at $q = q_c$, the critical end-point of this power-law ordered Neel phase, fits extremely well to the scaling function F_0, to which the more general prediction reduces when $\epsilon_0 = 0$.

6.5 Comparing numerical results with field theory results

In Fig (6.3), we have shown our data for the alternating part of the spin texture and compared it with the scaling prediction at the critical point $q = q_c$ for two of our largest system sizes. As can be seen from these two figures, the scaling prediction fits extremely well to all the data at both sizes. Also, a two-parameter fit using the RG-improved perturbation theory result yields a best-fit value of ϵ_0 indistinguishable from $\epsilon_0 = 0$. This confirms the location of the critical point, as the bare coefficient of the marginally irrelevant cosine interaction is expected to be zero at this quantum phase transition.

This almost perfect fit to the scaling prediction is contrasted with the results shown in Figs (6.2) and (6.1); which show numerical results at two representative points in the power-law Néel phase compared with the one-parameter fit obtained from the scaling prediction. As shown in these two figures, the scaling prediction cannot predict well the numerical results for $q < q_c$. Additionally we note that the misfit of scaling predictions with numerical results increases as we go further from the critical point(i.e. smaller q).

In the same figures, we also show the best two-parameter fit obtained by using our RG improved perturbation theory results. We show here that the best-fit values of $|\epsilon_0|$ increase as one goes further away from $q = q_c$, which is consistent with the expectation that the bare coefficient of the cosine interaction vanishes as q approaches q_c. Also we show that the RG improved perturbation theory provides a much better fit at $q = 0.02$ than at the Heisenberg point $q = 0$, consistent with the fact that our calculation is perturbative in the renormalized coupling $\epsilon(L)$, and is supposed to be a better approximation when the bare value of $|\epsilon_0|$ is smaller to begin with.

6.6 Discussion

The question one might ask, what can we conclude from these results about the possible origins of multiplicative logarithmic corrections to spin textures at other critical points ? To explore this, let us consider the same calculation of the spin texture, but at a different critical point with an *irrelevant* coupling g and a small scaling dimension α. In other words, we assume that $\beta(g) = -\alpha g + \ldots$ with α small and positive, and $\gamma(g) = \delta_0 + \delta_1 g + \ldots$. In this case, the Callan-Symanzik equation would predict that N_z satisfy the scaling law

$$N_z(\vec{r}) = \exp\left(-\int_{g_0}^{g(L)} \frac{\gamma(g)}{\beta(g)} dg\right) F\left(\frac{\vec{r}}{L}, g(L)\right) \tag{6.47}$$

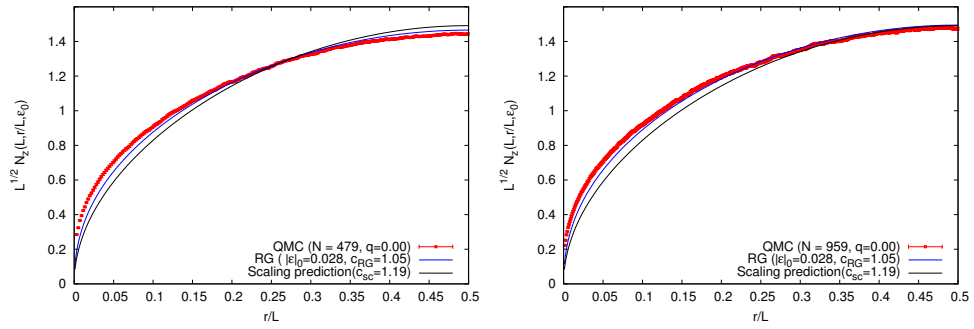

Figure 6.1: $L^{1/2}N_z(r)$ plotted versus r/L in the power-law ordered Néel phase at $q = 0.0$ (where $L = N + 1$ for chains with $N = 959$ and $N = 479$ spins and open boundary conditions) and compared with the scaling prediction with a common best-fit prefactor c_{sc}. Note that the deviation of the data from the scaling prediction cannot be simply ascribed to an overall multiplicative factor that grows with N, since the *shape* of the curves is slightly different. Data at both sizes is also fit to the best two-parameter fit corresponding to our RG improved perturbation theory result, and the agreement is seen to be quite reasonable, but not perfect, for the best fit values of c_{RG} and $|\epsilon_0|$ listed in the legend.

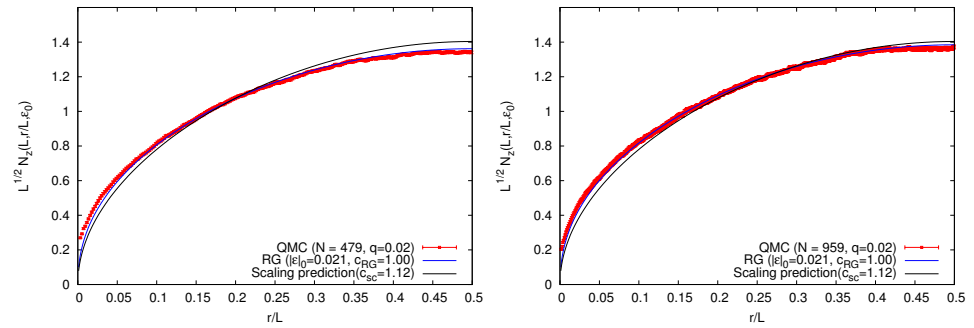

Figure 6.2: $L^{1/2}N_z(r)$ plotted versus r/L in the power-law ordered Néel phase at $q = 0.02$ (where $L = N+1$ for chains with $N = 959$ and $N = 479$ spins and open boundary conditions) and compared with the scaling prediction with a common best fit prefactor c_{sc}. Note that the deviation of the data from the scaling prediction cannot be simply ascribed to an overall multiplicative factor that grows with N, since the *shape* of the curves is slightly different. Data at both sizes is also fit to the best two-parameter fit corresponding to our RG improved perturbation theory result, and the agreement is seen to be excellent for the best fit values of c_{RG} and $|\epsilon_0|$ listed in the legend.

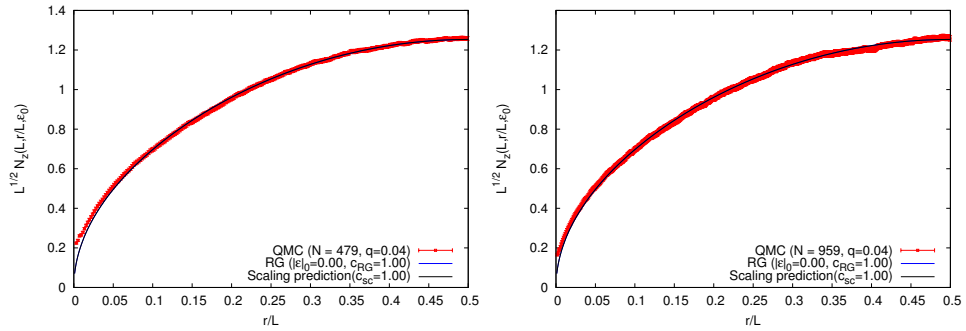

Figure 6.3: $L^{1/2}N_z(r)$ plotted versus r/L (where $L = N + 1$ for chains with $N = 959$ and $N = 479$ spins and open boundary conditions) and compared with the scaling prediction F_0 for $q = 0.04$, the approximate location of the quantum critical point separating the power-law Néel phase from the VBS ordered phase in the one dimensional JQ_3 model. Note the data at both sizes fits essentially perfectly to the scaling prediction with the same prefactor c_{sc}. Also note that the best two-parameter fit corresponding to our RG improved perturbation theory result also gives $|\epsilon_0| = 0$, and thus coincides with the scaling answer.

for some function F (that needs a more detailed analysis to determine). Using the postulated form of the β and γ functions, one can therefore conclude

$$N_z(\vec{r}) = \frac{\mathcal{C}}{L^{\delta_0}} F\left(\frac{\vec{r}}{L}, g_0/L^{\alpha}\right) \tag{6.48}$$

Thus, if the critical point in question has no marginal operators, the spin texture will quite generally obey scaling as long as the scaling function $F(x, y)$ does not diverge as $y \to 0$. Conversely, if the critical point in question has a marginal operator, scaling will always be violated by multiplicative logarithmic factors even if the scaling function $F(x, y)$ is perfectly analytic and well-defined in the $y \to 0$ limit. Indeed, in this marginal case, the only way of *evading* a multiplicative logarithmic correction would be to "arrange" for the $y \to 0$ limit of the scaling function $F(x, y)$ to have exactly the "right" kind of singularity needed to cancel the effects of the multiplicative logarithmic correction coming from the exponential prefactor. One may therefore conclude that unless the scaling function has a particularly "fine-tuned" form, scaling predictions for N_z will be *generically violated by multiplicative logarithmic corrections* in the presence of a marginal operator. Conversely, irrelevant operators can lead to violations of scaling only if the scaling function has a divergence as this operator renormalizes to zero.

Appendix A

Evaluating Density of states for randomly diluted bipartite hopping Hamiltonian

In this appendix we will discuss in detail our methods of calculating the density of states for the randomly diluted bipartite hopping Hamiltonian. As it was discussed before (section 3.2), our need in calculating density of states boils down to obtaining the spectrum of a very large matrix at very high precision. It turns out that calculation is possible without actually diagonalizing the matrix or storing the matrix. In this appendix first we will discuss the schemes we took for reduction of memory cost of the computation and then we will briefly review the tools we use to fetch reliable results at high precision. Finally we will discuss about the Sturm's method of calculating the spectral density without diagonalizing the matrix.

A.1 Reducing the matrix size

We already discussed (section 3.2) that for bipartite hopping Hamiltonian analyzing only half sized matrix $\mathbb{M}^2$ is enough. A further not so significant reduction in the matrix dimension is possible, by removing the array elements for deleted sites. So there is no need to analyze the $N^2_{A(B)}$(Number of site in A or B sublattices) size matrix, we can now analyze the compressed $dim^2_{A(B)}$ ($dim_{A(B)} = N_A(B) - I_{A(B)}$,$I_{A(B)}$ being number of vacancies in A or B sublattices and $N = N_A + N_B$ is the total number of sites) size matrix. However while doing this contraction we keep track of the correspondence between the compressed matrix elements and original full matrix elements. Here one of our goals is to get as large size of $N_{A(B)}$ as possible in order to reduce finite size corrections in low energy. In addition, as discussed in the introduction (section 2.2.1) that we are trying to see rare fluctuation events is very narrow energy range; so here we need to probe very low energy states of the system due to large number of impurities. So our another goal is to make our computation as accurate as possible for extremely small numbers.

A.2 Calculation of Density of states

The simplest way to calculate density of states is to diagonalize the matrix $\mathbb{M}^2$ by any standard procedure (like Gaussian elimination) and count the number of eigenvalues (we will call it λ_r) in all intervals $[\lambda, \lambda + \Delta]$. But the time-complexity of that process will be $O(N_A(B)^3)$, and the memory cost will be $O(N_A(B)^2)$. So one possible way to reduce that cost such that the problem fits into a standard computer capacity at large values of $N_A(B)$, is to use sparse matrix algorithms. For that we will use semi-open boundaries; which means in the $N \times N$ matrix $\mathbb{M}$ a site with index i can have the farthest connection to a site with index $i + 2L$, so the matrix will be a banded matrix with $2L$ leading diagonals. Similarly, for the $N_{A(B)} \times N_{A(B)}$ matrix $\mathbb{M}^2$ a site with index i can have the farthest connection to a site with index $i + 4L$. That reduces the memory cost to $O(4LN^2_{A(B)})$ and time-complexity to $O(4LN^2_{A(B)})$. Moreover, since $\mathbb{M}^2$ is a symmetric matrix, one can use standard Gaussian elimination type algorithms for symmetric band matrices to calculate the eigenvalues. There are available routines (like LAPACK [75]) which performs that task reliably using the standard computer floating point arithmetic.

Calculating with high precession It turns out that due to using the standard floating point arithmetic such routines are numerically unstable when the eigenvalues are very small. For instance the machine-ϵ[1] for double precision in IEEE 754 floating-point formats is given by 1.11×10^{-16}. So obviously when there are many eigenvalues that small, an instability is expected in determining those numbers. Since we are interested in the very low energy properties of the system induced by impurities, it is important for us to know the number of eigenvalues in an interval which is well below the standard machine-ϵ. For that purpose we make use of the GNU Multiple Precision Arithmetic Library[47], which uses numerically stable and efficient algorithms [48] to stretch the precision for basic arithmetic operations well beyond the machine precision. That task is accomplished by breaking down the asthmatic calculation into units which fits (known as limbs) withing the memory of a machine and then after performing calculation in each units they are recombined; depending on the required precision and the arithmetic operation different algorithms are used [48, 47]. However, the only limit in the maximum achievable precision by this is imposed by the virtual memory of the machine.

Calculating density of states without diagonalizing the matrix $\mathbb{M}$ We took an alternate approach here to calculate density of states. Since our main interest is knowing the number of eigenvalues in a certain interval of specified values, we make use of the Sturm sequence method. In brief the method gives a prescription to count the number of eigenvalues above a particular number λ, for any real symmetric matrix A by calculating the number of sign agreements between the successive leading principal minors of the matrix $(A - \lambda I)$. The ease the process of evaluating the principal minors the matrix $(A - \lambda I)$ can be first triangularized using Gaussian elimination process[46]. Even though there are several methods for triangularization, Gaussian elimination process is favored because it doesn't

[1] the smallest number ϵ for which the machine returns $1 + \epsilon > 1$

spoil the banded form of the matrix.

Sturm sequence The method of Sturm sequence is obtained as a corollary from a well-known theorem for hermitian matrices, which is states as:

Theorem 1. (Separation Theorem) *Consider an $N \times N$ Hermitian matrix A, with eigenvalues $\lambda_1 \geq \lambda_2 \geq ... > \lambda_N$. Suppose A_k denotes the principal submatrix of A obtained by deleting the kth row and kth column of H, where A_k has the eigenvalues $\alpha_1 \geq \alpha_2 \geq ... > \alpha_{N-1}$,*

then $\lambda_1 \geq \alpha_1 \geq \lambda_2 \geq \alpha_2 \geq ... \geq \alpha_{N-1} \geq \lambda_N$.

Corrolary 2. *From the Separation theorem it follows that if A_k is a principal submatrix of A of order k with eigenvalues $\alpha_1 \geq \alpha_2 \geq ... > \alpha_k$, then $\lambda_i \geq \alpha_i \geq \lambda_{N-k+i}$ for $i = 1, .., k$.*

The method of Sturm sequence follows from this corollary just by noticing the fact that the eigenvalues of the $(k-1)$-th leading principle minor, say A_{k-1}, of a symmetric matrix separates the eigenvalues of the k-th leading principle minors A_k, for $k = 1, .., N$. From here one can proof by induction that if one calculates the leading principle minors of the matrix $(A - \lambda I)$ i.e. the quantities $(A - \lambda I)_0, (A - \lambda I)_1, ..., (A - \lambda I)_N$- at a given λ, the number of agreements in the sign of consecutive principle minors will be the number of eigenvalues greater than λ(For details of the proof see Ref. [46]). In order to make this statement meaningful for all values of k, one can assume that $(A - \lambda I)_0 = 0$ and we associate $(A - \lambda I)_k$ a sign opposite to $(A - \lambda I)_{k-1}$ when $(A - \lambda I)_k = 0$ (also note the two consecutive $(A - \lambda I)_k$ cannot be zero).

In our calculation $A = \mathbb{M}^2$, so all eigenvalues above λ in A will be eigenvalues below λ for $\mathbb{M}^2$ and that gives us the integrated density of states $N(\lambda)$.

Appendix B

Spin wave theory calculations in closed systems

This appendix is complementary to 5.4. Here we show the details calculation to find the eigenvalues and eigenstates for the spin-wave Hamiltonian H^{sw} in periodic samples. As mentioned in chapter 2.3.3, we will exploit the translational invariance in periodic samples and work in Fourier space to obtain the spin-wave modes and their wavefunctions to calculate $m_0 = S - \Delta^{'}$ correct to leading order in the spin-wave expansion. We will discuss that calculation for all the models we study under spin wave theory, as described in the 5.1.

B.1 Nearest neighbor interaction model

Our nearest neighbor model Hamiltonian reads as follows:

$$H = J \sum_{\langle i,j \rangle} \mathbf{S}_i . \mathbf{S}_j . \tag{B.1}$$

After Holstein Primakoff transformation (Eq. 5.8, 5.9) and linear spin wave expansion it comes to Eq. 5.10, which for Heisenberg model with nearest neighbor interaction reads,

$$H^{sw} = JSz \sum_i b_i^\dagger b_i + \frac{JS}{2} \sum_{\langle ij \rangle} (b_i b_j + b_i^\dagger b_j^\dagger). \tag{B.2}$$

The Fourier transformation of the bosonic operators into reciprocal **k**-space is given by,

$$b_{\mathbf{k}} = \frac{1}{L} \sum_j e^{-i\mathbf{k}j} b_j \tag{B.3}$$

Applying the Fourier transformation (B.3) and using the delta function identity $\frac{1}{L^2} \sum_j e^{ij(\mathbf{k}-\mathbf{k}^{'})} = \delta_{\mathbf{k},\mathbf{k}'}$ on Eq.B.2, we will get the Hamiltonian in the k-space as,

$$H^{sw}(\mathbf{k}) = -\frac{JS^2L^2z}{2} + H_0(\mathbf{k}) + H_1(\mathbf{k}) + O(\frac{1}{S}). \tag{B.4}$$

Where $H^{sw}(\mathbf{k})$ is the quadratic Hamiltonian containing usual $b^\dagger b$ type term and bb or $b^\dagger b^\dagger$ type terms. $H_1(\mathbf{k})$ contains terms of the order $(1/S)^0$. We keep only terms upto lowest order in $1/S$ approximation, so the only term we want to deal with is the quadratic term $H_0(\mathbf{k})$,

$$H^{sw}(\mathbf{k}) = JSz\sum_{\mathbf{k}}[b^\dagger_{\mathbf{k}}b_{\mathbf{k}} + \frac{\eta_{\mathbf{k}}}{2}(b_{\mathbf{k}}b_{-\mathbf{k}} + b^\dagger_{\mathbf{k}}b^\dagger_{-\mathbf{k}})]. \tag{B.5}$$

where $\eta_{\mathbf{k}} = \frac{1}{z}\sum_{\mathbf{a}} e^{i\mathbf{k}.\mathbf{a}}$($\mathbf{a}$ being the lattice vector). For the diagonalization we have to perform a Bogoliuov transformation(equivalent to finding a transformation $\mathbb{S}$ of Eq. 5.15 in $\mathbf{k}$-space) as follows,

$$\gamma_{\mathbf{k}} = P_{\mathbf{k}}b_{\mathbf{k}} - Q_{\mathbf{k}}b^\dagger_{-\mathbf{k}} \tag{B.6}$$

To determine $P_{\mathbf{k}}$ and $Q_{\mathbf{k}}$ (in other words to know the matrix $\mathbb{S}$ in $\mathbf{k}$-space) we apply the following facts

- the Bogoliuov quasi particle i.e. γ is bosonic i.e. $[\gamma_{\mathbf{k}}, \gamma^\dagger_{\mathbf{k}'}] = \delta_{\mathbf{k}\mathbf{k}'}$,$[\gamma_{\mathbf{k}}, \gamma_{\mathbf{k}'}] = [\gamma^\dagger_{\mathbf{k}}, \gamma^\dagger_{\mathbf{k}'}] = 0$, this is equivalent to condition (25) of real space on $P_{\mathbf{k}}$, $Q_{\mathbf{k}}$.

  It turns out from this condition that we can take $P_{\mathbf{k}} = \cosh\theta_{\mathbf{k}}$,$Q_{\mathbf{k}} = \sinh\theta_{\mathbf{k}}$, where $\theta_{\mathbf{k}}$ is real and even in $\mathbf{k} \longrightarrow -\mathbf{k}$. Now in terms of the spin wave excitations i.e. Bogoliuov quasiparticles γ, the Hamiltonian is given by,

$$\begin{aligned} H_0(\mathbf{k}) &= JSz\sum_{\mathbf{k}}[(\cosh 2\theta_{\mathbf{k}} + \eta_{\mathbf{k}}\sinh 2\theta_{\mathbf{k}})\gamma^\dagger_{\mathbf{k}}\gamma_{\mathbf{k}} \\ &+ \frac{1}{2}(\sinh 2\theta_{\mathbf{k}} + \eta_{\mathbf{k}}\cosh 2\theta_{\mathbf{k}})(\gamma^\dagger_{\mathbf{k}}\gamma^\dagger_{-\mathbf{k}} + \gamma_{\mathbf{k}}\gamma_{-\mathbf{k}}) + \sinh^2\theta_{\mathbf{k}} + \eta_{\mathbf{k}}\sinh 2\theta_{\mathbf{k}}] \end{aligned} \tag{B.7}$$

- The Bogoliuov transformation diagonalizes the Hamiltonian i.e. $H_0(\mathbf{k})$ must come to the diagonal form $\lambda_{\mathbf{k}}\gamma_{\mathbf{k}}\gamma^\dagger_{\mathbf{k}}$, equivalent to condition Eq. 5.26 of real space.

  Condition (2) tells us to choose the $\theta_{\mathbf{k}}$ such that is satisfies the $\tanh\theta_{\mathbf{k}} = -\eta_{\mathbf{k}}$ in order to eliminate the unusual terms $\gamma\gamma$ or $\gamma^\dagger\gamma^\dagger$. Making that choice, $\lambda_{\mathbf{k}} = \sqrt{1-\eta_{\mathbf{k}}}$ and the final diagonalized Hamiltonian turns out to be

$$H = E_0 + \sum_{\mathbf{k}}\omega_{\mathbf{k}}(\gamma^\dagger_{\mathbf{k}}\gamma_{\mathbf{k}} + \frac{1}{2}). \tag{B.8}$$

  Where $\omega_{\mathbf{k}} = JSz\lambda_{\mathbf{k}}$ and $E_0 = \frac{-JL^2zS}{2}$. Thus our square lattice with antiferromagnetic interaction under the lowest order in $1/S$ approximation is mapped to a collection of independent harmonic oscillators with frequency ω.

Now let us calculate the $n^z_\uparrow$, from the definition of the same in Eq. 2.17 and applying Holstein-Primakoff transformation (Eq. 5.8, 5.9),

$$\begin{aligned} n^z_\uparrow &= \frac{1}{N_{\text{tot}}}\sum_{\mathbf{r}} \eta_{\mathbf{r}} \langle S^z_{\mathbf{r}} \rangle_\uparrow \\ &= \frac{1}{L^2}\langle \sum_i S^z_{iA} - \sum_j S^z_{jB} \rangle \\ &= S - \frac{1}{L^2}\sum_{\mathbf{k}} (\langle b^\dagger_{\mathbf{k}} b_{\mathbf{k}} \rangle) \\ &= S - \frac{1}{L^2}\sum_{\mathbf{k}} v^2_{\mathbf{k}} \\ &= S - \frac{1}{2L^2}\sum_{\mathbf{k}} [\frac{1}{\sqrt{1-\eta^2_{\mathbf{k}}}} - 1] \end{aligned} \tag{B.9}$$

So for a periodic infinite lattice we can convert this sum into an integral and write,

$$n^z_\uparrow = S - \Delta. \tag{B.10}$$

Where Δ is the quantum fluctuation which reduces the staggered magnetization $n^z_\uparrow$ from its classical value. And the integral form of Δ is given by

$$\Delta = \frac{1}{2}\int \frac{d^2k}{4\pi^2}[\frac{1}{\sqrt{1-\eta^2_{\mathbf{k}}}} - 1]. \tag{B.11}$$

Now another order parameter m^2 is given by (Eq. 2.16),

$$\begin{aligned} m^2_0 &= \frac{1}{N_{\text{tot}}}\sum_{\vec{r}\vec{r}'} \eta_{\vec{r}}\eta_{\vec{r}'} \langle \mathbf{S}_{\mathbf{r}} \cdot \mathbf{S}_{\mathbf{r}'} \rangle_0 \\ &= \frac{1}{L^2}[\sum_{ij} \langle \mathbf{S}_{Ai}\mathbf{S}_{Aj} + \mathbf{S}_{Bi}\mathbf{S}_{Bj} - 2\mathbf{S}_{Ai}\mathbf{S}_{Bj} \rangle] \end{aligned} \tag{B.12}$$

Applying the Holstein-Primakoff transformation transformation (Eq. 5.8, 5.9) and doing the lowest order in $1/S$ expansion,

$$m^2_0 = \frac{1}{L^2}[L^2S^2 + S\sum_{ij} \langle b_i b^\dagger_j + b^\dagger_i b_j - b_i b_j - b^\dagger_i b^\dagger_j - 2b^\dagger_i b_i \rangle]. \tag{B.13}$$

Applying the Fourier transform (B.3) and using the delta function identity,

$$\begin{aligned} m^2_0 &= \frac{1}{L^2}[L^2S^2 + S\sum_{\mathbf{k}} \langle b_0 b^\dagger_0 + b^\dagger_0 b_0 - b_0 b_0 - b^\dagger_0 b^\dagger_0 - 2b^\dagger_{\mathbf{k}} b_{\mathbf{k}} \rangle] \\ &= [S^2 + \frac{S}{L^2}\sum_{\mathbf{k}} \langle b_0 b^\dagger_0 + b^\dagger_0 b_0 - b_0 b_0 - b^\dagger_0 b^\dagger_0 - 2b^\dagger_{\mathbf{k}} b_{\mathbf{k}} \rangle]. \end{aligned} \tag{B.14}$$

Now using the Bogoliuov transformation (Eq. B.6) and taking the average we get,

$$\begin{aligned} m_0 &= S[1 - \frac{2}{L^2 S}\sum_{\mathbf{k}} v^2_k]^{\frac{1}{2}} \\ &= S - \frac{1}{2L^2}\sum_{\mathbf{k}} [\frac{1}{\sqrt{1-\eta^2_{\mathbf{k}}}} - 1], \end{aligned} \tag{B.15}$$

keeping terms upto lowest order in $1/S$. From the expression of m (B.16) we can see that it is same as the expression of $n^z_\uparrow$ (B.10) under the spin wave approximation of lowest order of $1/S$ terms. So exactly in the same manner we can write this sum as an integral for a periodic infinite lattice i.e.

$$m_0 = S - \Delta^{'}, \tag{B.16}$$

where $\Delta^{'} = \Delta$(Eq.B.11).

B.2 Next nearest neighbor interaction model

The next nearest neighbor model is described by the Hamiltonian H_{JJ_2}

$$H_{JJ_2} = J\sum_{\langle ij\rangle}\mathbf{S}_i.\mathbf{S}_j + J_2\sum_{\langle\langle ij\rangle\rangle}\mathbf{S}_i.\mathbf{S}_j. \tag{B.17}$$

Where $\langle.\rangle$ denotes nearest neighbors bonds and $\langle\langle.\rangle\rangle$ denotes next nearest neighbors bonds, see the models section 1.1 for more details. The calculation is same as before, so let us skip some of the steps and directly write down Hamiltonian in the **k** space in lowest order spin wave approximation i.e. the quadratic part,

$$H^{sw}_{JJ_2}(\mathbf{k}) = 2JSz\sum_{\mathbf{k}}[(1+\eta(\gamma^{'}_{\mathbf{k}}-1))b^\dagger_{\mathbf{k}}b_{\mathbf{k}} + \frac{\gamma_{\mathbf{k}}}{2}(b_{\mathbf{k}}b_{-\mathbf{k}} + b^\dagger_{\mathbf{k}}b^\dagger_{-\mathbf{k}})]. \tag{B.18}$$

We can write the Hamiltonian as

$$H^{sw}_{JJ_2}(\mathbf{k}) = 2JSz\sum_{\mathbf{k}}A_{\mathbf{k}}[b^\dagger_{\mathbf{k}}b_{\mathbf{k}} + \frac{\Gamma_{\mathbf{k}}}{2}(b_{\mathbf{k}}b_{-\mathbf{k}} + b^\dagger_{\mathbf{k}}b^\dagger_{-\mathbf{k}})]. \tag{B.19}$$

Where $A_{\mathbf{k}} = 1+\eta(\gamma^{'}_{\mathbf{k}}-1)$, $\Gamma_{\mathbf{k}} = \frac{\gamma_{\mathbf{k}}}{(1+\eta(\gamma^{'}_{\mathbf{k}}-1))}$ and $\eta = J_2/J$. Thus we wrote down the Hamiltonian in our known form as before,hence the rest of the calculation will just follow as before and the final results for JJ_2 will be,

$$n^z_\uparrow = S - \Delta_{JJ_2} \tag{B.20}$$

and

$$m_0 = S - \Delta^{'}_{JJ_2}. \tag{B.21}$$

Where $\Delta^{'}_{JJ_2} = \Delta_{JJ_2}$ and $\Delta_{JJ_2} = \int\frac{d^2k}{4\pi^2}[\frac{1}{\sqrt{1-\Gamma^2_{\mathbf{k}}}}-1]$.

B.3 Striped interaction model

The striped model is described by the Hamiltonian $H_{striped}$

$$H_{JJ'} = J\sum_{\langle ij\rangle}\mathbf{S}_i.\mathbf{S}_j + J'\sum_{\langle ij\rangle'}\mathbf{S}_i.\mathbf{S}_j. \tag{B.22}$$

Where $\langle.\rangle$ and $\langle.\rangle'$ denotes the red bonds and the blue dotted bonds in the Fig. 5.1 respectively. For more details look at 5.1.

Here the expression for $n^z_\uparrow$ is,

$$n^z_\uparrow = S - \Delta_{striped}. \tag{B.23}$$

Where

$$\Delta_{striped} = \frac{1}{2}\int \left(\sqrt{\frac{\lambda_2^+}{\lambda_1^-}} + \sqrt{\frac{\lambda_1^-}{\lambda_2^+}} + \sqrt{\frac{\lambda_2^-}{\lambda_1^+}} + \sqrt{\frac{\lambda_1^+}{\lambda_2^-}} - 1\right)\frac{d^2k}{(4\pi)^2}. \tag{B.24}$$

$$\lambda_1^\pm = -\frac{3}{2} - \frac{1}{2}\alpha \pm \frac{1}{2}\sqrt{1+\alpha^2+2\alpha\cos k_x} + \cos k_y \tag{B.25}$$

$$\lambda_2^\pm = -\frac{3}{2} - \frac{1}{2}\alpha \pm \frac{1}{2}\sqrt{1+\alpha^2+2\alpha\cos k_x} - \cos k_y \tag{B.26}$$

Here $\alpha = J'/J$. Point to notice is that the unit cell size is double here, so the normalization factor is different from before. In a similar manner we can calculate m for $JJ^{'}$ model,

$$m_0 = S - \Delta^{'}_{striped}. \tag{B.27}$$

Where $\Delta^{'}_{JJ'} = \Delta_{JJ'}$.

Appendix C

Bosonization

Bosonization is a procedure with which one can map quantities in a fermionic theory to quantities in a bosonic theory. The converse can also be used, which is called fermionization. Bosonization is often more useful as that can be used to tackle more difficult fermionic calculations with the help of tools developed for bosonic calculations. In brief, bosonization can be described as following: in one dimension, it is possible to express a fermion as a coherent state of a Bose field, or conversely, a boson as a bound state of fermionic theory. Such a connection is possible in one-dimension because in one dimension the low lying excitations have a linear form (Fig. C.1). So, Fermi surface is a pair of points about which the particle-hole excitation pair can have nearly the same group velocity and propagate together; in other words the pair dispersion relation near Fermi surface is narrow and like a coherent bound state.

In higher dimensions a particle-hole pair with a given momentum can have a continuous spectrum of energies depending on the shape of Fermi surface(Fig. C.2). Thus, the particle-hole spectrum is a continuum throughout and it is harder to form such a coherently propagating particle-hole bound state; in other words the pair-excitations are not bound state like. It is relatively straightforward to understand the functional form of boson to fermion mapping (dubbed as "bosonization dictionary") at the level of correlation functions. So in this appendix we will discuss the correlation functions of a free fermionic theory and a free bosonic theory; which will lead us to the bosonization dictionary. For a detailed review of this subject, look at references [76][77].

C.1 Correlation functions for free fermionic theory

Consider a system of free massless non-relativistic fermions(represented by the field ψ) in one dimension with the Hamiltonian

$$H_F = \int dx \left[\psi^\dagger \left(-\frac{i}{m} \partial_x^2 \right) \psi - \mu \psi^\dagger \psi \right]. \tag{C.1}$$

Here ψ is Fermi field satisfying canonical commutation relations $\{\psi^\dagger(x), \psi(x')\} = \delta(x - x')$, with the dispersion relation $E = \frac{k^2}{2m} - \mu$. The zero temperature ground state of this system will be all the

single particle eigenstates filled up upto the Fermi energy $\epsilon_F = \mu$ and the Fermi level will be made of two points at $k = \pm k_F$(Fig. C.1). If one is interested in the low energy physics of this system for all practical purposes it is a good enough approximation to linearize the dispersion relation near the Fermi levels as $E \approx \pm v_F(k \pm k_F)$, with $v_F(= k_F/m)$ being the Fermi velocity. Thus one can express the low energy excitations about this ground state in the chiral basis as

$$\psi(x) = \sqrt{a}\left(e^{-ik_F x}\psi_R(x) + e^{ik_F x}\psi_L(x)\right). \tag{C.2}$$

The corresponding low-energy Hamiltonian becomes,

$$H_F = -iv_F \int dx \left[\psi_R^\dagger \frac{d\psi_R}{dx} - \psi_L^\dagger i\frac{d\psi_L}{dx}\right]. \tag{C.3}$$

Where ψ_L and ψ_R are left propagating and right propagating modes respectively, containing only slowly varying Fourier modes near the points $E = v_F(k + k_F)$ and $E = -v_F(k - k_F)$ respectively. The canonical commutation relations followed here is $\{\psi^\dagger_{L(R)}(x), \psi_{L(R)}(x')\} = \delta(x - x')$. Now this Fermionic fields can be expanded in terms of the physical modes, which can have several kind of excitations. As mentioned before the ground state for this linearized Hamiltonian is made of all the negative energy states with respect to the Fermi energy i.e. the right moving negative k modes and left moving positive k modes. In the right moving sector the possible excitations are following: particles(holes) of momentum $k > 0$ with creation operator $\alpha^\dagger(k)(\beta^\dagger(k))$. Similarly for left moving sector the excitations are: particles(holes) of momentum $k < 0$ with creation operator $\gamma^\dagger(k)(\delta^\dagger(k))$. Those operators again satisfy all the canonical fermionic commutation relations $\{\alpha^\dagger(k), \alpha(k')\} = \{\beta^\dagger(k), \beta(k')\} = \{\gamma^\dagger(k), \gamma(k')\} = \{\delta^\dagger(k), \delta(k')\} = 2\pi\delta(k - k')$, rest other possible commutations are zero. The fermionic operators expressed in terms of this low energy modes are given by

$$\begin{aligned} \psi_R(z) &= \int_{k>0} \frac{dk}{2\pi}\left[e^{-kz}\alpha(k) + e^{kz}\beta^\dagger(k)\right] \\ \psi_L(\bar{z}) &= \int_{k>0} \frac{dk}{2\pi}\left[e^{-k\bar{z}}\gamma(k) + e^{k\bar{z}}\delta^\dagger(k)\right], \end{aligned} \tag{C.4}$$

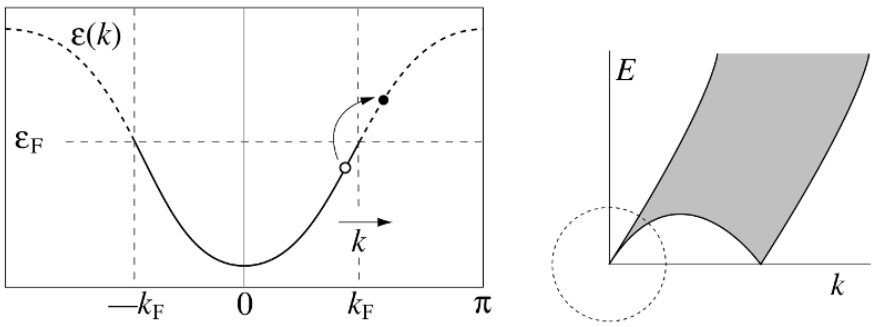

Figure C.1: Left panel: Dispersion relation for one-dimensional fermions. Right panel: electron-hole pair dispersion relation for one-dimensional fermions. Figure taken from ref [77].

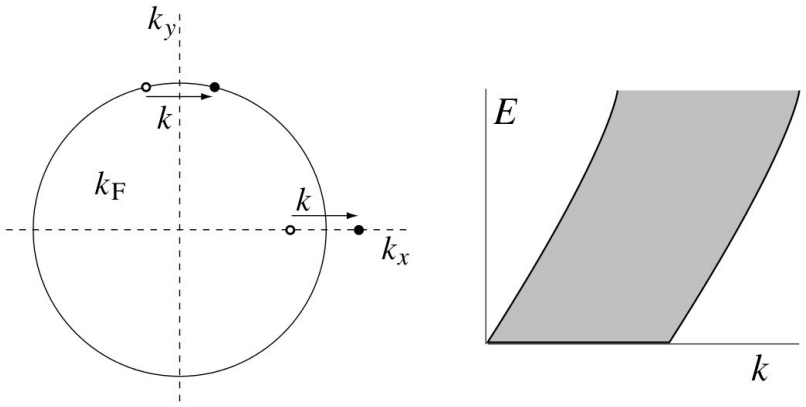

Figure C.2: Left panel: Dispersion relation for two-dimensional fermions, assuming a circular Fermi surface. Right panel: electron-hole pair dispersion relation for two-dimensional fermions with a circular Fermi surface. Figure taken from ref [77].

with the notation $v\tau - ix = z$, $v\tau + ix = \bar{z}$ and $\tau = it$ the imaginary time. In terms of this low energy modes the Hamiltonian is as follows:

$$H_F = v_F \int_0^\infty \frac{dk}{2\pi} k \left[\alpha^\dagger(k)\alpha(k) - \beta(k)\beta^\dagger(k) + \gamma^\dagger(k)\gamma(k) - \delta(k)\delta^\dagger(k)\right]. \tag{C.5}$$

The ground state of this Hamiltonian will have infinite negative energy $E_0 = -v_F \int_0^\infty \frac{dk}{2\pi} k = -\infty$. The way to deal with this infinity is by putting the creation operators to the left of annihilation operators i.e. working with the normal ordered Hamiltonian, where the E_0 is subtracted.

$$: H_F := v_F \int_0^\infty \frac{dk}{2\pi} k \left[\alpha^\dagger(k)\alpha(k) + \beta^\dagger(k)\beta(k) + \gamma^\dagger(k)\gamma(k) + \delta^\dagger(k)\delta(k)\right]. \tag{C.6}$$

Thus one can calculate the propagators as follows

$$\begin{aligned}
\langle \psi_R(z)\psi_R^\dagger(z')\rangle &= \langle \psi_R^\dagger(z)\psi_R(z')\rangle \\
&= \int_{k>0} \frac{dk}{2\pi} \int_{q>0} \frac{dk'}{2\pi} \langle \alpha(k)\beta^\dagger(k')\rangle e^{-kz+k'z'} \\
&= \int_{k>0} \frac{dk}{2\pi} \int_{q>0} \frac{dk'}{2\pi} 2\pi\delta(k-k') e^{-kz+k'z'} \\
&= \int_{k>0} \frac{dk}{2\pi} e^{-k(z-z')} \\
&= \frac{1}{2\pi(z-z')}.
\end{aligned} \tag{C.7}$$

Similarly,

$$\langle \psi_L(z)\psi_L^\dagger(z')\rangle = \langle \psi_L^\dagger(z)\psi_L(z')\rangle = \frac{1}{2\pi(z-z')}. \tag{C.8}$$

In the equal time limit,

$$\begin{aligned}
\langle \psi_L(x,0)\psi_L^\dagger(x,0)\rangle &= \lim_{\epsilon\to 0^+} \langle \psi_L^\dagger(x,\epsilon)\psi_L(x',0)\rangle \\
&= \lim_{\epsilon\to 0^+} \frac{1}{2\pi} \frac{1}{i(x-x')+\epsilon},
\end{aligned} \tag{C.9}$$

where time ordering is ensured by taking the limit as $\lim_{\epsilon\to 0^+}$.

C.2 Correlation functions for free bosonic theory

Now consider a free Boson Hamiltonian in one dimension as

$$H_B = \frac{v_F}{2}\int dx \left[\Pi(x)^2 + (\partial_x\phi)^2\right]. \tag{C.10}$$

If $\Pi(x)$ is the canonical conjugate momentum to the field $\phi(x)$, the equal time canonical conjugate relationship for bosons will be

$$\left[\phi(x), \Pi(x')\right] = i\delta(x-x'). \tag{C.11}$$

Like the fermionic case the standard modal expansion will be

$$\begin{aligned}\phi_R(x) &= \int_{k>0}\frac{dk}{2\pi}\frac{1}{\sqrt{2k}}\left[e^{-kz}a(k) + e^{kz}a(k)^\dagger(kz)\right] \\ \phi_L(x) &= \int_{k>0}\frac{dk}{2\pi}\frac{1}{\sqrt{2k}}\left[e^{-k\bar{z}}a(-k) + e^{k\bar{z}}a(-k)^\dagger(k)\right].\end{aligned} \tag{C.12}$$

With the usual bosonic commutation relation $[a(k), a(k')^\dagger] = 2\pi\delta(k-k')$. Here the dispersion relation $E = v_F|k|$ can thought of as two half lines with slope $\pm v_F$ above $E = 0$ and here the the infinity in ground state energy E_0(equivalent to "Fermi sea" for Dirac electrons) is due to the sum of the zero point energy of infinite harmonic oscillators. In terms of the above expansion the Hamiltonian is as follows:

$$H_B = \int\frac{dk}{2\pi}\frac{v_F|k|}{2}\left[a(k)^\dagger a(k) + a(k)a(k)^\dagger\right]. \tag{C.13}$$

And the normal ordered form,

$$:H_B: = \int\frac{dk}{2\pi}v_F|k|a(k)^\dagger a(k) \tag{C.14}$$

We can now switch to a convenient notation to work with a new field $\widetilde{\phi}$ defined as $\Pi = -\partial_x\widetilde{\phi}$. The new field follows the commutation relation

$$\left[\phi(x), \widetilde{\phi}(x')\right] = -i\theta(x-x'), \tag{C.15}$$

where $\theta(x)$ is the Heaviside step function as $\theta(x) = 1(x > 0)$, $\theta(x) = 0(x < 0)$. In terms of this new field $\widetilde{\phi} = -\int_\infty^x \Pi(y)dy$, one can write the normal ordered Bosonic Hamiltonian as

$$:H_B: = \frac{v_F}{2}\int dx\left[:(\partial_x\widetilde{\phi})^2: + :(\partial_x\phi)^2:\right]. \tag{C.16}$$

Switching to the chiral basis as $\phi = \phi_R + \phi_L$ and $\widetilde{\phi} = \phi_R - \phi_L$ one can re write the Hamiltonian as

$$:H_B: = \frac{v_F}{2}\int dx\left[:(\partial_x\phi_L)^2: + :(\partial_x\phi_R)^2:\right]. \tag{C.17}$$

Here one can calculate the propagators and correlation functions like before as

$$\langle\phi_R(z)\phi_R(z')\rangle = -\frac{1}{4}\ln\left(\mu(z-z')\right). \tag{C.18}$$

$$\langle\phi_L(z)\phi_L(z')\rangle = -\frac{1}{4}\ln\left(\mu(z-z')\right). \tag{C.19}$$

The equal time correlation is given by,

$$\langle \phi_R(x)\phi_R(x')\rangle = -\lim_{\epsilon\to 0^+}\frac{1}{4}\ln\left(i(z'-z)+\epsilon\right), \tag{C.20}$$

$$\langle \phi_L(x)\phi_L(x')\rangle = -\lim_{\epsilon\to 0^+}\frac{1}{4}\ln\left(i(z'-z)+\epsilon\right), \tag{C.21}$$

where $\mu(\sim 1/L$, L is the system size) is an IR cutoff, which is needed because the correlators are ill defined in the massless limit due to appearance of the integrals of type $\int \frac{dk}{k}e^{ikx}$. In later applications we will mostly need either the derivative of ϕ or $e^{i\beta\phi}$, for which the role of the IR cut-off is to ensure vanishing of the correlators when the total sum of β numbers doesn't vanish. For now we will assume $\mu = 1$.

C.3 Bosonization dictionary from correlation functions

A convenient way to see the boson-fermion connection could be from the algebra of current operator. For fermions one can easily calculate the charge density($J_0^F = \psi_R^\dagger\psi_R + \psi_L^\dagger\psi_L$) and current commutator($J_1^F = \psi_R^\dagger\psi_R - \psi_L^\dagger\psi_L$) at equal times in normal ordered form relative to the "Fermi-sea vacuum " ground state as

$$[J_0^F(z), J_1^F(z')] = -\frac{i}{\pi}\partial_z\delta(z-z'). \tag{C.22}$$

For free Bose field the corresponding normal ordered charge density and current operators are given by $J_0^B(x) = \frac{1}{\sqrt{\pi}}\partial_z\phi(z)$ and $J_1^B(z) = -\frac{1}{\sqrt{\pi}}\Pi(z)$ respectively. Taking a derivative on Eq.(C.11) we can see

$$\left[J_0^B(z), J_1^B(z')\right] = -\frac{i}{\pi}\partial_z\delta(z-z'). \tag{C.23}$$

Thus from the Eq.(C.22) and Eq.(C.23) one can conclude that for a free massless Dirac fermionic field in one dimension there exists a free bosonic field whose current coincides with the normal ordered Fermionic current as follows,

$$\begin{aligned} J_0^F(z) &= \frac{i}{\sqrt{\pi}}\partial_z\phi(z) \\ J_1^F(z) &= -\frac{i}{\sqrt{\pi}}\partial_z\widetilde{\phi}(z). \end{aligned} \tag{C.24}$$

To establish the mapping between bosonic and fermionic fields one can compare the field correlation functions and Eqs. C.8,C.8,C.10, C.18,C.19,C.20,C.21 from which a reasonable ansatz of the bosonic representation of fermionic operators can be following,

$$\psi(z) = Ae^{-iB\phi(z)}. \tag{C.25}$$

The constants A and B can be determined now by attempting to satisfy the fermionic anticommutation relations, with the help of bosonic commutation relations and the following identity

$$\begin{aligned} e^{i\alpha\phi(z)}e^{i\beta\phi(z')} &= e^{i\alpha\phi(z)+i\beta\phi(z')}e^{-\alpha\beta\phi(z)\phi(z')}\rangle \\ &= e^{i\alpha\phi(z)+i\beta\phi(z')}\left(z-z'\right)^{\frac{\alpha\beta}{4\pi}}, \end{aligned} \tag{C.26}$$

which can be proved with the Baker-Campbell-Housdroff formula[1].

Thus one can write in terms of the normal ordered expectation values of the fields,

$$\begin{aligned}\langle\psi_R(z)\psi_R^\dagger(z')\rangle &= A^2\langle e^{-iB\phi_R(z)}e^{iB\phi_R(z')}\rangle \\ &= A^2\langle e^{-iB(\phi_R(z)-\phi_R(z'))}\rangle\left(z-z'\right)^{-\frac{B^2}{4\pi}} \\ &= A^2\left(z-z'\right)^{-\frac{B^2}{4\pi}}\end{aligned} \tag{C.27}$$

Comparing Eq.(C.27) and (C.28) one can write down the following identity setting $A=\frac{1}{\sqrt{2\pi}}$ and $B=\sqrt{4\pi}$,

$$\langle\psi_R(x)\psi_R^\dagger(x')\rangle_F = \langle\frac{1}{\sqrt{2\pi}}:e^{i\sqrt{4\pi}\phi_R(x)}:\frac{1}{\sqrt{2\pi}}:e^{i\sqrt{4\pi}\phi_R(x')}:\rangle_B. \tag{C.28}$$

Where the fermionic and bosonic correlators are evaluated with respect to their own ground states and Hamiltonians respectively. So the relation between bosonic and fermionic fields is given by

$$\begin{aligned}\psi_R(x) &= \frac{1}{\sqrt{2\pi}}:e^{i\sqrt{4\pi}\phi_R(x)}: \\ \psi_L(x) &= \frac{1}{\sqrt{2\pi}}:e^{-i\sqrt{4\pi}\phi_L(x)}:\end{aligned} \tag{C.29}$$

The bosonization dictionary discussed so far is summarized in the table below.

Fermionic Theory	Bosonic Theory
$\psi_R(z)$	$\frac{1}{\sqrt{2\pi}}:e^{i\sqrt{4\pi}\phi_R(z)}:$
$\psi_L(z)$	$\frac{1}{\sqrt{2\pi}}:e^{-i\sqrt{4\pi}\phi_L(z)}:$
$J(z)$	$\frac{i}{\sqrt{\pi}}\partial_z\phi(z)$
$H_F=\int dx\left[\psi^\dagger i\left(-\frac{1}{m}\partial_x^2\right)\psi-\mu\psi^\dagger\psi\right]$	$H_B=\frac{v_F}{2}\int dx\left[\Pi(x)^2+(\partial_x\phi)^2\right]$

[1] for Bosonic fields A and B , $e^Ae^B=e^{A+B}e^{[A,B]/2}$

Appendix D

Bare perturbation theory for one dimensional open spin system

This appendix is supplementary to 6.4. Here we give the details of bare perturbation theory calculation leading to the calculation of 6.42, 6.43, 6.44, 6.45. As discussed in 6.3.2, when a spin is removed from a periodic spin chain of $N+1$ sites, the system can be visualized as a spin chain of N spins obeying open boundary condition. With those boundary conditions as in Eq. 6.31, the bosonic field $\phi(r)$ expanded in terms of bosonic normal modes are as in Eq. 6.32:

$$\begin{aligned} \phi(r) &= \pi R + \frac{q_0}{L} r + \sum_{n=1}^{\infty} \frac{\sin\left(\frac{n\pi r}{L}\right)(a_n + a_n^\dagger)}{\sqrt{\pi n}} \\ \widetilde{\phi}(r) &= \widetilde{\phi}_0 + i \sum_{n=1}^{\infty} \frac{\cos\left(\frac{n\pi r}{L}\right)(a_n - a_n^\dagger)}{\sqrt{\pi n}} \, . \end{aligned} \tag{D.1}$$

Here, the non zero bosonic commutation relations are $\left[\widetilde{\phi}(0), q_0\right] = i, \left[a_m, a_n^\dagger\right] = \delta_{mn}$, H_0 can be written (apart from an infinite constant $\frac{u}{2}\sum_{n=1}^{\infty}\frac{n\pi}{L}$, the sum of zero point energies of all the oscillators) in the canonical form

$$H_0 = \frac{u}{2}\frac{q_0^2}{L} + \sum_{n=1}^{\infty}\left(\frac{un\pi}{L}\right) a_n^\dagger a_n \, . \tag{D.2}$$

Thus the ground state $|G_0\rangle$ of the unperturbed Hamiltonian is the vacuum for all the a_n operators, and an eigenstate of the zero mode q_0. Indeed, $q_0|G_0\rangle = \pi R|G_0\rangle$ for the $S_{tot} = 1/2$, $S^z_{tot} = 1/2$ ground state that we wish to model (more generally $|G_0\rangle$ is an eigenstate of q_0 with eigenvalue $2\pi R S^z_{tot}$).

Now, the ground state corrected to first order in ϵ_0 can be written formally as

$$|G\rangle \cong |G_0\rangle - \sum_{k \neq G_0} \left(\frac{\langle k|H_1|G_0\rangle}{E_k^0 - E_{G_0}^0}\right)|k\rangle. \tag{D.3}$$

Here $k \equiv \{N_n\}$ with $n = 1, 2 \ldots \infty$ and N_n being the number of bosons in mode n. For an arbitrary excited state, we have the unperturbed energy

$$E^0(\{N_n\}) = \frac{u}{2}\frac{q_0^2}{L} + \sum_n \omega_n \left(N_n + \frac{1}{2}\right) \tag{D.4}$$

with $\omega_n = \frac{un\pi}{L}$, which gives us the following expression for the energy denominators:

$$E^0(\{N_n\}) - E_g^0 = \sum_n \omega_n N_n. \tag{D.5}$$

As a result, our formal expression for the ground state corrected to first order in ϵ_0 now reads

$$|G\rangle = |\{N_n = 0\}\rangle + \frac{u\epsilon_0}{r_0^2} \sum_{\{N_n\}\neq\{0\}} \left(\frac{\langle\{N_n\}| \int_0^L \cos(\frac{2\phi(x)}{R})|\{0\}\rangle}{u\sum_n \frac{n\pi}{L} N_n} \right) |\{N_n\}\rangle \tag{D.6}$$

This gives the following formal expression for the one point function:

$$\begin{aligned} S\left(L, \frac{r}{L}, \epsilon_0\right) &= \langle G| \frac{1}{\sqrt{r_0}} \sin\left(\frac{\phi(r)}{R}\right) |G\rangle \\ &\cong \langle\{0\}| \frac{1}{\sqrt{r_0}} \sin\left(\frac{\phi(r)}{R}\right) |\{0\}\rangle \\ &+ \frac{\epsilon_0}{r_0^2} \sum_{\{N_n\}\neq\{0\}} \frac{\langle\{0\}| \frac{1}{\sqrt{r_0}} \sin\left(\frac{\phi(r)}{R}\right) |\{N_n\}\rangle\langle\{N_n\}| \int_0^L \cos\left(\frac{2\phi(x)}{R}\right) |\{0\}\rangle}{\sum_n \frac{n\pi}{L} N_n} \\ &+ \frac{\epsilon_0}{r_0^2} \sum_{\{N_n\}\neq\{0\}} \frac{\langle\{N_n\}| \frac{1}{\sqrt{r_0}} \sin(\frac{\phi(r)}{R})|\{0\}\rangle\langle\{0\}| \int_0^L \cos\left(\frac{2\phi(x)}{R}\right) |\{N_n\}\rangle}{\sum_n \frac{n\pi}{L} N_n}. \end{aligned} \tag{D.7}$$

where we can set $R = 1/\sqrt{2\pi}$ in the contributions that arise from the $\mathcal{O}(\epsilon_0)$ corrections to $|G_0\rangle$, as long as we are careful to use the full expression $R = (2\pi - 2\pi^2\epsilon_0)^{-1/2} \approx (1 + \pi\epsilon_0/2)/\sqrt{2\pi}$ when evaluating the first "unperturbed" term in order to obtain the latter correct to $\mathcal{O}(\epsilon_0)$. To evaluate the matrix elements and expectation values, it is useful to write the state $|\{N_n\}\rangle$ in "coordinate" representation as

$$\langle\{y_n\}|\{N_n\}\rangle = \prod_{n=1}^{\infty} \left(\frac{1}{\pi^{\frac{1}{4}} 2^{\frac{N_n}{2}}} \frac{1}{\sqrt{N_n!}} e^{-\frac{y_n^2}{2}} H_{N_n}(y_n) \right) \tag{D.8}$$

where the coordinates $y_n = \frac{a_n + a_n^\dagger}{\sqrt{2}}$ are conjugate to "momenta" $\pi_n = \frac{a_n - a_n^\dagger}{i\sqrt{2}}$ and $H_m(x)$ is the m^{th} Hermite polynomial of x.

Now

$$\begin{aligned} \langle\{0\}| \frac{1}{\sqrt{r_0}} \sin\left(\frac{\phi(r)}{R}\right) |\{N_n\}\rangle &= \frac{(-1)}{\sqrt{r_0}} \Im\left[e^{\frac{i\pi r}{L}} \prod_n \left\{ \frac{\int_{-\infty}^{+\infty} dy_n e^{-y_n^2} H_{N_n}(y_n)}{\sqrt{\pi}\sqrt{2^{N_n}}\sqrt{N_n!}} e^{2i\frac{\sin\left(\frac{\pi n r}{L}\right)}{\sqrt{2\pi R^2 n}} y_n} \right\} \right] \\ &= \frac{(-1)}{\sqrt{r_0}} \Im\left[e^{\frac{i\pi r}{L}} \prod_n \left\{ \frac{\int_{-\infty}^{+\infty} dy_n e^{-\left(y_n - i\frac{\sin\left(\frac{\pi n r}{L}\right)}{\sqrt{2\pi R^2 n}}\right)^2} H_{N_n}(y_n)}{\sqrt{\pi}\sqrt{2^{N_n}}\sqrt{N_n!}} e^{-\frac{\sin^2\left(\frac{\pi n r}{L}\right)}{2\pi R^2 n} y_n} \right\} \right]. \end{aligned} \tag{D.9}$$

Using the formula $\int_{-\infty}^{+\infty} e^{-(x-y)^2} H_N(x)dx = \sqrt{\pi} y^N 2^N$. So

$$\begin{aligned}
&\langle \quad \{0\} \quad |\frac{1}{\sqrt{r_0}} \sin\left(\frac{\phi(r)}{R}\right) |\{N_n\}\rangle \qquad (D.10)\\
&= \quad -\frac{1}{\sqrt{r_0}} \Im \left[e^{\frac{i\pi r}{L}} e^{-\sum_{n=1}^{\infty} \frac{\sin^2\left(\frac{\pi n r}{L}\right)}{2\pi R^2 n}} \prod_n \left\{ \frac{\left(\sqrt{2}\right)^{N_n}}{\sqrt{N_n!}} (i)^{N_n} \left(\frac{\sin\left(\frac{\pi n r}{L}\right)}{\sqrt{2\pi R^2 n}} \right)^{N_n} \right\} \right] \\
&= \quad -\frac{1}{\sqrt{r_0}} e^{-\sum_{n=1}^{\infty} \frac{\sin^2\left(\frac{\pi n r}{L}\right)}{2\pi R^2 n}} \prod_n \left\{ \left(\frac{\sqrt{2}\sin(\frac{\pi n r}{L})}{\sqrt{2\pi R^2 n}} \right)^{N_n} \frac{1}{\sqrt{N_n!}} \right\} \times \Im \left[e^{\frac{i\pi r}{L}} (i)^{(\sum_n N_n)} \right] \\
&= \quad -\frac{1}{\sqrt{r_0}} e^{-\sum_{n=1}^{\infty} \frac{\sin^2\left(\frac{\pi n r}{L}\right)}{2\pi R^2 n}} \prod_n \left\{ \left(\frac{\sqrt{2}\sin(\frac{\pi n r}{L})}{\sqrt{2\pi R^2 n}} \right)^{N_n} \frac{1}{\sqrt{N_n!}} \right\} \\
&\times \quad \left[\sin\left(\frac{\pi r}{L}\right) (-1)^{\sum \frac{N_n}{2}} \left(\frac{1+(-1)^{\sum N_n}}{2} \right) + \cos\left(\frac{\pi r}{L}\right) (-1)^{\left(\frac{\sum N_n)-1}{2}\right)} \left(\frac{1-(-1)^{\sum N_n}}{2} \right) \right].
\end{aligned}$$

Thus

$$\langle \{0\} | \frac{\sin\left(\frac{\phi(r)}{R}\right)}{\sqrt{r_0}} | \{0\} \rangle = -\frac{1}{\sqrt{r_0}} \sin\left(\frac{\pi r}{L}\right) e^{-\sum_{n=0}^{\infty} \frac{\sin^2\left(\frac{\pi n r}{L}\right)}{2\pi R^2 n}}. \qquad (D.11)$$

Similarly,

$$\begin{aligned}
\langle \{0\} | \cos\left(\frac{2\phi(x)}{R}\right) |\{N_n\}\rangle &= \Re \left[e^{\frac{2\pi i x}{L}} \prod_n \left\{ \frac{\int_{-\infty}^{+\infty} dy_n e^{-y_n^2} H_{N_n}(y_n)}{\sqrt{\pi}\sqrt{2}^{N_n}\sqrt{N_n!}} e^{4i \frac{\sin\left(\frac{\pi n x}{L}\right)}{\sqrt{2\pi R^2 n}} y_n} \right\} \right] \qquad (D.12)\\
&= \Re \left[e^{\frac{2\pi i x}{L}} \prod_n \left\{ \frac{\int_{-\infty}^{+\infty} dy_n e^{-\left(y_n - 2i \frac{\sin\left(\frac{\pi n x}{L}\right)}{\sqrt{2\pi R^2 n}}\right)^2} H_{N_n}(y_n)}{\sqrt{\pi}\sqrt{2}^{N_n}\sqrt{N_n!}} e^{-4\frac{\sin^2\left(\frac{\pi n x}{L}\right)}{2\pi R^2 n} y_n} \right\} \right].
\end{aligned}$$

$$\begin{aligned}
&\langle \quad \{0\} \quad |\cos\left(\frac{2\phi(x)}{R}\right) |\{N_n\}\rangle \qquad (D.13)\\
&= \quad e^{-\sum_{n=1}^{\infty} \frac{4\sin^2\left(\frac{\pi n x}{L}\right)}{2\pi R^2 n}} \prod_n \left\{ \left(\frac{2\sqrt{2}\sin\left(\frac{\pi n x}{L}\right)}{\sqrt{2\pi R^2 n}} \right)^{N_n} \frac{1}{\sqrt{N_n!}} \right\} \times \Re \left[e^{\frac{2\pi i x}{L}} (i)^{(\sum_n N_n)} \right] \\
&= \quad e^{-\sum_{n=1}^{\infty} \frac{4\sin^2\left(\frac{\pi n x}{L}\right)}{2\pi R^2 n}} \prod_n \left\{ \left(\frac{2\sqrt{2}\sin(\frac{\pi n x}{L})}{\sqrt{2\pi R^2 n}} \right)^{N_n} \frac{1}{\sqrt{N_n!}} \right\} \\
&\times \quad \left[\cos\left(\frac{2\pi x}{L}\right) (-1)^{\sum \frac{N_n}{2}} \left(\frac{1+(-1)^{\sum N_n}}{2} \right) - \sin\left(\frac{2\pi x}{L}\right) (-1)^{\frac{\sum N_n - 1}{2}} \left(\frac{1-(-1)^{\sum N_n}}{2} \right) \right].
\end{aligned}$$

So,

$$\begin{aligned}
\langle \quad \{0\} \quad & |\cos(\frac{2\phi(x)}{R})|\{N_n\}\rangle\langle\{N_n\}|\frac{\sin(\frac{\phi(r)}{R})}{\sqrt{r_0}}|\{0\}\rangle + h.c. \qquad \text{(D.14)}\\
= \quad & -\frac{2}{\sqrt{r_0}}e^{-\sum_{n=1}^{\infty}\left(\frac{4\sin^2\left(\frac{2\pi nx}{L}\right)}{2\pi R^2 n}+\frac{\sin^2\left(\frac{\pi nr}{L}\right)}{2\pi R^2 n}\right)}\\
\times \quad & \prod_n\left\{\left(\frac{4\sin\left(\frac{\pi nr}{L}\right)\sin\left(\frac{\pi nx}{L}\right)}{2\pi R^2 n}\right)^{N_n}\frac{1}{N_n!}\right\}\\
\times \quad & \left[\sin\left(\frac{\pi r}{L}\right)\cos\left(\frac{2\pi x}{L}\right)\left(\frac{1+(-1)^{\sum N_n}}{2}\right)\right.\\
- \quad & \left.\sin\left(\frac{2\pi x}{L}\right)\cos\left(\frac{\pi r}{L}\right)\left(\frac{1-(-1)^{\sum N_n}}{2}\right)\right]\\
= \quad & -\frac{2}{\sqrt{r_0}}e^{-\sum_{n=1}^{\infty}\left(\frac{4\sin^2\left(\frac{\pi nx}{L}\right)}{2\pi R^2 n}+\frac{\sin^2\left(\frac{\pi nr}{L}\right)}{2\pi R^2 n}\right)}\\
\times \quad & \left[\sin\left(\frac{\pi(r-2x)}{L}\right)\prod_n\left\{\left(\frac{4\sin\left(\frac{\pi nr}{L}\right)\sin\left(\frac{\pi nx}{L}\right)}{2\pi R^2 n}\right)^{N_n}\frac{1}{N_n!}\right\}\right.\\
+ \quad & \left.\sin\left(\frac{\pi(r+2x)}{L}\right)\prod_n\left\{\left(-\frac{4\sin\left(\frac{\pi nr}{L}\right)\sin\left(\frac{\pi nx}{L}\right)}{2\pi R^2 n}\right)^{N_n}\frac{1}{N_n!}\right\}\right]
\end{aligned}$$

Now

$$\begin{aligned}
& \frac{\langle\{0\}|\cos(\frac{2\phi(x)}{R})|\{N_n\}\rangle\langle\{N_n\}|\frac{\sin(\frac{\phi(r)}{R})}{\sqrt{r_0}}|\{0\}\rangle + h.c.}{\sum_n \frac{n\pi}{L}N_n} \qquad \text{(D.15)}\\
\equiv & \int_0^\infty d\mathcal{T}(\langle\{0\}|\cos\left(\frac{2\phi(x)}{R}\right)|\{N_n\}\rangle\langle\{N_n\}|\frac{\sin\left(\frac{\phi(r)}{R}\right)}{\sqrt{r_0}}|\{0\}\rangle + h.c.)e^{-\mathcal{T}\sum_n \frac{n\pi}{L}N_n}\\
& = -\frac{1}{\sqrt{r_0}}e^{-\sum_{n=1}^{\infty}\left(\frac{4\sin^2\left(\frac{\pi nx}{L}\right)}{2\pi R^2 n}+\frac{\sin^2\left(\frac{\pi nr}{L}\right)}{2\pi R^2 n}\right)}\\
& \times\left[\sin\left(\frac{\pi(r-2x)}{L}\right)\int_0^\infty d\mathcal{T}\left[\prod_n\left\{\left(\frac{4\sin\left(\frac{\pi nr}{L}\right)\sin\left(\frac{\pi nx}{L}\right)}{2\pi R^2 n}e^{-\frac{n\pi\mathcal{T}}{L}}\right)^{N_n}\frac{1}{N_n!}\right\}\right]\right.\\
& \left.+\sin\left(\frac{\pi(r+2x)}{L}\right)\int_0^\infty d\mathcal{T}\left[\prod_n\left\{\left(-\frac{4\sin\left(\frac{\pi nr}{L}\right)\sin\left(\frac{\pi nx}{L}\right)}{2\pi R^2 n}e^{-\frac{n\pi\mathcal{T}}{L}}\right)^{N_n}\frac{1}{N_n!}\right\}\right]\right]
\end{aligned}$$

So

$$\begin{aligned}
&\frac{\epsilon_0}{r_0^2} \sum_{\{N_n\}\neq\{0\}} \frac{\langle\{0\}|\cos(\frac{2\phi(x)}{R})|\{N_n\}\rangle\langle\{N_n\}|\frac{\sin(\frac{\phi(r)}{R})}{\sqrt{r_0}}|\{0\}\rangle + h.c.}{\sum_n \frac{n\pi}{L}N_n} \qquad \text{(D.16)}\\
&= -\frac{\epsilon_0}{r_0^{\frac{5}{2}}} e^{-\sum_{n=1}^{\infty}\left(\frac{4\sin^2\left(\frac{\pi n x}{L}\right)}{2\pi R^2 n}+\frac{\sin^2\left(\frac{\pi n r}{L}\right)}{2\pi R^2 n}\right)}\\
&\times \left[\sin\left(\frac{\pi(r-2x)}{L}\right)\int_0^{\infty} d\mathcal{T}\left[\prod_n\left\{\sum_n\left[\left(\frac{4\sin\left(\frac{\pi n r}{L}\right)\sin\left(\frac{\pi n x}{L}\right)}{2\pi R^2 n}e^{-\frac{n\pi\mathcal{T}}{L}}\right)^{N_n}\frac{1}{N_n!}\right]\right\}-1\right]\right.\\
&+ \left.\sin\left(\frac{\pi(r+2x)}{L}\right)\int_0^{\infty} d\mathcal{T}\left[\prod_n\left\{\sum_n\left[\left(-\frac{4\sin(\frac{\pi n r}{L})\sin(\frac{\pi n x}{L})}{2\pi R^2 n}e^{-\frac{n\pi\mathcal{T}}{L}}\right)^{N_n}\frac{1}{N_n!}\right]\right\}-1\right]\right]
\end{aligned}$$

Therefore we now have to do summations $\sum_{n=1}^{\infty}\frac{\sin^2\frac{\pi n()}{L}}{2\pi R^2 n}$ and $\sum_{n=1}^{\infty}\frac{\sin\frac{\pi n()}{L}\sin\frac{\pi n\widetilde{()}}{L}}{2\pi R^2 n}e^{-\frac{n\pi\mathcal{T}}{L}}$.

It is at this stage the UV regulator of the field theory (r_0) comes into our calculation. We calculate these summations as follows using the formula $\sum_{n=1}^{\infty}\frac{p^n\cos(nx)}{n} = \log(\frac{1}{\sqrt{1-2p\cos x+p^2}})$(for us $p \equiv e^{-\frac{\pi r_0}{L}}$) , as follows.

$$\begin{aligned}
\sum_{n=1}^{\infty}\frac{\sin^2\frac{\pi n r}{L}}{n}e^{-\frac{\pi n r_0}{L}} &= \frac{1}{2}\sum_{n=1}^{\infty}\frac{\left(1-\cos\frac{2\pi n r}{L}\right)}{n}e^{-\frac{\pi n r_0}{L}} \qquad \text{(D.17)}\\
&= \frac{1}{2}\log\frac{1}{\sqrt{1-2e^{-\frac{\pi r_0}{L}}+e^{-\frac{2\pi r_0}{L}}}} - \frac{1}{2}\log\frac{1}{\sqrt{1-2e^{-\frac{\pi r_0}{L}}\cos\frac{2\pi r}{L}+e^{-\frac{2\pi r_0}{L}}}}\\
&= \frac{1}{4}\log\left[\frac{1-2e^{-\frac{\pi r_0}{L}}\cos\frac{2\pi r}{L}+e^{-\frac{2\pi r_0}{L}}}{1-2e^{-\frac{\pi r_0}{L}}+e^{-\frac{2\pi r_0}{L}}}\right]\\
&= \frac{1}{4}\log\left[\frac{\cosh\frac{\pi r_0}{L}-\cos\frac{2\pi r}{L}}{\cosh\frac{\pi r_0}{L}-1}\right]\\
&\cong \frac{1}{4}\log\left[\frac{1+\frac{1}{2}\left(\frac{\pi r_0}{L}\right)^2-\cos\frac{2\pi r}{L}}{\frac{1}{2}\left(\frac{\pi r_0}{L}\right)^2}\right]\\
&\cong \frac{1}{4}\log\left[\frac{4\sin^2\frac{\pi r}{L}}{\frac{1}{2}\left(\frac{\pi r_0}{L}\right)^2}\right]\\
&\equiv \frac{1}{2}\log\left(\frac{2L\sin\left(\frac{\pi r}{L}\right)}{\pi r_0}\right).
\end{aligned}$$

Similarly,

$$
\begin{aligned}
\sum_{n=1}^{\infty} \quad & \frac{\sin\frac{\pi n r}{L}\sin\frac{\pi n x}{L}}{n} e^{-\frac{n\pi\mathcal{T}}{L}} \qquad (D.18)\\
= \quad & \frac{1}{2}\sum_{n=1}^{\infty}\frac{\left[\cos\frac{\pi n}{L}(r-x)-\cos\frac{\pi n}{L}(r+x)\right]}{n} e^{-\frac{n\pi\mathcal{T}}{L}}\\
= \quad & \frac{1}{2}\log\frac{1}{\sqrt{1-2e^{-\frac{\pi\mathcal{T}}{L}}\cos\frac{2\pi(r-x)}{L}+e^{-\frac{2\pi\mathcal{T}}{L}}}} - \frac{1}{2}\log\frac{1}{\sqrt{1-2e^{-\frac{\pi\mathcal{T}}{L}}\cos\frac{2\pi(r+x)}{L}+e^{-\frac{2\pi\mathcal{T}}{L}}}}\\
= \quad & \frac{1}{4}\log\left[\frac{1-2e^{-\frac{\pi\mathcal{T}}{L}}\cos\frac{\pi(r+x)}{L}+e^{-\frac{2\pi\mathcal{T}}{L}}}{1-2e^{-\frac{\pi\mathcal{T}}{L}}\cos\frac{\pi(r-x)}{L}+e^{-\frac{2\pi\mathcal{T}}{L}}}\right]\\
= \quad & \frac{1}{4}\log\left[\frac{\cosh\frac{\pi\mathcal{T}}{L}-\cos\frac{2\pi(r+x)}{L}}{\cosh\frac{\pi\mathcal{T}}{L}-\cos\frac{2\pi(r-x)}{L}}\right]
\end{aligned}
$$

So,

$$
\begin{aligned}
\tfrac{\epsilon_0}{r_0^2} \quad & \sum_{\{N_n\}\neq\{0\}} \frac{\langle\{0\}|\cos(\frac{2\phi(x)}{R})|\{N_n\}\rangle\langle\{N_n\}|\frac{\sin(\frac{\phi(r)}{R})}{\sqrt{r_0}}|\{0\}\rangle + h.c.}{\sum_n \frac{n\pi}{L}N_n} \qquad (D.19)\\
= \quad & -\frac{\epsilon_0}{r_0^{\frac{5}{2}}}\sqrt{\frac{\pi r_0}{2L\sin\frac{\pi r}{L}}}\left(\frac{\pi r_0}{2L\sin\frac{\pi r}{L}}\right)^2\\
\times \quad & \left[\sin\Big(\frac{\pi}{L}(r-2x)\Big)\int_0^{\infty} d\mathcal{T}\left(\frac{\cosh\frac{\pi\mathcal{T}}{L}-\cos\frac{2\pi(r+x)}{L}}{\cosh\frac{\pi\mathcal{T}}{L}-\cos\frac{\pi(r-x)}{L}}-1\right)\right.\\
+ \quad & \left.\sin\Big(\frac{\pi}{L}(r+2x)\Big)\int_0^{\infty} d\mathcal{T}\left(\frac{\cosh\frac{\pi\mathcal{T}}{L}-\cos\frac{\pi(r-x)}{L}}{\cosh\frac{\pi\mathcal{T}}{L}-\cos\frac{\pi(r+x)}{L}}-1\right)\right]\\
= \quad & -\epsilon_0\sqrt{\frac{\pi}{2L\sin\frac{\pi r}{L}}}\left(\frac{\pi}{2L\sin\frac{\pi r}{L}}\right)^2\\
\times \quad & \left[\sin\Big(\frac{\pi}{L}(r-2x)\Big)\int_0^{\infty} d\mathcal{T}\left(\frac{\cos\frac{\pi(r-x)}{L}-\cos\frac{\pi(r+x)}{L}}{\cosh\frac{\pi\mathcal{T}}{L}-\cos\frac{\pi(r-x)}{L}}\right)\right.\\
+ \quad & \left.\sin\Big(\frac{\pi}{L}(r+2x)\Big)\int_0^{\infty} d\mathcal{T}\left(\frac{\cos\frac{\pi(r+x)}{L}-\cos\frac{\pi(r-x)}{L}}{\cosh\frac{\pi\mathcal{T}}{L}-\cos\frac{\pi(r+x)}{L}}\right)\right].
\end{aligned}
$$

And the unperturbed part

$$
\begin{aligned}
\langle\{0\}|\frac{\sin\left(\frac{\phi(r)}{R}\right)}{\sqrt{r_0}}|\{0\}\rangle \quad & = \quad -\frac{1}{\sqrt{r_0}}\sin\left(\frac{\pi r}{L}\right)e^{-\sum_{n=0}^{\infty}\frac{\sin^2\left(\frac{\pi n r}{L}\right)}{2\pi R^2 n}}. \qquad (D.20)\\
& = \quad -\frac{1}{\sqrt{r_0}}\sin\left(\frac{\pi r}{L}\right)\left(\frac{\pi r_0}{2L\sin\frac{\pi r}{L}}\right)^{\frac{1}{2}\frac{1}{2\pi R^2}}\\
& = \quad -\frac{1}{\sqrt{r_0}}\sin\left(\frac{\pi r}{L}\right)\left(\frac{\pi r_0}{2L\sin\frac{\pi r}{L}}\right)^{\frac{1}{2}-\frac{\pi\epsilon_0}{2}}\\
& = \quad -\frac{1}{\sqrt{r_0}}\sin\left(\frac{\pi r}{L}\right)\left(\frac{\pi r_0}{2L\sin\frac{\pi r}{L}}\right)^{\frac{1}{2}}\left(1-\frac{\pi\epsilon_0}{2}\log\frac{\pi r_0}{2L\sin\frac{\pi r}{L}}\right).
\end{aligned}
$$

So

$$
\begin{aligned}
S\left(L,\frac{r}{L},\epsilon_0\right) &= -\sqrt{\frac{\pi\sin\frac{\pi r}{L}}{2L}}\left(1-\frac{\pi\epsilon_0}{2}\log\frac{\pi r_0}{2L\sin\frac{\pi r}{L}}\right) \\
&- \epsilon_0\sqrt{\frac{\pi\sin\frac{\pi r}{L}}{2L}}\frac{\pi^2}{4L^2}\frac{1}{\sin\frac{\pi r}{L}} \\
&\times \left[\int_0^\infty\int_0^L d\mathcal{T}dx\frac{\sin\left(\frac{\pi}{L}(r-2x)\right)}{\sin^2\frac{\pi x}{L}}\left(\frac{\cos\frac{\pi(r-x)}{L}-\cos\frac{\pi(r+x)}{L}}{\cosh\frac{\pi\mathcal{T}}{L}-\cos\frac{\pi(r-x)}{L}}\right)\right. \\
&+ \left.\int_0^\infty\int_0^L d\mathcal{T}dx\,\frac{\sin\left(\frac{\pi}{L}(r+2x)\right)}{\sin^2\frac{\pi x}{L}}\int_0^\infty d\mathcal{T}\left(\frac{\cos\frac{\pi(r+x)}{L}-\cos\frac{\pi(r-x)}{L}}{\cosh\frac{\pi\mathcal{T}}{L}-\cos\frac{\pi(r+x)}{L}}\right)\right].
\end{aligned}
\tag{D.21}
$$

Variable change

$$
\begin{aligned}
\frac{\pi r}{L} &= \theta_r \\
\frac{\pi x}{L} &= \phi \\
\frac{\pi\mathcal{T}}{L} &= s.
\end{aligned}
\tag{D.22}
$$

In new variables the last expression becomes

$$
\begin{aligned}
S\left(L,\frac{r}{L},\epsilon_0\right) &= -\sqrt{\frac{\pi\sin\theta_r}{2L}}\left(1-\frac{\pi\epsilon_0}{2}\log\frac{\pi r_0}{2L\sin\theta_r}\right) \\
&- \epsilon_0\sqrt{\frac{\pi\sin\theta_r}{2L}}\frac{1}{4\sin\theta_r} \\
&\times \left[\int_0^\infty\int_0^\pi dsd\phi\frac{\sin(\theta_r-2\phi)}{\sin^2\phi}\left(\frac{\cos(\theta_r-\phi)-\cos(\theta_r+\phi)}{\cosh s-\cos(\theta_r-\phi)}\right)\right. \\
&+ \left.\int_0^\infty\int_0^\pi dsd\phi\,\frac{\sin(\theta_r+2\phi)}{\sin^2\phi}\int_0^\infty ds\left(\frac{\cos(\theta_r+\phi)-\cos(\theta_r-\phi)}{\cosh s-\cos(\theta_r+\phi)}\right)\right].
\end{aligned}
\tag{D.23}
$$

The ranges of $\theta_r+\phi$ and $-\theta_r+\phi$ are $\theta_r+\phi\epsilon_0[\theta_r,\theta_r+\pi]$ and $\phi-\theta_r\epsilon_0[-\theta_r,\pi-\theta_r]$ respectively. In order to use the standard integrals let us express

$$
\cos(\theta_r+\phi)=\cos t_+, t_+\epsilon_0(0,\pi) \tag{D.24}
$$

$$
\cos(\phi-\theta_r)=\cos t_-, t_-\epsilon_0(0,\pi). \tag{D.25}
$$

Let us do the s integral as ,

$$
I_\pm=\int_0^\infty\frac{1}{\cosh s-\cos t_\pm} \tag{D.26}
$$

So,

$$
\begin{aligned}
I_\pm &= \int_0^\infty\frac{1}{\cosh s-\cos t_\pm} \\
&= \int_0^\infty\frac{1}{\cosh s-\cos t_\pm} \\
&= \frac{2}{\sqrt{1-\cos^2 t_\pm}}\tan^{-1}\left(\frac{\sqrt{1-\cos^2 t_\pm}}{1-\cos^2 t_\pm}\right).
\end{aligned}
\tag{D.27}
$$

Now,

$$I_{\pm} = \frac{u_{\pm}}{\sin u_{\pm}} \tag{D.28}$$

where $u_{\pm} = \pi - t_{\pm}$ and $t_{\pm} \in (0, \pi)$ hence $u_{\pm} \in (\pi, 0)$ or $x \in (\mp r, (L+1) \mp r)$.

$$I_{\pm} = \frac{v_{\pm}}{\sin v_{\pm}} \tag{D.29}$$

where $v_{\pm} = t_{\pm} - \pi$ and $t_{\pm} \in (\pi, 2\pi)$ hence $v_{\pm} \in (0, \pi)$ or $x \in ((L+1) \mp r, 2(L+1) \mp r)$.

$$I_{\pm} = \frac{w_{\pm}}{\sin w_{\pm}} \tag{D.30}$$

where $w_{\pm} = \pi + t_{\pm}$ and $t_{\pm} \in (\pi, 0)$ hence $w_{\pm} \in (0, \pi)$ or $x \in (-(L+1) \mp r, \mp r)$. So

$$\begin{aligned} I_+ &= u_+ \in [0, (L+1) - r] \\ &= v_+ \in [(L+1) - r, L]. \end{aligned} \tag{D.31}$$

$$\begin{aligned} I_- &= w_- \in [0, r] \\ &= u_- \in [r, L]. \end{aligned} \tag{D.32}$$

$$\begin{aligned} S\left(L, \frac{r}{L}, \epsilon_0\right) &= -\sqrt{\frac{\pi \sin\theta_r}{2L}} \left(1 - \frac{\pi\epsilon_0}{2} \log \frac{\pi r_0}{2L \sin\theta_r}\right) \\ &+ \frac{\epsilon_0}{2} \left(\frac{\pi}{2L}\right)^{\frac{1}{2}} \\ &\times \left[\int_0^{\pi-\theta_r} d\phi \frac{2\sin\phi\sin\theta_r}{\sqrt{\sin\theta_r}\sin^2\phi} \sin(2\phi+\theta_r) \frac{\pi - (\phi+\theta_r)}{\sin(\pi - (\phi+\theta_r))} \right. \\ &+ \int_{\pi-\theta_r}^{\pi} d\phi \frac{2\sin\phi\sin\theta_r}{\sqrt{\sin\theta_r}\sin^2\phi} \sin(2\phi+\theta_r) \frac{(\phi+\theta_r) - \pi}{\sin((\phi+\theta_r) - \pi)} \\ &+ \int_0^{\theta_r} d\phi \frac{2\sin\phi\sin\theta_r}{\sqrt{\sin\theta_r}\sin^2\phi} \sin(2\phi-\theta_r) \frac{(\phi-\theta_r) + \pi}{\sin((\phi-\theta_r) + \pi)} \\ &+ \left. \int_{\theta_r}^{\pi} d\phi \frac{2\sin\phi\sin\theta_r}{\sqrt{\sin\theta_r}\sin^2\phi} \sin(2\phi-\theta_r) \frac{\pi - (\phi-\theta_r)}{\sin(\pi - (\phi-\theta_r))} \right]. \end{aligned} \tag{D.33}$$

Putting cut offs to remove divergences at $\phi = 0, \pi, \theta_r$,

$$\begin{aligned} S\left(L, \frac{r}{L}, \epsilon_0\right) &= -\sqrt{\frac{\pi \sin\theta_r}{2L}} \left(1 - \frac{\pi\epsilon_0}{2} \log \frac{\pi r_0}{2L \sin\theta_r}\right) \\ &- \frac{\epsilon_0}{4} \left(\frac{\pi}{2L}\right)^{\frac{1}{2}} \\ &\times \left[\int_{\alpha}^{\pi-\theta_r} d\phi \frac{2\sin\phi\sin\theta_r}{\sqrt{\sin\theta_r}\sin^2\phi} \sin(2\phi+\theta_r) \frac{-\pi + (\phi+\theta_r)}{\sin(\phi+\theta_r)} \right. \\ &+ \int_{\pi-\theta_r}^{\pi-\beta} d\phi \frac{2\sin\phi\sin\theta_r}{\sqrt{\sin\theta_r}\sin^2\phi} \sin(2\phi+\theta_r) \frac{(\phi+\theta_r) - \pi}{\sin(\phi+\theta_r)} \\ &+ \int_{\alpha}^{\theta_r-\zeta} d\phi \frac{2\sin\phi\sin\theta_r}{\sqrt{\sin\theta_r}\sin^2\phi} \sin(2\phi-\theta_r) \frac{(\phi-\theta_r) + \pi}{\sin(\phi-\theta_r)} \\ &+ \left. \int_{\theta_r+\zeta}^{\pi-\beta} d\phi \frac{2\sin\phi\sin\theta_r}{\sqrt{\sin\theta_r}\sin^2\phi} \sin(2\phi-\theta_r) \frac{-\pi + (\phi-\theta_r)}{\sin(\phi-\theta_r)} \right] \end{aligned} \tag{D.34}$$

$$
\begin{aligned}
S\left(L,\frac{r}{L},\epsilon_0\right) &= -\sqrt{\frac{\pi\sin\theta_r}{2L}}\left(1-\frac{\pi\epsilon_0}{2}\log\frac{\pi r_0}{2L\sin\theta_r}\right) \qquad \text{(D.35)}\\
&- \frac{\epsilon_0}{2}\left(\frac{\pi}{2L}\right)^{\frac{1}{2}}\sqrt{\sin\theta_r}\\
&\times \Big[\int_\alpha^{\pi-\theta_r}\phi\cot\phi d\phi+\theta_r\int_\alpha^{\pi-\theta_r}\cot\phi d\phi+\int_\alpha^{\pi-\theta_r}(\phi+\theta_r)\cot(\phi+\theta_r)d\phi\\
&- \int_\alpha^{\pi-\theta_r}\pi\cot\phi d\phi-\int_\alpha^{\pi-\theta_r}\pi\cot(\phi+\theta_r)d\phi+\int_{\pi-\theta_r}^{\pi-\beta}\phi\cot\phi d\phi\\
&+ \theta_r\int_{\pi-\theta_r}^{\pi-\beta}\cot\phi d\phi+\int_{\pi-\theta_r}^{\pi-\beta}(\phi+\theta_r)\cot(\phi+\theta_r)d\phi-\int_{\pi-\theta_r}^{\pi-\beta}\pi\cot\phi d\phi\\
&- \int_{\pi-\theta_r}^{\pi-\beta}\pi\cot(\phi+\theta_r)d\phi+\int_\alpha^{\theta_r-\zeta}(\phi-\theta_r)\cot(\phi-\theta_r)d\phi+\int_\alpha^{\theta_r-\zeta}\phi\cot\phi d\phi\\
&- \theta_r\int_\alpha^{\theta_r-\zeta}\cot\phi d\phi+\int_\alpha^{\theta_r-\zeta}\pi\cot(\phi-\theta_r)d\phi+\int_\alpha^{\theta_r-\zeta}\pi\cot\phi d\phi\\
nonumber &+ \int_{\theta_r+\zeta}^{\pi-\beta}(\phi-\theta_r)\cot(\phi-\theta_r)d\phi+\int_{\theta_r+\zeta}^{\pi-\beta}\phi\cot\phi d\phi-\theta_r\int_{\theta_r+\zeta}^{\pi-\beta}\cot\phi d\phi \qquad \text{(D.36)}\\
&- \int_{\theta_r+\zeta}^{\pi-\beta}\pi\cot(\phi-\theta_r)d\phi-\int_{\theta_r+\zeta}^{\pi-\beta}\pi\cot\phi d\phi\ \Big]
\end{aligned}
$$

$$
\begin{aligned}
S\left(L,\frac{r}{L},\epsilon_0\right) &= -\sqrt{\frac{\pi\sin\theta_r}{2L}}\left(1-\frac{\pi\epsilon_0}{2}\log\frac{\pi r_0}{2L\sin\theta_r}\right) \qquad \text{(D.37)}\\
&- \frac{\epsilon_0}{2}\left(\frac{\pi}{2L}\right)^{\frac{1}{2}}\sqrt{\sin\theta_r}\\
&\times \Big[\int_\alpha^{\pi-\theta_r}\phi\cot\phi d\phi+\int_\alpha^{\pi-\theta_r}(\phi+\theta_r)\cot(\phi+\theta_r)d\phi\\
&+ \int_\alpha^{\theta_r-\zeta}\pi\cot\phi d\phi-\int_\alpha^{\pi-\theta_r}\pi\cot\phi d\phi-\int_\alpha^{\pi-\theta_r}\pi\cot(\phi+\theta_r)d\phi+\int_{\pi-\theta_r}^{\pi-\beta}(\phi-1)\cot\phi d\phi\\
&+ \int_{\pi-\theta_r}^{\pi-\beta}(\phi+\theta_r)\cot(\phi+\theta_r)d\phi-\int_{\pi-\theta_r}^{\pi-\beta}\pi\cot\phi d\phi\\
&- \int_{\pi-\theta_r}^{\pi-\beta}\pi\cot(\phi+\theta_r)d\phi+\int_\alpha^{\theta_r-\zeta}(\phi-\theta_r)\cot(\phi-\theta_r)d\phi+\int_\alpha^{\theta_r-\zeta}\phi\cot\phi d\phi\\
&+ \int_\alpha^{\theta_r-\zeta}\pi\cot(\phi-\theta_r)d\phi+\int_{\theta_r+\zeta}^{\pi-\beta}(\phi-\theta_r)\cot(\phi-\theta_r)d\phi+\int_{\theta_r+\zeta}^{\pi-\beta}(\phi-1)\cot\phi d\phi\\
&- \int_{\theta_r+\zeta}^{\pi-\beta}\pi\cot(\phi-\theta_r)d\phi\ \Big].
\end{aligned}
$$

Now let us assume $r > \frac{L}{2}$ and remove the cutoffs everywhere except at the divergent integrals ,

$$
\begin{aligned}
S\left(L, \frac{r}{L}, \epsilon_0\right) &= -\sqrt{\frac{\pi \sin\theta_r}{2L}}\left(1 - \frac{\pi\epsilon_0}{2}\log\frac{\pi r_0}{2L\sin\theta_r}\right) \\
&- \frac{\epsilon_0}{2}\left(\frac{\pi}{2L}\right)^{\frac{1}{2}}\sqrt{\sin\theta_r} \\
&\times \Big[\int_0^{\pi-\theta_r}\phi\cot\phi d\phi + \int_0^{\pi-\theta_r}(\phi+\theta_r)\cot(\phi+\theta_r)d\phi \\
&- \int_0^{\pi-\theta_r}\pi\cot(\phi+\theta_r)d\phi + \int_{\pi-\theta_r}^{\pi}(\phi+\theta_r)\cot(\phi+\theta_r)d\phi \\
&- \int_{\pi-\theta_r}^{\pi}\pi\cot(\phi+\theta_r)d\phi + \int_0^{\theta_r}(\phi-\theta_r)\cot(\phi-\theta_r)d\phi + \int_0^{\theta_r}\phi\cot\phi d\phi \\
&+ \int_{\theta_r}^{\pi}(\phi-\theta_r)\cot(\phi-\theta_r)d\phi + \int_{\pi-\theta_r}^{\theta_r}\pi\cot\phi d\phi \\
&+ \left(\int_{\theta_r}^{\pi} + \int_{\pi-\theta_r}^{\pi}\right)(\phi-1)\cot\phi d\phi + \left(\int_0^{\theta_r-\zeta} - \int_{\theta_r-\zeta}^{\pi}\right)\pi\cot(\phi-\theta_r)d\phi\,\Big].
\end{aligned}
\tag{D.38}
$$

Substitute $\phi + \theta_r = \xi$ and $\phi - \theta_r = \rho$.

$$
\begin{aligned}
S\left(L, \frac{r}{L}, \epsilon_0\right) &= -\sqrt{\frac{\pi \sin\theta_r}{2L}}\left(1 - \frac{\pi\epsilon_0}{2}\log\frac{\pi r_0}{2L\sin\theta_r}\right) \\
&- \frac{\epsilon_0}{2}\left(\frac{\pi}{2L}\right)^{\frac{1}{2}}\sqrt{\sin\theta_r} \\
&\times \Big[\int_0^{\pi-\theta_r}\phi\cot\phi d\phi + \int_{\theta_r}^{\pi}\xi\cot\xi d\xi \\
&- \int_{\theta_r}^{\pi}\pi\cot\xi d\xi + \int_{\pi}^{\pi+\theta_r}\xi\cot\xi d\xi \\
&- \int_{\pi}^{\pi+\theta_r}\pi\cot\xi d\xi + \int_{-\theta_r}^{0}\rho\cot\rho d\rho + \int_0^{\theta_r}\phi\cot\phi d\phi \\
&+ \int_0^{\pi-\theta_r}\rho\cot\rho d\rho + \int_{\pi-\theta_r}^{\theta_r}\pi\cot\phi d\phi \\
&+ \left(\int_{\theta_r}^{\pi} + \int_{\pi-\theta_r}^{\pi}\right)(\phi-1)\cot\phi d\phi + \left(\int_{-\theta_r}^{-\zeta} - \int_{\zeta}^{\pi-\theta_r}\right)\pi\cot\rho d\rho\,\Big].
\end{aligned}
\tag{D.39}
$$

Substituting $\pi - \tau = \tau$ we have $\int_{\theta_r}^{\pi}(\tau-1)\cot\tau d\tau = \int_0^{\pi-\theta_r}\tau\cot\tau d\tau$. Similarly substituting

$\pi+\tau=\tau$ we have $\int_{\pi}^{\pi+\theta_r}(\tau-1)\cot\tau d\tau=\int_0^{\theta_r}\tau\cot\tau d\tau$. Using the above substitutions we can write

$$
\begin{aligned}
S\left(L,\frac{r}{L},\epsilon_0\right) &= -\sqrt{\frac{\pi\sin\theta_r}{2L}}\left(1-\frac{\pi\epsilon_0}{2}\log\frac{\pi r_0}{2L\sin\theta_r}\right) \qquad \text{(D.40)}\\
&- \frac{\epsilon_0}{2}\left(\frac{\pi}{2L}\right)^{\frac{1}{2}}\sqrt{\sin\theta_r}\\
&\times \left[3\int_0^{\pi-\theta_r}\phi\cot\phi d\phi+3\int_0^{\theta_r}\phi\cot\phi d\phi+\int_{\pi-\theta_r}^{\theta_r}\pi\cot\phi d\phi\right.\\
&+ \left.\left(\int_{\theta_r}^{\pi}+\int_{\pi-\theta_r}^{\pi}\right)(\phi-1)\cot\phi d\phi+\left(\int_{-\theta_r}^{-\zeta}-\int_{\zeta}^{\pi-\theta_r}\right)\pi\cot\rho d\rho\ \right]\\
&= -\sqrt{\frac{\pi\sin\theta_r}{2L}}\left(1-\frac{\pi\epsilon_0}{2}\log\frac{\pi r_0}{2L\sin\theta_r}\right)\\
&- \frac{\epsilon_0}{2}\left(\frac{\pi}{2L}\right)^{\frac{1}{2}}\sqrt{\sin\theta_r}\\
&\times \left[2\int_{\theta_r}^{\pi}(\phi-1)\cot\phi d\phi+\int_{\pi-\theta_r}^{\theta_r}\pi\cot\phi d\phi\right.\\
&+ \left.3\left(\int_0^{\theta_r}+\int_0^{\pi-\theta_r}\right)\phi\cot\phi d\phi+\left(\int_{-\theta_r}^{-\zeta}-\int_{\zeta}^{\pi-\theta_r}\right)\pi\cot\rho d\rho\ \right]\\
&= -\sqrt{\frac{\pi\sin\theta_r}{2L}}(1-\frac{\pi\epsilon_0}{2}\log\frac{\pi r_0}{2L\sin\theta_r})\\
&- \frac{\epsilon_0}{2}\left(\frac{\pi}{2L}\right)^{\frac{1}{2}}\sqrt{\sin\theta_r}\\
&\times [4\int_0^{\theta_r}\phi\cot\phi d\phi+4\int_0^{\pi-\theta_r}\phi\cot\phi d\phi\\
&+ \pi\log\left(\frac{\sin\zeta}{\sin\theta_r}\right)-\pi\log\left(\frac{\sin(\pi-\theta_r}{\sin\zeta}\right)]\\
&= -\sqrt{\frac{\pi\sin\theta_r}{2L}}(1-\frac{\pi\epsilon_0}{2}\log\frac{\pi r_0}{2L\sin\theta_r})\\
&- \frac{\epsilon_0}{2}\left(\frac{\pi}{2L}\right)^{\frac{1}{2}}\sqrt{\sin\theta_r}\\
&\times [4\int_0^{\theta_r}\phi\cot\phi d\phi+4\int_0^{\pi-\theta_r}\cot\phi d\phi\\
&+ 2\pi\log(\pi r_0)-2\pi\log\sin\theta_r].
\end{aligned}
$$

Write $\zeta=\pi r_0$.

$$
\begin{aligned}
S\left(L,\frac{r}{L},\epsilon_0\right) &= -\sqrt{\frac{\pi\sin\theta_r}{2L}}\left(1-\frac{\pi\epsilon_0}{2}\log\frac{\pi r_0}{2L\sin\theta_r}\right) \\
&- \epsilon_0\left(\frac{\pi\sin\theta_r}{2L}\right)^{\frac{1}{2}}\left(2\left(\int_0^{\theta_r}+\int_0^{\pi-\theta_r}\right)\phi\cot\phi d\phi+\pi\log\frac{\pi r_0}{\sin\theta_r}\right) \\
&= -\sqrt{\frac{\pi\sin\theta_r}{2L}}\left(1-\frac{\pi\epsilon_0}{2}\log\frac{\pi r_0}{2L\sin\theta_r}+\pi\epsilon_0\log\frac{\pi r_0}{\sin\theta_r}+2\epsilon_0\left(\int_0^{\theta_r}+\int_0^{\pi-\theta_r}\right)\phi\cot\phi d\phi\right) \\
&= -\sqrt{\frac{\pi\sin\theta_r}{2L}}\left(1+\frac{\pi\epsilon_0}{2}\log\frac{2\pi r_0}{L\sin\theta_r}+2\epsilon_0\left(\int_0^{\theta_r}+\int_0^{\pi-\theta_r}\right)\phi\cot\phi d\phi\right) \\
&= -\sqrt{\frac{\pi\sin\theta_r}{2L}}\left(1-\frac{\pi\epsilon_0}{2}\log\frac{L}{r_0}+\frac{\pi\epsilon_0}{2}\log\frac{2\pi}{\sin\theta_r}+2\epsilon_0\left(\int_0^{\theta_r}+\int_0^{\pi-\theta_r}\right)\phi\cot\phi d\phi\right)
\end{aligned}
\tag{D.41}
$$

Comparing with Eq. 6.42 we can write

$$
F_0(\frac{r}{L}) = -\sqrt{\frac{\pi\sin\theta_r}{2}}. \tag{D.42}
$$

and

$$
R(\frac{r}{L}) = \frac{\pi}{2}\log\frac{2\pi}{\sin\theta_r}+2\left(\int_0^{\theta_r}+\int_0^{\pi-\theta_r}\right)\phi\cot\phi d\phi \tag{D.43}
$$

To summarize, we have regulated mode sums $\sum_{m=1}^{\infty} g_m$ over the harmonic oscillator modes by replacing them with $\sum_{m=1}^{\infty} g_m \exp(-\pi m r_0/L)$ whenever necessary. And the integral representations are again regulated with the short distance cut-off r_0 by requiring that the ϕ integrals are to be done by excluding the region $[\theta_r - \pi r_0/L, \theta_r + \pi r_0/L]$ from the integration range. Somewhat remarkably, it is possible to obtain explicit expressions for all integrals sensitive to this ultraviolet cutoff, and thereby reduce this integral representation to the following compact and simple form:

$$
S\left(L,\frac{r}{L},\epsilon_0\right) = -\sqrt{\frac{\pi\sin\theta_r}{2L}}\left(1-\frac{\pi\epsilon_0}{2}\log\frac{L}{r_0}+\frac{\pi\epsilon_0}{2}\log\frac{2\pi}{\sin\theta_r}+2\epsilon_0\left(\int_0^{\theta_r}+\int_0^{\pi-\theta_r}\right)\phi\cot\phi d\phi\right) \tag{D.44}
$$

Comparing with the general expectation from our RG analysis (Eq. 6.42), we therefore obtain

$$
F_0(\frac{r}{L}) = -\sqrt{\frac{\pi\sin\theta_r}{2}}. \tag{D.45}
$$

and

$$
R(\frac{r}{L}) = \frac{\pi}{2}\log\frac{2\pi}{\sin\theta_r}+2\left(\int_0^{\theta_r}+\int_0^{\pi-\theta_r}\right)\phi\cot\phi d\phi. \tag{D.46}
$$

Bibliography

[1] S. Sanyal, A. Banerjee, and K. Damle. Vacancy-induced spin texture in a one-dimensional S=1/2 Heisenberg antiferromagnet. *Physical Review B*, 84(23):235129, December 2011.

[2] O. P. Vajk, P. K. Mang, M. Greven, P. M. Gehring, and J. W. Lynn. Quantum Impurities in the Two-Dimensional Spin One-Half Heisenberg Antiferromagnet. *Science*, 295:1961–1695, March 2002.

[3] A. W. Sandvik. Evidence for Deconfined Quantum Criticality in a Two-Dimensional Heisenberg Model with Four-Spin Interactions. *Physical Review Letters*, 98(22):227202, June 2007.

[4] M. A. Metlitski and S. Sachdev. Edge and impurity response in two-dimensional quantum antiferromagnets. *Physical Review B*, 78(17):174410, November 2008.

[5] S. Sanyal, A. Banerjee, K. Damle, and A. W. Sandvik. Antiferromagnetic order in systems with doublet S_{tot}=1/2 ground states. *Physical Review B*, 86(6):064418, August 2012.

[6] Y. Shimizu, K. Miyagawa, K. Kanoda, M. Maesato, and G. Saito. Spin Liquid State in an Organic Mott Insulator with a Triangular Lattice. *Physical Review Letters*, 91(10):107001, September 2003.

[7] S. Yamashita, Y. Nakazawa, M. Oguni, Y. Oshima, H. Nojiri, Y. Shimizu, K. Miyagawa, and K. Kanoda. Thermodynamic properties of a spin-1/2 spin-liquid state in a κ-type organic salt. *Nature Physics*, 4:459–462, April 2008.

[8] Y. Qi, C. Xu, and S. Sachdev. Dynamics and Transport of the Z_2 Spin Liquid: Application to κ-$(ET)_2Cu_2(CN)_3$. *Physical Review Letters*, 102(17):176401, May 2009.

[9] J. S. Helton, K. Matan, M. P. Shores, E. A. Nytko, B. M. Bartlett, Y. Yoshida, Y. Takano, A. Suslov, Y. Qiu, J.-H. Chung, D. G. Nocera, and Y. S. Lee. Spin Dynamics of the Spin-1/2 Kagome Lattice Antiferromagnet $ZnCu_3(OH)_6Cl_2$. *Physical Review Letters*, 98(10):107204, March 2007.

[10] R. R. Biswas, L. Fu, C. R. Laumann, and S. Sachdev. SU(2)-invariant spin liquids on the triangular lattice with spinful Majorana excitations. *Physical Review B*, 83(24):245131, June 2011.

[11] T. Itou, A. Oyamada, S. Maegawa, and R. Kato. Instability of a quantum spin liquid in an organic triangular-lattice antiferromagnet. *Nature Physics*, 6:673–676, September 2010.

[12] T. Itou, A. Oyamada, S. Maegawa, M. Tamura, and R. Kato. Quantum spin liquid in the spin-1/2 triangular antiferromagnet $EtMe_3Sb[Pd(dmit)_2]_2$. *Physical Review B*, 77(10):104413, March 2008.

[13] H. Yao and D.-H. Lee. Fermionic Magnons, Non-Abelian Spinons, and the Spin Quantum Hall Effect from an Exactly Solvable Spin-1/2 Kitaev Model with SU(2) Symmetry. *Physical Review Letters*, 107(8):087205, August 2011.

[14] H. Bethe. Zur Theorie der Metalle. *Zeitschrift fur Physik*, 71:205–226, March 1931.

[15] P. A. de Sa and A. M. Tsvelik. Anisotropic spin-1/2 Heisenberg chain with open boundary conditions. *Physical Review B*, 52:3067–3070, August 1995.

[16] I. Affleck. Field theory methods and quantum critical phenomena. In E. Brezin and J. Zinn-Justin, editors, *Fields, Strings, and Critical Phenomena*, pages 563–640. Les Houches 1988, North-Holland, Amsterdam, 1990.

[17] A. Banerjee, K. Damle, and F. Alet. Impurity spin texture at a deconfined quantum critical point. *Physical Review B*, 82(15):155139, October 2010.

[18] T. Senthil, A. Vishwanath, L. Balents, S. Sachdev, and M. P. A. Fisher. Deconfined Quantum Critical Points. *Science*, 303:1490–1494, March 2004.

[19] A. Banerjee, K. Damle, and F. Alet. Impurity spin texture at the critical point between Néel-ordered and valence-bond-solid states in two-dimensional SU(3) quantum antiferromagnets. *Physical Review B*, 83(23):235111, June 2011.

[20] S. Pujari, K. Damle, and F. Alet. Néel-State to Valence-Bond-Solid Transition on the Honeycomb Lattice: Evidence for Deconfined Criticality. *Physical Review Letters*, 111(8):087203, August 2013.

[21] F.-J. Jiang, M. Nyfeler, S. Chandrasekharan, and U.-J. Wiese. From an antiferromagnet to a valence bond solid: evidence for a first-order phase transition. *Journal of Statistical Mechanics: Theory and Experiment*, 2:9, February 2008.

[22] A. B. Kuklov, M. Matsumoto, N. V. Prokof'Ev, B. V. Svistunov, and M. Troyer. Deconfined Criticality: Generic First-Order Transition in the SU(2) Symmetry Case. *Physical Review Letters*, 101(5):050405, August 2008.

[23] E. Orignac. Quantitative expression of the spin gap via bosonization for a dimerized spin-1/2 chain. *European Physical Journal B*, 39:335–339, June 2004.

[24] I. Affleck, D. Gepner, H. J. Schulz, and T. Ziman. Critical behaviour of spin-s Heisenberg antiferromagnetic chains: analytic and numerical results. *Journal of Physics A Mathematical General*, 22:511–529, March 1989.

[25] V. Barzykin and I. Affleck. Finite-size scaling for the spin-1/2 Heisenberg antiferromagnetic chain. *Journal of Physics A Mathematical General*, 32:867–874, February 1999.

[26] H. Neuberger and T. Ziman. Finite-size effects in Heisenberg antiferromagnets. *Physical Review B*, 39:2608–2618, February 1989.

[27] S. R. White and A. L. Chernyshev. Neél Order in Square and Triangular Lattice Heisenberg Models. *Physical Review Letters*, 99(12):127004, September 2007.

[28] A. W. Sandvik. Finite-size scaling of the ground-state parameters of the two-dimensional Heisenberg model. *Physical Review B*, 56:11678–11690, November 1997.

[29] B. B. Beard, R. J. Birgeneau, M. Greven, and U.-J. Wiese. Square-Lattice Heisenberg Antiferromagnet at Very Large Correlation Lengths. *Physical Review Letters*, 80:1742–1745, February 1998.

[30] E. Lieb and D. Mattis. Ordering Energy Levels of Interacting Spin Systems. *Journal of Mathematical Physics*, 3:749–751, July 1962.

[31] Z. Weihong and C. J. Hamer. Spin-wave theory and finite-size scaling for the Heisenberg antiferromagnet. *Physical Review B*, 47:7961–7970, April 1993.

[32] T. Holstein and H. Primakoff. Field Dependence of the Intrinsic Domain Magnetization of a Ferromagnet. *Physical Review*, 58:1098–1113, December 1940.

[33] P. Chandra and B. Doucot. Possible spin-liquid state at large S for the frustrated square Heisenberg lattice. *Physical Review B*, 38:9335–9338, November 1988.

[34] S. Wenzel and W. Janke. Comprehensive quantum Monte Carlo study of the quantum critical points in planar dimerized/quadrumerized Heisenberg models. *Physical Review B*, 79(1):014410, January 2009.

[35] P. W. Anderson. An Approximate Quantum Theory of the Antiferromagnetic Ground State. *Physical Review*, 86:694–701, June 1952.

[36] S. Chandrasekharan, F.-J. Jiang, M. Pepe, and U.-J. Wiese. Rotor spectra, berry phases, and monopole fields: From antiferromagnets to QCD. *Physical Review D*, 78(7):077901, October 2008.

[37] T. T. Wu and C. N. Yang. Some properties of monopole harmonics. *Physical Review D*, 16:1018–1021, August 1977.

[38] A. J. Willans, J. T. Chalker, and R. Moessner. Site dilution in the Kitaev honeycomb model. *Physical Review B*, 84(11):115146, September 2011.

[39] O. Motrunich, K. Damle, and D. A. Huse. Particle-hole symmetric localization in two dimensions. *Physical Review B*, 65(6):064206, February 2002.

[40] R. Gade. Anderson localization for sublattice models. *Nuclear Physics B*, 398:499–515, June 1993.

[41] R. B. Griffiths. Nonanalytic Behavior Above the Critical Point in a Random Ising Ferromagnet. *Physical Review Letters*, 23:17–19, July 1969.

[42] S.-K. Ma, C. Dasgupta, and C.-K. Hu. Random Antiferromagnetic Chain. *Physical Review Letters*, 43:1434–1437, November 1979.

[43] D. S. Fisher. Random antiferromagnetic quantum spin chains. *Physical Review B*, 50:3799–3821, August 1994.

[44] R. N. Bhatt and P. A. Lee. Scaling Studies of Highly Disordered Spin- 1/2 Antiferromagnetic Systems. *Physical Review Letters*, 48:344–347, February 1982.

[45] B. S. Shastry and D. Sen. Majorana fermion representation for an antiferromagnetic spin chain. *Physical Review B*, 55:2988–2994, February 1997.

[46] R. S. Martin and J. H. Wilkinson. Solution of symmetric and unsymmetric band equations and calculation of eigenvectors of band matrices. In J. H. Wilkinson and C. Reinsh, editors, *Linear Algebra*, volume 2, pages 70–92. Springer-Verlag,, 1971.

[47] Torbjørn Granlund and the GMP development team. *The GNU Multiple Precision Arithmetic Library*. 5.1.2 edition.

[48] D. E. Knuth. *Seminumerical Algorithms,The Art of Computer Programming*, volume 2. Addison-Wesley, 1998.

[49] E. H. Lieb. Flux phase of the half-filled band. *Physical Review Letters*, 73:2158–2161, October 1994.

[50] P. W. Anderson. Absence of Diffusion in Certain Random Lattices. *Physical Review*, 109:1492–1505, March 1958.

[51] N. F. Mott. The Basis of the Electron Theory of Metals, with Special Reference to the Transition Metals. *Proceedings of the Physical Society A*, 62:416–422, July 1949.

[52] R. N. Bhatt and P. A. Lee. A scaling method for low temperature behavior of random antiferromagnetic systems (invited). *Journal of Applied Physics*, 52:1703–1707, March 1981.

[53] I. M. Lifshitz. The energy spectrum of disordered systems. *Advances in Physics*, 13:483–536, October 1964.

[54] A. Altland and M. R. Zirnbauer. Nonstandard symmetry classes in mesoscopic normal-superconducting hybrid structures. *prb*, 55:1142–1161, January 1997.

[55] F. J. Dyson. The Dynamics of a Disordered Linear Chain. *Physical Review*, 92:1331–1338, December 1953.

[56] T. F. Rosenbaum, R. F. Milligan, M. A. Paalanen, G. A. Thomas, R. N. Bhatt, and W. Lin. Metal-insulator transition in a doped semiconductor. *prb*, 27:7509–7523, June 1983.

[57] L. C. Tippie and W. G. Clark. Low-temperature magnetism of quinolinium $(\mathrm{TCNQ})_2$, a random-exchange heisenberg antiferromagnetic chain. i. static properties. *Phys. Rev. B*, 23:5846–5853, Jun 1981.

[58] M. Takigawa, N. Motoyama, H. Eisaki, and S. Uchida. Field-induced staggered magnetization near impurities in the S= one-dimensional Heisenberg antiferromagnet Sr_2CuO_3. *Physical Review B*, 55:14129–14132, June 1997.

[59] B. Lake, D. A. Tennant, C. D. Frost, and S. E. Nagler. Quantum criticality and universal scaling of a quantum antiferromagnet. *Nature Materials*, 4:329–334, April 2005.

[60] B. Lake, D. A. Tennant, and S. E. Nagler. Longitudinal magnetic dynamics and dimensional crossover in the quasi-one-dimensional spin- (1)/(2) Heisenberg antiferromagnet $KCuF_3$. *Physical Review B*, 71(13):134412, April 2005.

[61] S. Eggert, I. Affleck, and M. Takahashi. Susceptibility of the spin 1/2 Heisenberg antiferromagnetic chain. *Physical Review Letters*, 73:332–335, July 1994.

[62] A. W. Sandvik. Evidence for Deconfined Quantum Criticality in a Two-Dimensional Heisenberg Model with Four-Spin Interactions. *Physical Review Letters*, 98(22):227202, June 2007.

[63] P. W. Kasteleyn. The statistics of dimers on a lattice : I. The number of dimer arrangements on a quadratic lattice. *Physica*, 27:1209–1225, December 1961.

[64] E. Lieb and M. Loss. Fluxes, Laplacians and Kasteleyn's Theorem. *eprint arXiv:cond-mat/9209031*, September 1992.

[65] A. Auerbach and D. P. Arovas. *Schwinger Bosons Approaches to Quantum Antiferromagnetism*, page 365. 2011.

[66] S. Esposito, E. Recami, A. van der Merwe, and R. Battiston. *Ettore Majorana: Unpublished Research Notes on Theoretical Physics*. 2009.

[67] J. Lou, A. W. Sandvik, and N. Kawashima. Antiferromagnetic to valence-bond-solid transitions in two-dimensional SU(N) Heisenberg models with multispin interactions. *prb*, 80(18):180414, November 2009.

[68] A. Banerjee and K. Damle. Generalization of the singlet sector valence-bond loop algorithm to antiferromagnetic ground states with total spin S_{tot} = 1/2. *Journal of Statistical Mechanics: Theory and Experiment*, 8:17, August 2010.

[69] A. W. Sandvik. Ground State Projection of Quantum Spin Systems in the Valence-Bond Basis. *Physical Review Letters*, 95(20):207203, November 2005.

[70] A. W. Sandvik and H. G. Evertz. Loop updates for variational and projector quantum Monte Carlo simulations in the valence-bond basis. *prb*, 82(2):024407, July 2010.

[71] A. W. Sandvik. Multichain Mean-Field Theory of Quasi-One-Dimensional Quantum Spin Systems. *Physical Review Letters*, 83:3069–3072, October 1999.

[72] S. Eggert. Numerical evidence for multiplicative logarithmic corrections from marginal operators. *prb*, 54:9612, October 1996.

[73] T. Hikihara and A. Furusaki. Spin correlations in the two-leg antiferromagnetic ladder in a magnetic field. *prb*, 63(13):134438, April 2001.

[74] J. V. José, L. P. Kadanoff, S. Kirkpatrick, and D. R. Nelson. Renormalization, vortices, and symmetry-breaking perturbations in the two-dimensional planar model. *prb*, 16:1217–1241, August 1977.

[75] E. Anderson, Z. Bai, C. Bischof, S. Blackford, J. Demmel, J. Dongarra, J. Du Croz, A. Greenbaum, S. Hammarling, A. McKenney, and D. Sorensen. *LAPACK Users' Guide*. Society for Industrial and Applied Mathematics, Philadelphia, PA, third edition, 1999.

[76] Alexei M. Tsvelik Alexander O. Gogolin, Alexander A. Nersesyan. *Bosonization and Strongly Correlated Systems*. (Cambridge University Press), first edition, 1998.

[77] D. Sénéchal. An introduction to bosonization. *eprint arXiv:cond-mat/9908262*, August 1999.